NASA/TM—2012-217450

Acoustic Performance of the GEAE UPS Research Fan in the NASA Glenn 9- by 15-Foot Low-Speed Wind Tunnel

Richard P. Woodward and Christopher E. Hughes
Glenn Research Center, Cleveland, Ohio

May 2012

NASA STI Program . . . in Profile

Since its founding, NASA has been dedicated to the advancement of aeronautics and space science. The NASA Scientific and Technical Information (STI) program plays a key part in helping NASA maintain this important role.

The NASA STI Program operates under the auspices of the Agency Chief Information Officer. It collects, organizes, provides for archiving, and disseminates NASA's STI. The NASA STI program provides access to the NASA Aeronautics and Space Database and its public interface, the NASA Technical Reports Server, thus providing one of the largest collections of aeronautical and space science STI in the world. Results are published in both non-NASA channels and by NASA in the NASA STI Report Series, which includes the following report types:

- TECHNICAL PUBLICATION. Reports of completed research or a major significant phase of research that present the results of NASA programs and include extensive data or theoretical analysis. Includes compilations of significant scientific and technical data and information deemed to be of continuing reference value. NASA counterpart of peer-reviewed formal professional papers but has less stringent limitations on manuscript length and extent of graphic presentations.

- TECHNICAL MEMORANDUM. Scientific and technical findings that are preliminary or of specialized interest, e.g., quick release reports, working papers, and bibliographies that contain minimal annotation. Does not contain extensive analysis.

- CONTRACTOR REPORT. Scientific and technical findings by NASA-sponsored contractors and grantees.

- CONFERENCE PUBLICATION. Collected papers from scientific and technical conferences, symposia, seminars, or other meetings sponsored or cosponsored by NASA.

- SPECIAL PUBLICATION. Scientific, technical, or historical information from NASA programs, projects, and missions, often concerned with subjects having substantial public interest.

- TECHNICAL TRANSLATION. English-language translations of foreign scientific and technical material pertinent to NASA's mission.

Specialized services also include creating custom thesauri, building customized databases, organizing and publishing research results.

For more information about the NASA STI program, see the following:

- Access the NASA STI program home page at *http://www.sti.nasa.gov*

- E-mail your question via the Internet to *help@sti.nasa.gov*

- Fax your question to the NASA STI Help Desk at 443–757–5803

- Telephone the NASA STI Help Desk at 443–757–5802

- Write to:
  NASA Center for AeroSpace Information (CASI)
  7115 Standard Drive
  Hanover, MD 21076–1320

NASA/TM—2012-217450

Acoustic Performance of the GEAE UPS Research Fan in the NASA Glenn 9- by 15-Foot Low-Speed Wind Tunnel

Richard P. Woodward and Christopher E. Hughes
Glenn Research Center, Cleveland, Ohio

National Aeronautics and
Space Administration

Glenn Research Center
Cleveland, Ohio 44135

May 2012

This work was sponsored by the Fundamental Aeronautics Program at the NASA Glenn Research Center.

Level of Review: This material has been technically reviewed by technical management.

Available from

NASA Center for Aerospace Information
7115 Standard Drive
Hanover, MD 21076–1320

National Technical Information Service
5301 Shawnee Road
Alexandria, VA 22312

Available electronically at http://www.sti.nasa.gov

Acoustic Performance of the GEAE UPS Research Fan in the NASA Glenn 9- by 15-Foot Low-Speed Wind Tunnel

Richard P. Woodward and Christopher E. Hughes
National Aeronautics and Space Administration
Glenn Research Center
Cleveland, Ohio 44135

Abstract

A model advanced turbofan was acoustically tested in the NASA Glenn 9- by 15-Foot Low-Speed Wind Tunnel in 1994. The Universal Propulsion Simulator fan was designed and manufactured by General Electric Aircraft Engines, and included an active core, as well as bypass, flow paths. The fan was tested with several rotors featuring unswept, forward-swept and aft-swept designs of both metal and composite construction. Sideline acoustic data were taken with both hard and acoustically treated walls in the flow passages. The fan was tested within an airflow at a Mach number of 0.20, which is representative of aircraft takeoff/approach conditions. All rotors showed similar aerodynamic performance. However, the composite rotors typically showed higher noise levels than did corresponding metal rotors. Aft and forward rotor sweep showed at most modest reductions of transonic multiple pure tone levels. However, rotor sweep often introduced increased rotor-stator interaction tone levels. Broadband noise was typically higher for the composite rotors and also for the aft-swept metal rotor. Transonic MPT generation was reduced with increasing fan axis angle of attack (AOA); however, higher downstream noise levels did increase with AOA resulting in higher overall Effective Perceived Noise Level.

Introduction

The Universal Propulsion Simulator (UPS) fan was designed and built by General Electric Aircraft Engines (GEAE) to explore advanced fan stage concepts for future quiet turbofan engines. The 1994 UPS fan tests were conducted in the NASA Glenn 9- by 15-Foot Low-Speed Wind Tunnel (henceforth referred to as the 9×15 LSWT) using several rotor designs. These acoustic tests explored the fan performance with unswept, forward-swept, and aft-swept rotors of both metal and composite construction. The fan stage was tested with, and without acoustic treatment on the inlet and exhaust flow passages. Acoustic testing was performed with air flowing in the tunnel at a Mach number of 0.20, which is representative of aircraft takeoff/approach conditions.

The primary focus of these tests was to acquire representative UPS fan data in the NASA Glenn Research Center 9×15 LSWT and in two other world class facilities—the Boeing Low-Speed Aeroacoustic Facility (LSAF) free jet, and the German-Dutch Wind Tunnel (DNW) free jet facility. The acoustic results of the UPS fan tests in these three facilities can be found in References 1 and 2. Data comparisons for the UPS fan in these three facilities showed the NASA 9×15 LSWT to be an acceptable facility for fan far-field aeroacoustic measurements under simulated flight conditions.

Description of Test

Research Fan

The UPS fan is representative of current state-of-the-art high bypass ratio turbofan engines. Figure 1 is a cross-sectional sketch of the UPS fan. The bypass rotor diameter is 55.9 cm (22.0 in.). The rotor bypass-vane ratio is adequate to achieve cutoff of the fundamental interaction tone (Refs. 3 and 4). The UPS fan has an active core flow that includes a powered rotor (same rotational speed as the bypass fan) with inlet and outlet vanes. The core flow passage has de-swirl struts slightly downstream of the core

outlet guide vanes, and aft load struts further downstream which have the potential of generating rotor-strut interaction noise. The core passage also has a full passage screen to adjust flow rates, and subsequently stage bypass ratio. Table 1 is a listing of the fan design parameters. The fan was powered by a high-pressure air turbine drive (Ref. 5) with the drive air and instrumentation supplied through a support strut mounted on the wind tunnel test section floor.

The UPS fan stage was tested with several bypass rotor configurations as shown in Figure 2. (The bypass stator and core stage were the same throughout this test series.) The baseline rotor, designated "M4" was unswept and fabricated of metal. Additional test rotors allowed investigation of rotor forward and aft sweep effects, and relative performance of composite versus metal rotor construction.

The acoustic results reported herein are for the UPS bypass fan stage with either hard or acoustically treated walls. Figure 1 shows the presence of acoustic treatment in the inlet and bypass ducts. The acoustic treatment was always present on the inner wall of the bypass duct upstream and downstream of the bypass stator. The inlet and outer wall bypass duct treatment panels were removable and could be replaced with hard-wall panels. However for the tests reported here, the acoustic treatment was always present on the outer bypass duct wall between the rotor and stator. Letter designations are used in this report to distinguish between different configurations of hard-wall and treated wall panels in the inlet and outlet sections of the bypass duct. The letter "H" designates a hard-wall panel. The initial acoustic treatment or the original acoustic treatment as provided by GEAE, is designated by the letter "T." A new or alternative acoustic treatment, designed by NASA, is designated by the letter "N." Thus, the hard-wall configuration is designated "HTH" and the treated configurations are designated "TTT" or "NTN."

9×15 LSWT and Acoustic Instrumentation

The NASA Glenn 9×15 LSWT is located in the low speed return leg of the 8×6 Supersonic Wind Tunnel (Fig. 3). The tunnel test section walls, floor and ceiling have acoustic treatment to produce an anechoic test environment (Refs. 6 to 8). Figure 4 is a sketch of the test fan installed in the 9×15 LSWT. Sideline acoustic data were acquired with a computer-controlled translating microphone probe (also seen in the photograph of Figure 5) and with an array of fixed microphones mounted on the tunnel wall. The translating microphone probe acquired data at 48 sideline geometric angles from 29° to 138° relative to the fan inlet highlight. The translating probe traverse was at 226 cm (89-in.) from the fan rotational axis (approximately four fan diameters). The acoustic data were acquired through a digital computer system and stored for post-run analysis. Acoustic data were acquired at a tunnel Mach number of 0.20, which is representative of takeoff and approach conditions and provides flight acoustic conditions (Ref. 9). Acoustic data were taken at 0°, 3°, and 9° of fan axis angles of attack.

Acoustic data acquired in the 9×15 LSWT were processed as constant bandwidth spectra. Spectra were acquired and averaged at each translating probe position with 6 and 118 Hz bandwidths. These constant bandwidth spectra were electronically merged and used to generate 1/3rd octave spectra. The results presented herein are in terms of both constant bandwidth and 1/3rd octave spectra. The survey data were instrument corrected and corrected for atmospheric attenuation using Doppler-shifted frequencies over the propagation path. Geometric (observed) sideline angles were converted to emission angles according to the relationship:

$$\Theta_{em} = \Theta_{geom} - \sin^{-1}(M_o \sin \Theta_{geom})$$

where Θ_{em} and Θ_{geom} are, respectively, the emission and observed sideline angles, and M_o is the test section Mach number.

There was initially some concern as to the validity of data acquired with the translating microphone probe as opposed to data acquired with conventional fixed microphones. The fixed wall microphone array was vertically staggered to minimize wake interaction from upstream microphone holders. Acoustic data acquired during the UPS test were used to compare fixed and translating microphone data quality (Ref. 8). Wakes from upstream microphone holders were shown to persist a significant distance downstream, thus possibly impinging on downstream microphones with a consequent compromise in the data quality from these microphones. Also, the vertical stagger used to minimize this wake interaction introduced a new, azimuthal variation in the sideline data—a problem not associated with a single traversing microphone. The traversing microphone probe is not restricted as to the number of discrete measurement positions (48 positions were used for this test). Acoustic data presented herein is for the translating microphone probe.

Results and Discussion

Aerodynamic Performance

Limited aerodynamic results are available for the UPS tests in the NASA 9×15 LSWT. Data were taken at a tunnel Mach number of 0.20 over a range of fan speeds from 7400 to 14000 corrected revolutions per minute (rpm) (see Table 2). The fan design tip speed (Table 1) was 1214 ft/sec (metal rotors, such as M4) and 1274 ft/sec (composite rotors).

The UPS fan was tested in the 9×15 LSWT with several rotor configurations (Table 3). As discussed previously, acoustic treatment was always present between the rotor and the stator on the bypass duct outer wall (see Fig. 1). Data were taken with two types of acoustic treatment on the inlet and bypass ducts as well as for hard-wall in those locations. Acoustic data were acquired for the first 9 configurations, listed as C-1 to C-9 in Table 3, followed by a series of aerodynamic and flow visualization tests (not reported herein). A rather severe drive system oil leak developed at the end of these non-acoustic tests, necessitating the insertion of an oil drain pipe extending from the drive through the downstream flow passages. Consequently, aeroacoustic results for the last four test configurations (listed as C-44 a and b and C-45 a and b in Table 3) utilizing the advanced unswept composite rotor were compromised with extraneous noise by the insertion of this oil drainpipe, and are not included herein.

Representative fan aerodynamic performance for the UPS tests are shown in Figures 6 and 7. Figure 6 shows the aerodynamic performance in terms of the bypass pressure ratio as a function of bypass corrected weight flow for the hard-wall test configurations. These results show similar performance for each of the 4 bypass rotors; the unswept (M4) and the aft-swept metal rotors, and the unswept and forward-swept composite rotors (see Fig. 2). Figure 7 shows corresponding results for the test configurations with acoustically treated inlet and exhaust ducts.

Acoustic Performance

Expected Acoustic Propagation

Table 4 shows the expected frequencies for the first four rotor bypass rotor-stator interaction tone orders and first two core stage tone orders for each of the fan test speeds. These results are presented in graphical form in Figure 8. Blade and vane numbers for the bypass and core stages were selected to acoustically cutoff the propagation of the fundamental blade passing frequency (BPF) tone at lower fan speeds, according to the acoustic mode theory of References 3 and 4.

Effective Perceived Noise Level

The Effective Perceived Noise Level (EPNL) provides a subjective measure of the aircraft flyover and sideline noise levels. This value is derived from the flyover or sideline sound pressure level profiles and is a function of frequency, duration, and tone content. Effective perceived noise levels were calculated by GEAE using the NASA 9×15 LSWT results. The furthest downstream emission angle measured by the traverse microphone at $M_0 = 0.20$ flow was 130°, which was not sufficiently downstream to define a 10 dB drop off from the peak sideline values. (Later acoustic tests in the 9×15 LSWT used three fixed downstream microphones to better define aft fan noise.) Therefore, an assumed downstream directivity shape was used to complete the EPNL calculations. A scale factor of 5.6 was used. EPNL values are calculated from "full-scale engine" sound pressure data up to 10 kHz. Thus, with this scale factor, model acoustic data up to about 60 kHz were utilized.

An unexpected tone in the acoustic spectra was associated with the composite rotor (configurations 4 through 7, Table 3). The tones were found to be caused by the presence of bolt access holes in the rotor spinner used for the composite blade configurations. Another spinner with slightly different bolt hole geometry was used for the metal rotor configurations and did not generate these unexpected tones. (The acoustic impact of the spinner holes was investigated with the advanced unswept composite rotor of configurations 44 and 45 using metallic tape to cover the spinner holes.) The spinner-induced tones were electronically removed from the spectra for the composite rotor configurations. Figure 9 shows the adverse effect of these spinner bolt holes as a function of rotor tip speed, with the noise difference being most significant at lower tip speeds.

Figure 10 compares EPNL levels for several hard-wall (HTH) configurations at 0° fan axis angle of attack. The noise levels for the metal baseline M4 rotor are significantly lower than those for the aft-swept metal rotor or the unswept and forward-swept composite rotors—especially near 950 ft/sec rotor tip speed. The relatively higher noise levels for the aft-swept metal rotor may be the result of increased rotor wake-vane interaction because of reduced blade-vane spacing toward the tip region. The composite rotors were consistently noisier than their metal counterparts. This may be due, at least in part, to adverse flexing of the composite rotors under load.

Figure 11 shows corresponding EPNL results for the test configurations with inlet and bypass exhaust duct treatment. Two wall treatment configurations were tested, as provided by GEAE. As indicated before, the original treatment configurations are designated TTT. New treatment panels, designated NTN were introduced for some of the later configurations. Once again, the lowest EPNL values were associated with the baseline M4 metal rotor. The M4 rotor with the original wall treatment (TTT) was typically slightly quieter than with the new treatment (NTN). The composite rotors were typically noisier than the M4 rotor, although the difference between metal and composite rotors was not as pronounced as for the hardwall configurations of Figure 10.

Figure 12 compares the baseline M4 configurations with (TTT) and without (HTH) wall treatment. The wall treatment varied in effectiveness through the range of test speeds from about 2 EPNdB at the lowest speeds to about 5 EPNdB at the higher speeds—the exception was near 950 ft/sec rotor tip speed, which showed no treatment benefit. Rotor multiple pure tone generation will occur as the tip Mach number approaches unity. The results of Figure 12 show lower perceived noise levels with liner treatment, most likely due to MPT absorption by the liner.

Effect of Rotor Design and Construction

The UPS fan was tested with several metal and composite rotors featuring mild forward and aft sweep as well as metal and composite unswept rotors (see Fig. 2). The EPNL results, given in the previous section, showed that, in general, the noise levels were somewhat lower with the metal rotors than with composite rotors, even though all rotors showed comparable aerodynamic performance, (Figs. 6 and 7). The following discussion presents spectral and directivity comparisons for these test

rotors. Results are presented for six rotor comparisons first showing EPNL versus fan speed. Results are then presented for constant bandwidth (6 Hz) spectra at 10 and 12 k corrected rpm, or rpm_c at 47°, 102°, and 130° sideline emission angles. The fan tangential tip speed is subsonic at 10 k rpm_c (nominal 980 ft/sec), and supersonic at 12 k rpm_c (nominal 1180 ft/sec), which is the speed where maximum MPT generation occurs. These comparisons are then concluded with 1/3rd octave sideline directivities at these two fan speeds.

Unswept Rotor

Figures 13 to 30 compare acoustic performance of the baseline unswept M4 metal rotor and the unswept composite rotor. Figures 13 to 21 are for the hardwall duct, and Figures 22 to 30 are for the "new" duct acoustic treatment (NTN). These results continue to show higher noise levels associated with the composite rotor.

Figure 13 compares EPNL for the two rotors as a function of rotor tip speed, showing the composite rotor configuration to be up to 4 EPNdB noisier than the M4 metal rotor. Figure 14 compares constant bandwidth spectra at 10 k rpm_c at the upstream, 47° emission angle. There is a "haystack" noise region associated with the composite rotor near 2 kHz that is not seen for the metal rotor. It is possible that MPT generation occurs slightly sooner (at a lower tip speed) for the composite rotor than for the metal rotor. Likewise, there are several pure tones above the bypass blade passage frequency (BPF) which are only seen for the composite rotor. There is evidence of the fundamental rotor tone (BPF) in these spectra even though the blade and vane numbers were chosen to cutoff the fundamental BPF tone. The fan tip speed is approaching transonic at 10 k rpm_c such that a rotor-alone BPF tone is possible. The bypass 2BPF tone, which is clearly seen for the metal rotor, is essentially missing from the spectra for the composite rotor at this sideline angle. Broadband levels tend to be higher for the composite rotor. The 2 kHz "haystack" is not seen for the composite rotor at the 102° and 130° emission angles (Figs. 15 and 16). Broadband levels are still slightly higher for the composite rotor at the further aft sideline locations. MPT generation appears to be well established for both rotors (Figs. 17 to 19) at 12 k rpm_c, where the broadband level is still higher for the composite rotor.

Figure 20 compares 1/3rd octave directivities for the metal and composite unswept rotors at 10 k rpm_c. Noise levels for the composite rotor are especially higher toward upstream angles at 2 and 2.5 kHz (Figs. 20(a) and (b)), which correspond to the spectral "haystack" (possibly early MPT generation) observed in the spectra of Figure 15. Higher noise levels for the composite rotor become more consistent across the directivity survey with increasing frequency, eventually becoming aft dominated at 5 kHz (Fig. 20(e)). The directivity surveys for the bypass 2BPF and core BPF tones (8 kHz, Fig. 20(f), See also Table 4) show a somewhat higher level for the composite rotor, although these noise levels are significantly affected by differences in broadband levels for the two rotors.

Directivities at 12 k rpm_c (Fig. 21) again show high noise levels associated with the composite rotor at forward sideline angles and low frequencies. However, unlike the directivity results at 10 k rpm_c, noise level differences between the two rotors become insignificant at frequencies above 4 kHz.

Figures 22 to 30 present a similar comparison for the unswept metal and composite rotors with the "new" bypass duct acoustic treatment (NTN) in place. EPNL differences are significantly smaller with duct acoustic treatment, although the composite rotor is typically still noisier (Fig. 22, compare with Fig. 13). The EPNL difference tends to be less as the rotor tip speed exceeds the sonic speed where MPT energy (rather than broadband) tends to dominate the noise spectra.

The constant bandwidth spectral comparisons at 10 k and 12 k rpm_c (Figs. 23 to 28) correspond to the previously discussed figures for the hard-wall (HTH) configuration (Figs. 14 to 19). At 10 k rpm_c the new acoustic treatment greatly reduced the 2BPF tone—especially at 47° and 102° sideline angles. However, there was some increase in the fundamental, BPF tone associated with the NTN treatment.

There is considerable MPT generation at 12 k rpm_c for both the hard-wall and treated bypass ducts, although subjectively, duct treatment somewhat reduced the severity of these MPT tones. Also, the new duct treatment was more effective in reducing the fundamental tone level at this fan speed than was seen at the lower, 10 k rpm_c fan speed.

Figures 29 and 30 show, respectively, 1/3rd octave directivities at 10 k and 12 k rpm_c for the unswept metal and composite rotors with duct wall acoustic treatment (NTN). The 10 k rpm_c results are similar to those for the hard-wall duct (higher noise levels associated with the composite rotor), although the noise level differences between the two rotors are less with duct treatment in place. At 12 k rpm_c the composite rotor shows significantly higher noise levels at upstream angles for 2 and 2.5 kHz (Figs. 30(a) and (b)). However, noise differences between the two rotors become minimal at 3.15 kHz. (Fig. 30(c)) and above.

In summary, comparisons between the unswept metal and composite rotors consistently showed higher noise levels associated with the composite rotor. These differences are primarily in the broadband, and are more pronounced at lower frequencies. There are also consistent spectral differences between the metal and composite rotors. In particular, an upstream "haystack" region is exclusively seen for the composite rotor in the constant bandwidth spectra near 2 kHz. The composite rotor tends to have a higher bypass BPF tone at 10 k rpm_c; however, the bypass 2BPF tone for this rotor and fan speed is much lower than that tone for the metal rotor.

Effect of Rotor Aft Sweep

Rotor aft sweep may retard and/or reduce MPT generation. However, aft rotor sweep may decrease the rotor-stator separation distance toward the tip region, thereby increase the potential for rotor-stator interaction noise. Figures 31 to 39 compare acoustic results for the unswept M4 metal rotor and the aft-swept metal rotor (Fig. 2) with the hardwall bypass duct (HTH). Similar results are presented for the unswept M4 and modified aft-swept metal rotors with the "new" bypass duct acoustic treatment (NTN) in Figures 40 to 48.

Figure 31 compares EPNL's as a function of fan speed for the baseline M4 unswept and aft-swept metal rotors for the hard-wall configuration. Noise levels are consistently higher for the aft-swept rotor, especially for near transonic tip speeds, being 4 EPNdB higher than the baseline rotor at 970 ft/sec rotor tip speed.

Figures 32 to 37 present constant bandwidth spectra at 10 and 12 k rpm_c for 47°, 102°, and 130° emission angles. There are several spectral differences between the two rotors at 10 k rpm_c (Figs. 32 to 34). The fundamental bypass interaction tone is consistently higher for the aft-swept rotor as might be expected with the somewhat closer rotor-stator axial spacing toward the tip region. However, the bypass 2BPF tone is much stronger for the baseline M4 rotor. Additionally, broadband levels for the aft-swept rotor are as much as 6 dB higher than those for the baseline rotor.

Fundamental bypass interaction tone levels continue to be higher for the aft-swept rotor at 12 k rpm_c (Figs. 35 to 37), especially at further aft sideline angles. Again, broadband noise levels are higher for the aft-swept rotor. There is some indication that MPT generation may be slightly less for the aft-swept rotor, although the difference is insignificant.

Figures 38 and 39 present 1/3rd octave directivities for the unswept and aft-swept metal rotors. At 10 k rpm_c (Fig. 38) broadband levels are consistently higher for the aft-swept rotor throughout the sideline survey. The directivities at 4 kHz (Fig. 38(d)), which contain the bypass BPF tone, are significantly higher for the aft-swept rotor compared to the other frequency bands shown, suggesting increased rotor-stator wake interaction for this rotor (or possibly rotor-alone BPF tone as a consequence of transonic flow over the rotor). The directivities at 8 kHz (Fig. 38(f)), which contain the bypass 2BPF and core BPF tones are also somewhat higher for the aft-swept rotor. However, it is likely that the higher broadband levels for the aft-swept rotor largely control these levels.

The directivities at 12 k rpm_c (Fig. 39) tell a different story, suggesting that there may be a measurable reduction in MPT noise for the aft-swept rotor. As seen in the constant bandwidth spectra of Figures 35 to 37, both rotors generate significant MPTs at this rotor speed with somewhat higher broadband levels associated with the aft-swept rotor. At 2 kHz (Fig. 39(a)), the directivities for both rotors are essentially similar, if slightly higher for the unswept rotor. Directivity levels continue to be lower for the aft-swept rotor at 2.5 and 3.15 kHz. However a tendency for higher noise for the aft-swept rotor at downstream angles begins to be seen at 3.15 kHz and above. This is especially evident for the bypass BPF tone at 5 kHz, which is much stronger for the aft-swept rotor than for the unswept rotor. Increased tone noise for the aft-swept rotor is consistent with the idea that decreased blade-vane tip spacing should show increased rotor-stator interaction noise.

The EPNL for the unswept M4 and modified aft-swept metal rotors with the "new" acoustic treatment (NTN) are in good agreement at subsonic and supersonic tip speeds (Fig. 40). The modified aft-swept rotor is about 2 EPNdB noisier than the baseline rotor in the transonic tip speed region.

The constant bandwidth spectral comparisons for the two rotors are shown in Figures 41 to 46. The bypass stage interaction tones are typically higher for the baseline rotor at 10 k rpm_c. Relative BPF and 2BPF tone levels vary with sideline angles (Figs. 41 to 43). However, at 12 k rpm_c (Figs. 44 to 46) the fundamental bypass interaction tone is typically higher for the modified aft-swept rotor. The modified aft-swept rotor was consistently effective in reducing MPT generation at 12 k rpm_c.

Figure 47 presents $1/3^{rd}$ octave directivities for the unswept and modified aft-swept rotors with bypass duct acoustic treatment at 10 k rpm_c. These results are again similar to the hardwall results of Figure 38, showing somewhat higher noise levels for the modified aft-swept rotor, especially in the aft part for the directivities at 4 kHz (Fig. 47(d)) which contain the bypass BPF tone.

Figure 48 presents the corresponding $1/3^{rd}$ octave directivities at 12 k rpm_c. There is clear evidence that MPT generation for the modified aft-swept rotor is significantly less than for the unswept rotor at frequencies below bypass BPF at upstream sideline angles. However, the bypass BPF tone is higher for the modified aft-swept rotor at further downstream sideline angles, consistent with increased rotor-stator interaction for the aft-swept rotor.

The aft-swept rotor was expected to show reduced MPT generation, but with possibly increased rotor-stator interaction tones due to reduced blade row spacing (especially near the tip region). These results showed that the modified aft-swept rotor did a better job of reducing MPTs than did the original aft-swept design, although this observation is somewhat qualified in that the original aft-swept rotor was tested with a hard bypass duct (HTH) while the modified aft-swept rotor was tested with a treated duct (NTN). In particular, the modified aft-swept rotor showed significantly less MPT generation in the region of transonic tip speed. However, the fundamental rotor-stator interaction tone, in particular, was higher for the aft-swept rotors. In addition, there is evidence of higher broadband levels associated with the aft-swept design, especially at subsonic tip speeds.

Effect of Rotor Forward Sweep

In concept, rotor forward sweep could combine the MPT reductions associated with aft sweep while further increasing the blade row spacing in the tip region with resultant reductions in rotor-stator tone noise levels. Mechanically, forward sweep imposes additional blade stress considerations, which could include a tendency to "untwist" under aerodynamic loading. Test results were obtained with the unswept and forward-swept composite rotors in both the hard-wall (HTH) and "new" acoustic treatment (NTN) configurations. Results for the hardwall bypass duct are shown in Figures 49 to 57, while corresponding results with the new bypass duct acoustic treatment are shown in Figures 58 to 66.

Figure 49 compares EPNLs for the unswept and forward-swept composite rotors (Fig. 2) for the hardwall bypass duct. Noise levels are essentially the same for both rotors. Figure 50 compares constant bandwidth spectra at the 47° emission angle and 10 k rpm_c for the two rotors. The spectra are mostly similar, showing the previously seen "haystack" at 2 kHz, which was previously shown for composite

rotor noise (Fig. 14). The bypass 2BPF tone is significantly higher for the forward-swept rotor at this sideline angle. Spectra at 102° and 130° sideline emission angles (Figs. 51 and 52) do not show the "haystack" region; however, the bypass BPF and 2BPF tones are both higher for the forward-swept rotor.

There is little difference in the MPT generation for the two rotors at 12 k rpm_c at 47° and 130° sideline angles, with some decrease in MPT generation for the forward-swept rotor at 102° sideline angle (Figs. 53 to 55). The bypass rotor-stator interaction tones (BPF and 2BPF) continue to be somewhat stronger for the forward-swept rotor.

Figure 56 shows 1/3rd octave directivities at 10 k rpm_c. There is an indication of reduced broadband noise level associated with the forward-swept rotor (in contrast to the aft-swept rotor results of Figure 38 in which the broadband noise for the aft-swept rotor was greater than that for the unswept rotor). There is essentially no difference in blade row interaction tone levels at 4 and 8 kHz (Figs. 56(d) and (f)).

The 1/3rd octave directivity results at 12 k rpm_c (Fig. 57) show little difference in the broadband levels for the two rotors at 2 and 2.5 kHz. (there is significant MPT content at this speed). There is an indication of reduced broadband level for the forward-swept rotor at 3.15 k and especially 4 kHz. The stronger bypass BPF tone for the forward-swept rotor, noted in the spectra of Figure 55, is evident in the directivities at 5 kHz (Fig. 57(e)) which include the bypass BPF tone.

The comparison of forward-swept and unswept composite rotors (with the hard-wall duct configuration) showed mixed relative benefits for the two rotor designs. There was little evidence that MPT generation was significantly reduced with the forward-swept rotor, although that was the main expected benefit of the forward-swept design. Surprisingly, broadband levels were sometimes lower for the forward-swept rotor. Somewhat higher bypass interaction tone levels for the forward-swept rotor suggest that downstream wakes from this rotor were somewhat higher despite the increased rotor tip-stator axial spacing.

Figures 58 to 66 show the corresponding comparisons between the unswept and forward-swept composite rotors with the "new" bypass duct acoustic treatment (NTN). EPNL is essentially the same for the two rotors throughout the range of test speeds (Fig. 58). Representative constant bandwidth spectra at 10 k and 12 k rpm_c for the two rotors are shown in Figures 59 to 64. The forward-swept composite rotor again shows higher bypass BPF tone levels at aft angles. MPT generation is about the same for the two rotors at 12 k rpm_c.

There is little difference in the 1/3rd octave directivity levels for the two rotors at 10 k rpm_c (Fig. 65), although broadband levels are slightly lower for the forward-swept composite rotor at downstream sideline angles at 3.15 k and 5 kHz (Figs. 65(c) and (e)). The 1/3rd octave directivities at 12 k rpm_c (Fig. 66) are essentially the same for the two rotors. There is a small increase in the bypass BPF tone level for the forward-swept rotor at 5 kHz, but Figure 66(e) shows the apparent effect of absorption by the acoustic liner (compare with Fig. 57(e)).

The acoustic results for the forward-swept and unswept composite rotor with bypass duct acoustic treatment suggest that forward sweep may slightly reduce broadband levels at some fan speeds and frequencies. Expected reductions in MPT noise with forward sweep relative to unswept were not observed. The bypass BPF tone level tended to increase, rather than decrease with forward sweep, indicating an increase in the forward-swept rotor wake.

Fan Axis Angle of Attack

The UPS fan was tested at fan axis angles-of-attack (AOA) of 0°, 3°, and 9°. Figures 67 to 69 show EPNL levels for these AOAs as a function of rotor tip speed for the baseline M4 metal rotor with hard-wall bypass duct and two types of bypass inlet and exhaust wall treatment. The EPNL levels typically increase with AOA.

Figures 70 to 72 show representative constant bandwidth (6 Hz) spectra for these three configurations for 0°, 3°, and 9° AOA at 12 k rpm_c. The spectra of Figure 70 are for the hard-wall, HTH, configuration. MPT generation is significant at this transonic fan speed. There is a significant decrease in MPT activity as

the AOA is increased from 0° to 9°. Data were not taken at 3° AOA for this configuration and speed. Similar results are seen for the M4 rotor with wall treatment in Figures 71 and 72.

Figures 73 to 78 show 1/3rd octave directivities taken with the translating sideline microphone for these three M4 rotor configurations. Figure 73 shows directivities for 8 kHz (broadband) noise at 8200 rpm_c. The broadband levels are particularly high for 9° AOA toward the aft (typically peak noise) angles. There is a small decrease in noise levels for the TTT configuration at 3° AOA that is not observed for the HTH or NTN configurations. Noise levels at upstream angles are seen to decrease slightly with AOA for the TTT and NTN configurations.

Figure 74 shows directivity changes with AOA for the 3BPF bypass interaction tone with the fan operating at 8200 rpm_c. Noise levels are again seen to increase with AOA at aft angles, with some decrease in the upstream levels with increasing AOA.

The UPS fan shows maximum MPT generation near 12 k rpm_c Figure 75 shows 1/3rd octave directivities for the three M4 rotor configurations at 2 kHz. These results illustrate the reduction in MPT generation that was seen in the previously discussed constant bandwidth spectra. In particular, there is a significant reduction in noise level with increasing AOA for the hard-wall configuration. Earlier results presented in this paper (Fig. 11) suggested that the initial duct wall treatment (TTT) was somewhat more effective than was the redesigned (NTN) treatment. It was also shown that duct wall treatment can significantly reduce MPT levels. This observation is further confirmed in Figure 76 where changes in MPT generation with AOA are essentially not seen for the TTT configuration, since these tones are effectively removed by the duct wall treatment. Such was not the case for the NTN treatment, which still showed reductions in MPT levels with increasing AOA.

Finally, Figure 77 shows 1/3rd octave directivities at 12 k rpm_c and 8 kHz, which contains the bypass 2BPF tone. There is still significant MPT content at this frequency (see Figs. 70 to 72) and the results are somewhat similar to those of the two preceding figures, showing a level reduction with increasing AOA. However, this effect is also seen for the TTT configuration, possibly due to the presence of the bypass 2BPF tone which was not as easily absorbed by the duct wall treatment.

There has been some question as to the origin of the "periodic" nature of the bypass tone directivity as illustrated in the preceding directivity plots. An initial concern was that the treated walls of the 9×15 LSWT were, in fact, reflecting some noise, resulting in a cancellation pattern. Directivity results for the UPS fan tested in the German-Dutch Wind Tunnel (DNW) likewise showed this periodic nature (Ref. 1). Tests were made with the same UPS configuration using the same microphone assembly and holder as was used for the NASA 9×15 LSWT tests and data were taken at a 224 cm (88 in.) sideline within a $M_0 = 0.20$ airflow. However, as a free jet facility, the DNW did not introduce the possibility of acoustically reflecting tunnel walls. These DNW directivity results show that the likely source of the "periodic" noise levels is acoustic interaction (periodic reinforcement and cancellation) between fan noise at a particular frequency radiating from the fan inlet and exhaust. Reference 10 is a theoretical study of model fan noise radiating from separate inlet and exhaust sources. Tone directivity results in this reference likewise show this periodic nature.

Concluding Remarks

The Universal Propulsion Simulator (UPS) fan was designed and built by General Electric Aircraft Engines to explore advanced fan stage concepts for future quiet turbofan engines. The fan stage was tested in the NASA Glenn 9×15 LSWT using several rotor designs. These acoustic tests explored the fan performance with unswept, forward-swept, and aft-swept rotors of both metal and composite construction. The fan stage was tested with, and without acoustic treatment on the outer wall of the bypass flow duct. Acoustic testing was performed within a $M_0 = 0.20$ tunnel flow, which is representative of aircraft takeoff and approach conditions.

Noise levels were compared for the various rotors and bypass duct treatments. These comparisons showed that there was a significant noise increase associated with the composite rotors relative to that for metal rotors. This noise increase appears to be largely due to increases in broadband noise for the composite rotors (although a modest reduction in broadband noise was sometimes observed for the composite forward-swept rotor). There was a significant spectral "haystack" noise region associated with the composite rotors at upstream sideline locations. Aerodynamic performance of the various rotors was essentially similar.

The use of aft or forward rotor sweep could somewhat reduce multiple pure tone (MPT) generation for transonic rotational speeds. However, aft rotor sweep introduces the potential for increased rotor-stator interaction noise due to reduced blade-vane spacing. Acoustic results for two aft-swept metal rotor designs were compared with those for the baseline, unswept metal rotor. While MPT generation was reduced for the aft-swept rotors, there was also an increase in the bypass stage BPF tone associated with the reduced blade-vane spacing. Also, there was evidence of higher broadband levels associated with the aft-swept rotors. Consequently, overall EPNL were similar for the aft-swept and unswept rotors.

The effect of rotor forward sweep was explored with composite forward-swept and unswept rotor designs. These comparisons suggest that there may be a slight reduction in broadband noise level associated with forward sweep. However, the bypass BPF tone was higher for the forward-swept rotor, indicating that the wake from the forward-swept rotor is more severe than that for the unswept rotor. EPNL comparisons for the forward-swept and upswept rotor were essentially the same for both configurations.

The UPS fan was tested at three fan axis angles-of-attack in the NASA 9×15 LSWT. The fan was shown to exhibit reduced MPT generation with increased AOA, although overall effective perceived noise levels typically increased with AOA. Additionally, EPNL values were typically higher for bypass rotors of composite material compared to the metal rotors. This may be due to increased flexure of the composite rotors changing their acoustic (but apparently not gross aerodynamic) properties under load.

References

1. Woodward, R.P., and Hughes, C.E., "Acoustic Performance of Several GEAE UPS Research Fans in Three Test Facilities," Pending NASA TM.
2. Gliebe, P.R., Ho, P.Y., and Mickol, J.D., "Low-Speed Wind Tunnel (LSWT)/Universal Propulsion Simulator (UPS) Acoustic Calibration," GEAE Technical Memorandum 96-166, August, 1996.
3. Tyler, J.M., and Sofrin, T.G., "Axial Flow Compressor Noise Studies," Society of Automotive Engineers Transactions, Vol. 70, 1962, pp. 309-332.
4. Rice, E.J., and Heidmann, M.F., "Modal Propagation Angles in a Cylindrical Duct with Flow and their Relation to Sound Radiation," AIAA-79-0183, January, 1979.
5. Balan, C., and Hoff, G.E., "Propulsion Simulator for High Bypass Turbofan Performance Evaluation," SAE Paper 931410, Jan. 1993.
6. Dahl, Milo D., and Woodward, Richard P., "Comparison Between Design and Installed Acoustic Characteristics of the NASA Glenn 9- by 15-Foot Low-Speed Wind Tunnel Acoustic Treatment," NASA TP-2996, April, 1990.
7. Dahl, Milo D., and Woodward, Richard P., "Acoustical Evaluation of the NASA Glenn 9- by 15-Foot Low-Speed Wind Tunnel," NASA TP-3274, November, 1992.
8. Woodward, Richard P., Dittmar, James H., Hall, David G., and Kee-Bowling, Bonnie, "Background Noise Levels Measured in the NASA Glenn 9- by 15-Foot Low-Speed Wind Tunnel, AIAA = 95-0720, NASA TM 106817, January, 1995.
9. Chestnutt, D., "Flight Effects of Fan Noise," NASA CP-2242, January, 1982.
10. Envia, Edmane, and Nallasamy, M., "Design Selection and Analysis of a Swept & Leaned Stator Concept," NASA TM-1998-208662, 1998.

TABLE 1.—UPS DESIGN PARAMETERS

Bypass Stage:	
Rotor blades	22
Stator vanes	54
Core (booster):	
Inlet guide vanes	90
Rotor blades	48
Outlet guide vanes	70
Deswirl vanes	50
Forward load struts	8
Full passage screen	1
Aft load struts	8
Rotor-stator axial spacing (mean rotor chords)	2.75
Bypass stage:	
Pressure ratio:	
M4 rotor	1.49
Composite rotors	1.53
Bypass ratio:	
M4 rotor	8.85
Composite rotors	8.24
Mass flow, kg/sec (lbm/sec):	
M4 rotor	46.3 (102.1)
Composite rotors	47.5 (104.7)
Rotor diameter, cm (in.)	55.9 (22.0)
Rotor tip speed, m/sec (ft/sec):	
M4 rotor	370 (1214)
Composite rotors	388 (1274)
Acoustic Rating Rotor Tip Speeds, m/sec (ft./sec)	
Approach	216 (710)
Cutback	293 (960)
Sideline	351 (1152)

TABLE 2.—ACOUSTIC TEST SPEEDS
[Nominal Values.]

Corrected, rpm	Point of interest	Corrected tip speed m/sec (ft/sec)	Tip Mach (Tangential)
[a]1330	Windmill	38.9 (127.7)	0.11
7400	Low approach	216.5 (710.3)	0.63
8200	High approach	239.9 (787.1)	0.70
10000	Low cutback	292.6 (959.9)	0.85
11000	High cutback	321.8 (1055.9)	0.94
12000	MPT peak	351.1 (1151.9)	1.02
13000	Low takeoff	380.4 (1247.9)	1.11
13500	High takeoff	395.0 (1295.9)	1.15
14000	Overspeed	409.6 (1343.9)	1.19

[a]Windmill speed is approximate, depending on tunnel conditions

TABLE 3.—ACOUSTIC TEST CONFIGURATIONS IN THE NASA 9×15 LSWT

Blade design	Duct treatment		
	Inlet	Fan case	Exhaust
C-1, Baseline (M4, metal)	T (treated)	T	T
C-2, Baseline (M4, metal)	H (hard-wall)	T	H
C-3, Aft-Swept (metal)	H	T	H
C-4, Unswept (composite)	H	T	H
C-5, Forward-Swept (composite)	H	T	H
C-6, Forward-Swept (composite)	N (new treatment)	T	N
C-7, Unswept (composite)	N	T	N
C-7, Modified Aft-Swept (metal)	N	T	N
C-9, Baseline (M4, metal)	N	T	N
C-44(a), Advanced Unswept[a] (composite)	H	T	H
C- 44(b), Advanced Unswept[a,b] (composite)	H	T	H
C-45, Advanced Unswept[a,b] (composite)	N	T	H
C-45(a), Advanced Unswept[a,b] (composite)	T	T	H

[a]Lube oil scavenge line in bypass aft duct
[b]Taped spinner to eliminate extraneous tones

TABLE 4.—NOMINAL BLADE PASSING FREQUENCY (BPF) TONES AS A FUNCTION OF FAN SPEED

Nominal, rpm		Bypass tones, Hz					Core tones, Hz	
Corrected speed	Actual speed	BPF	2BPF	3BPF	4BPF	5BPF	BPF_C	$2BPF_C$
7400	7500	2750	5500	8250	11000	13750	6000	12000
8200	8300	3043	6087	9130	12173	15217	6640	13280
10000	10220	3747	7495	11242	14989	18737	8176	16352
11000	11150	4088	8177	12265	16353	20442	8920	17840
12000	12275	4501	9002	13503	18003	22504	9820	19640
13000	13300	4877	9753	14630	19507	24383	10640	21280
13500	13800	5060	10120	15180	20240	25300	11040	22080

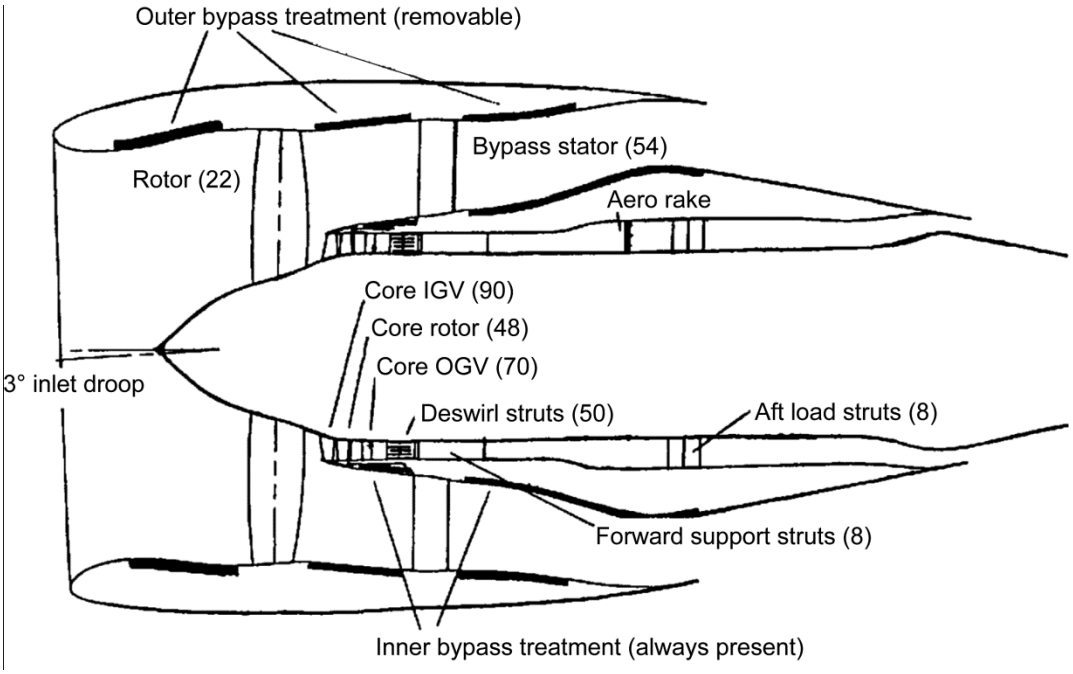

Figure 1.—Cross-sectional view of the UPS fan stage.

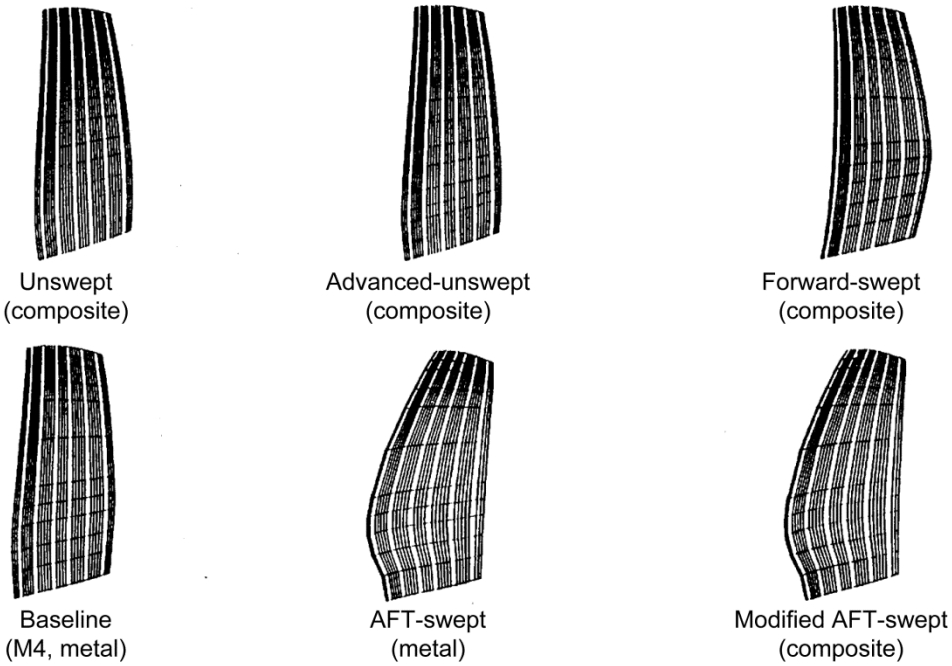

Figure 2.—UPS rotors tested in the NASA Glenn 9×15 LSWT.

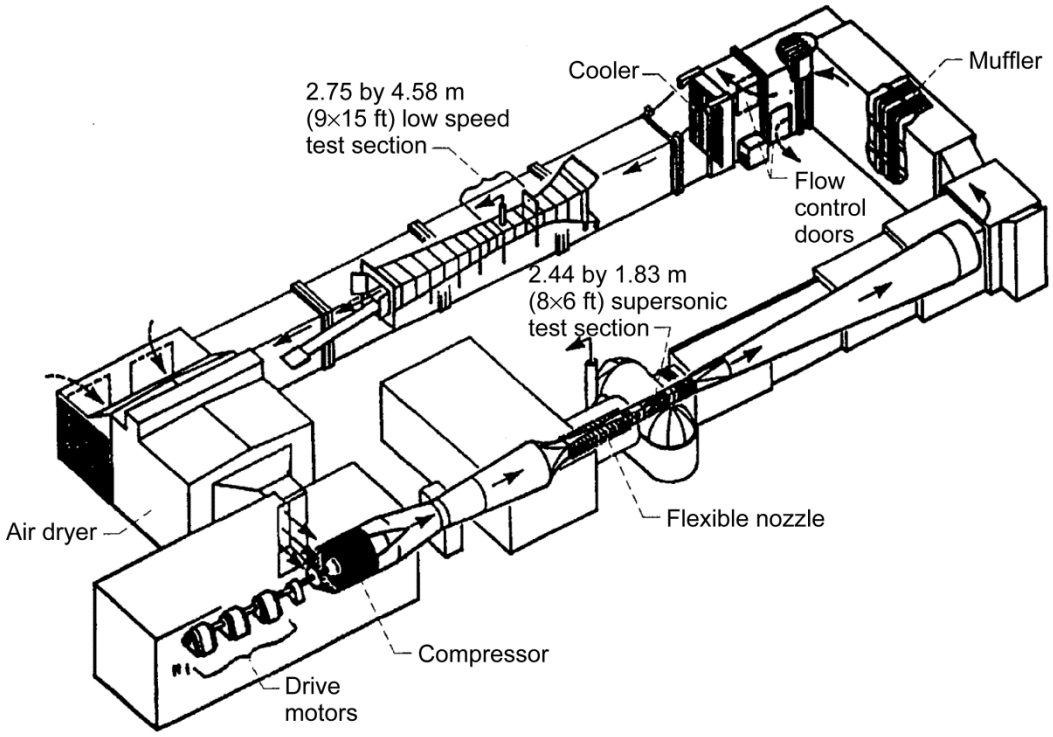

Figure 3.—NASA Glenn 9×15 low-speed anechoic wind tunnel.

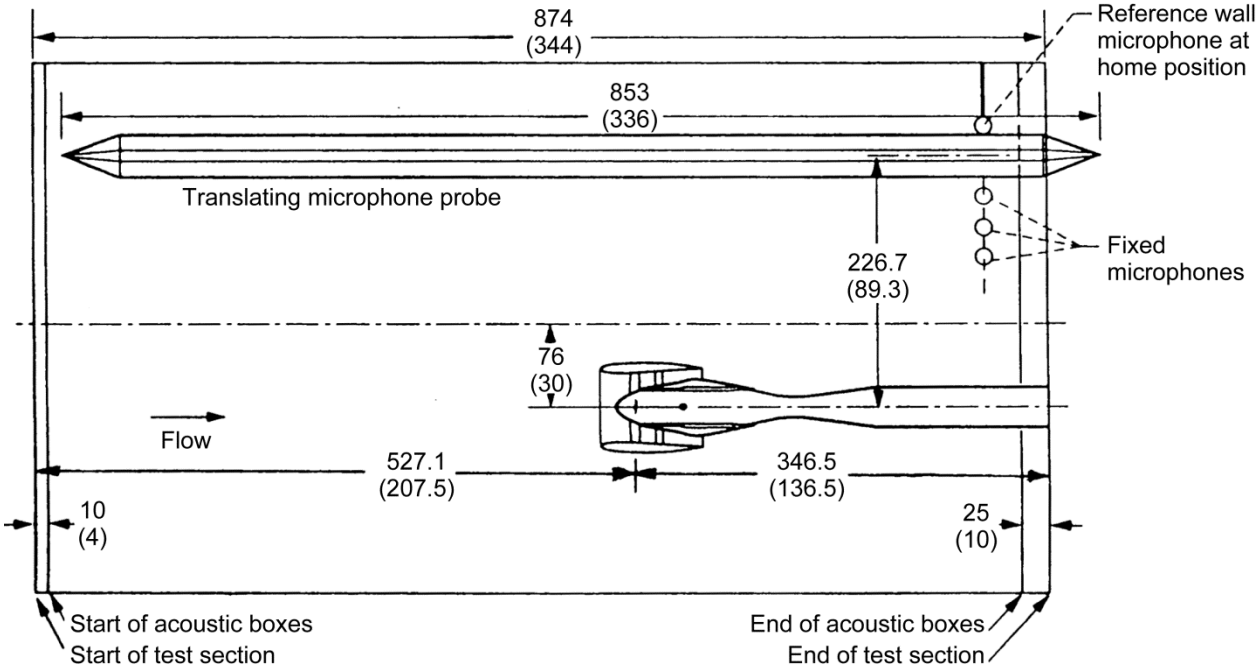

Figure 4.—Sketch of the UPS model installed in the NASA Glenn 9×15 LSWT (dimensions are cm (in.)).

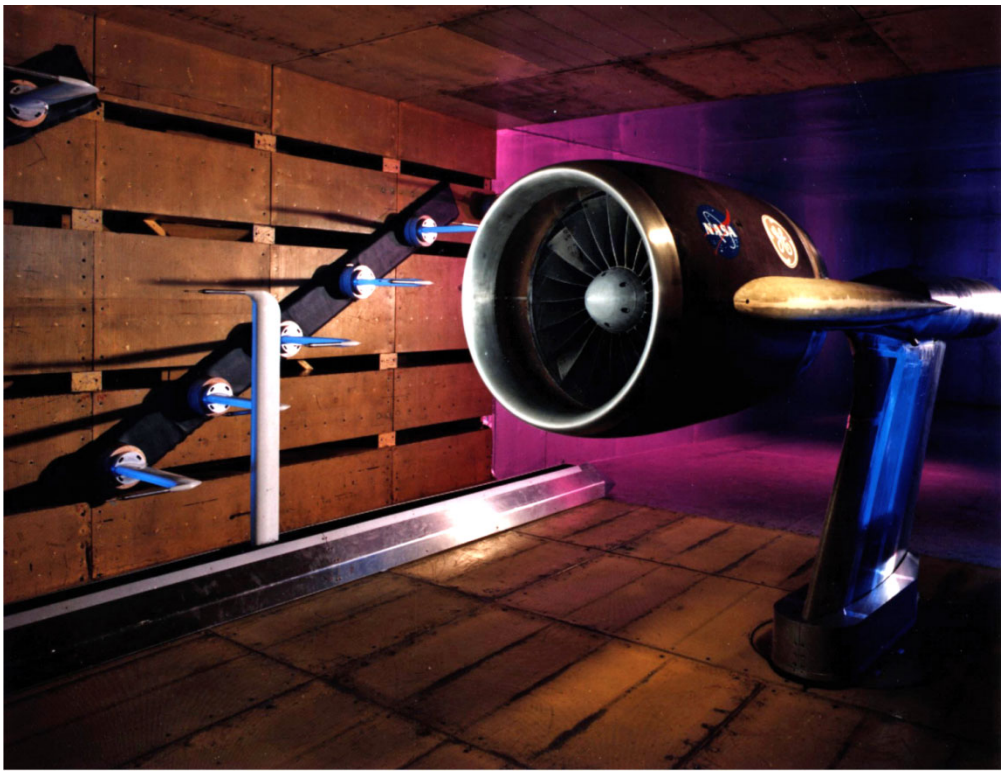

Figure 5.—Photograph of the UPS model installed in the NASA Glenn 9×15 LSWT.

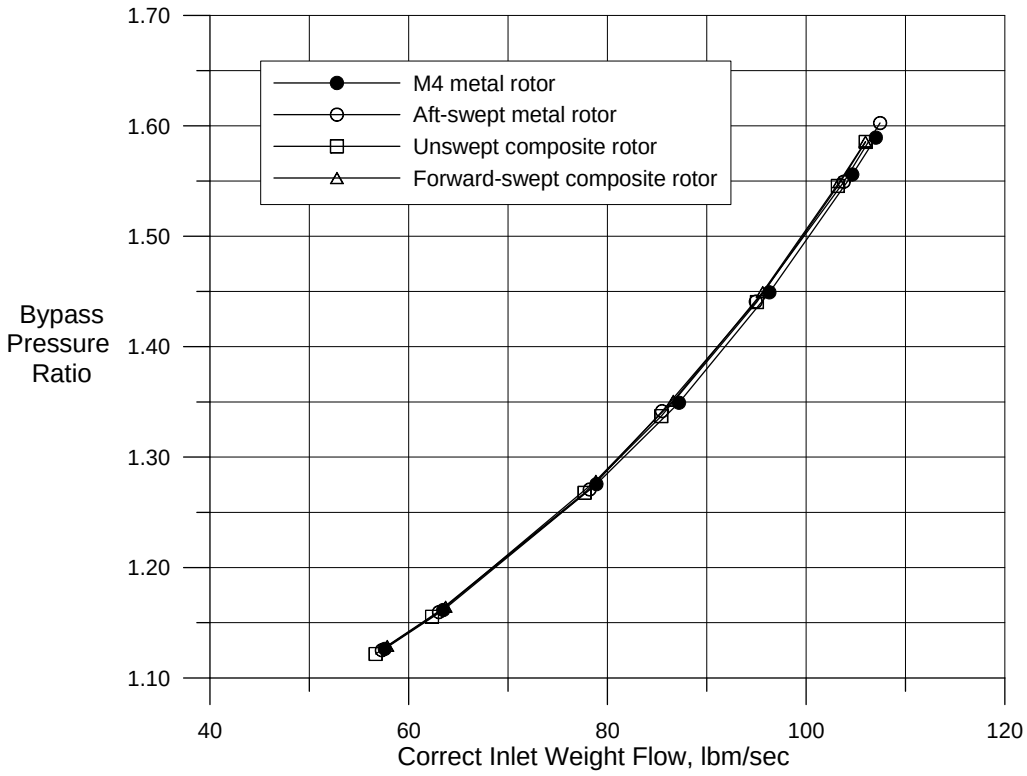

Figure 6.—Fan stage aerodynamic performance for the hard-wall flow duct configurations.

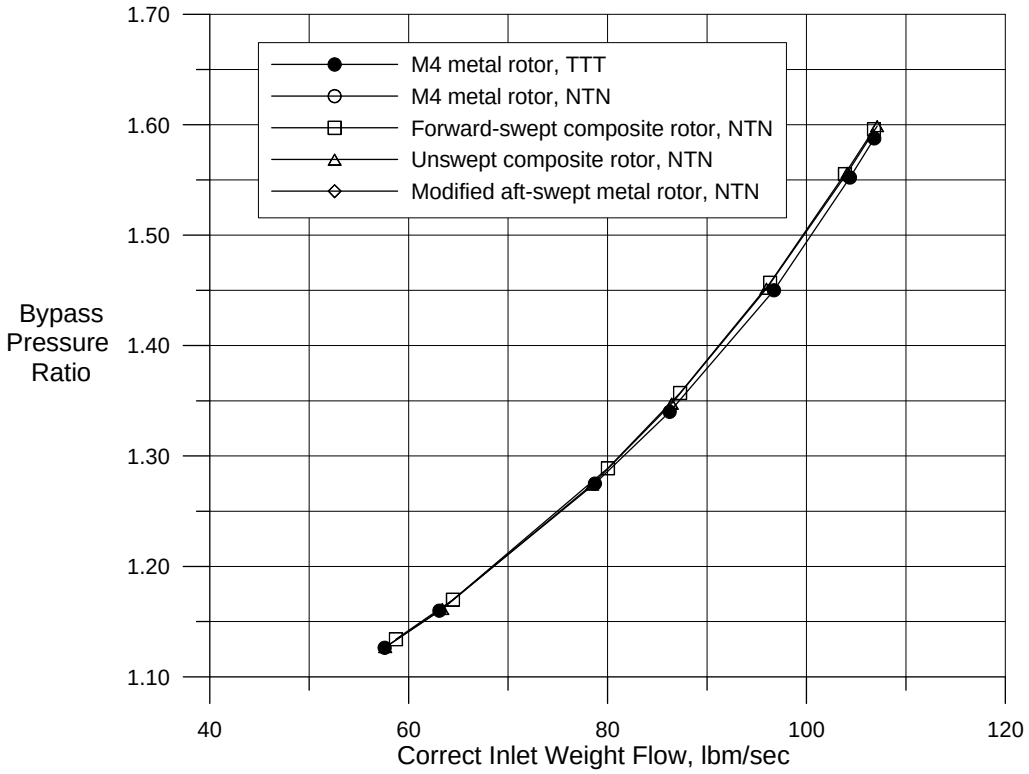

Figure 7.—Fan stage aerodynamic performance for the treated flow duct configurations.

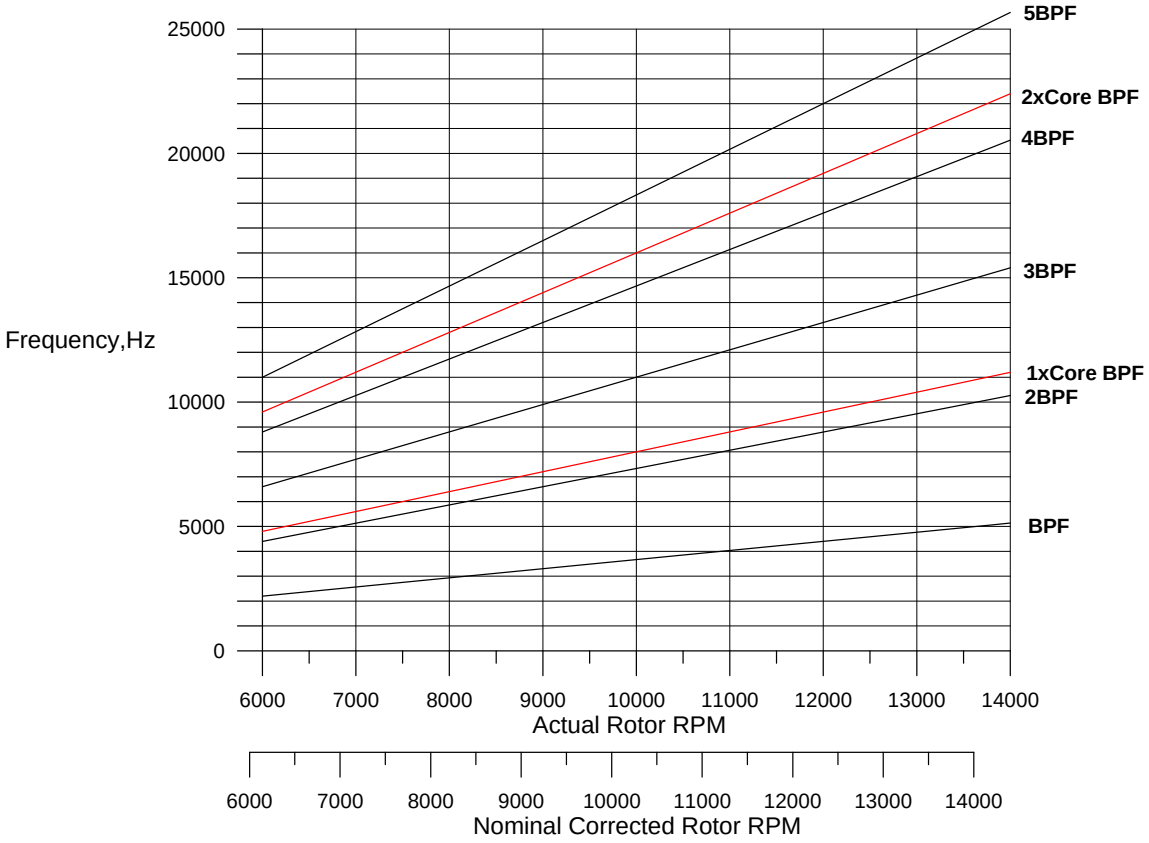

Figure 8.—UPS bypass and core tone frequencies as a function of rotor speed.

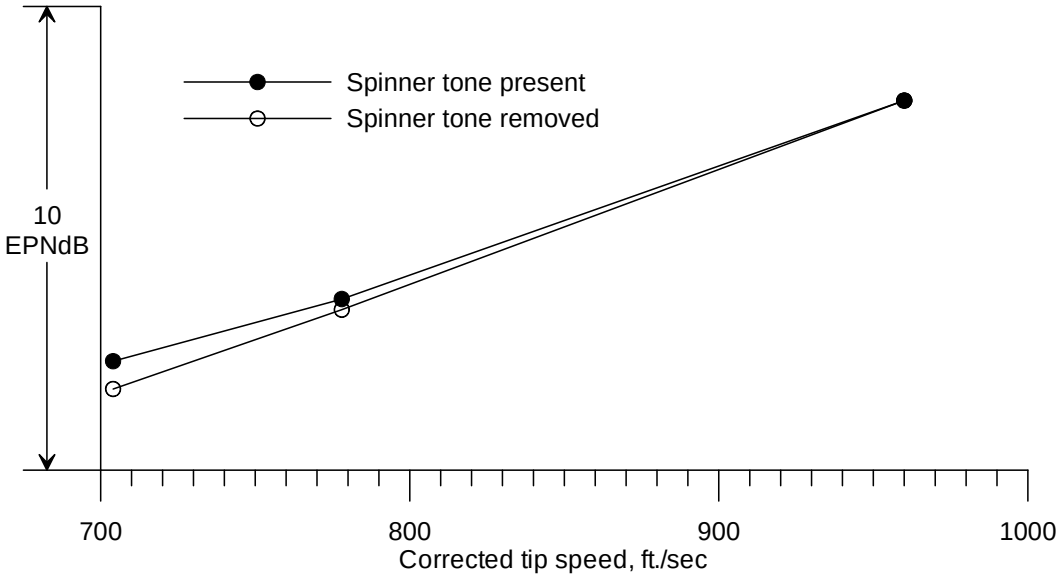

Figure 9.—Effect of electronically removing the “spinner tone” from the unswept composite rotor, HTH configuration (EPNL calculated from 9×15 LSWT sideline data, 0° AOA, 5.6 scale factor, 304.8-m (1000-ft) flyover).

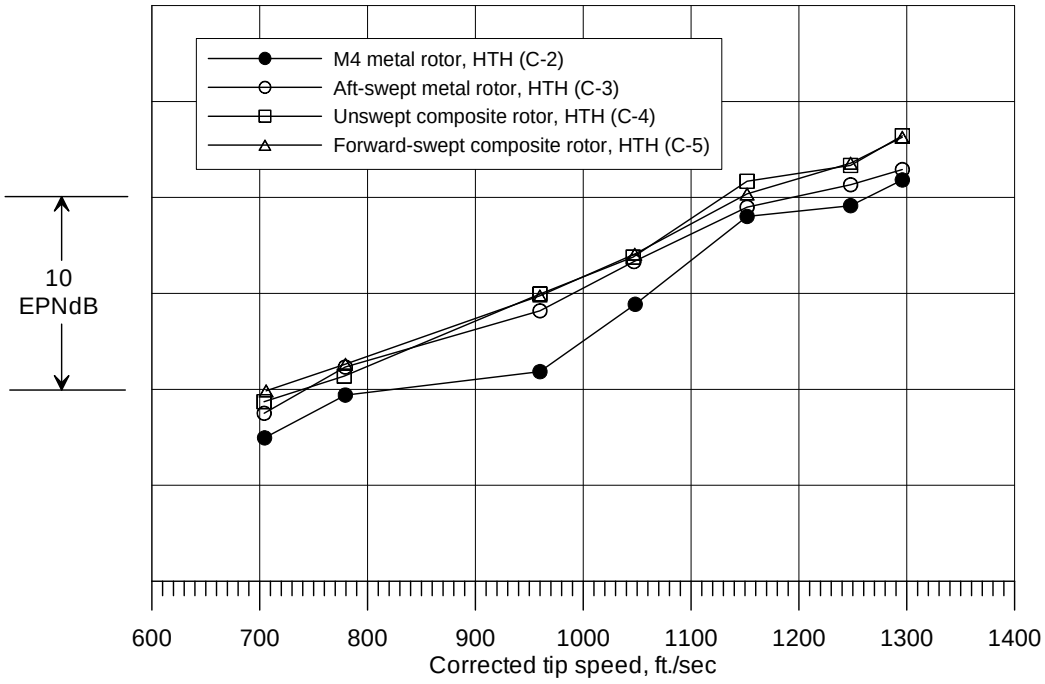

Figure 10.—Effect of rotor configuration with hardwall bypass duct. (EPNL calculated from 9×15 LSWT sideline data, 0° AOA, 5.6 scale factor, 304.8-m (1000-ft) flyover).

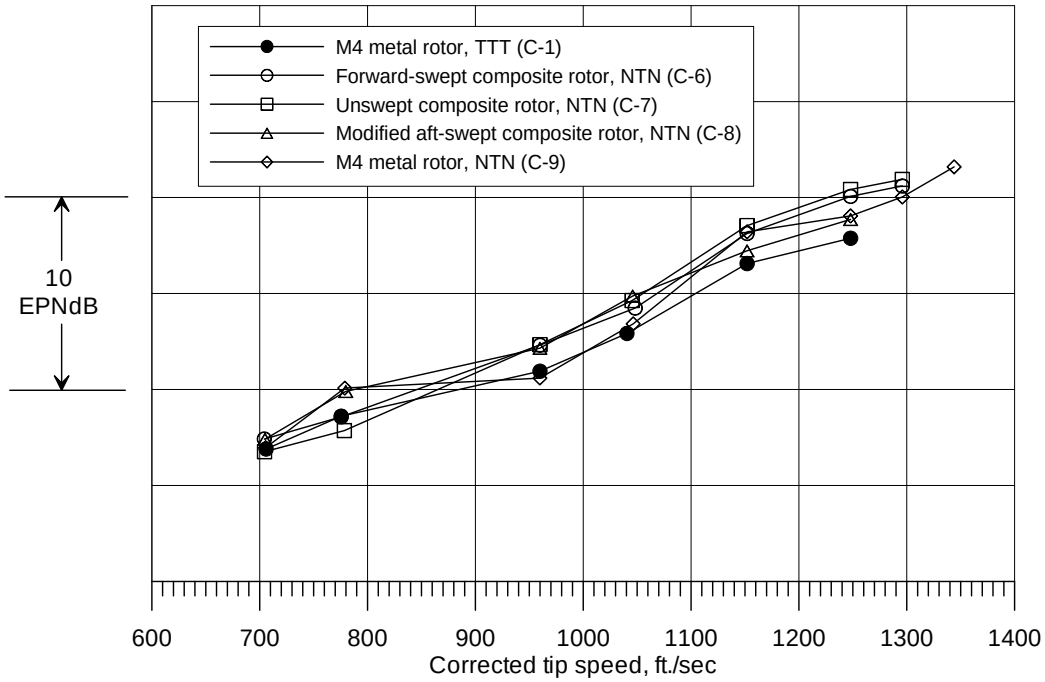

Figure 11.—Effect of rotor configuration with acoustically treated bypass duct. (EPNL calculated from 9×15 LSWT sideline data, 0° AOA, 5.6 scale factor, 304.8-m (1000-ft) flyover).

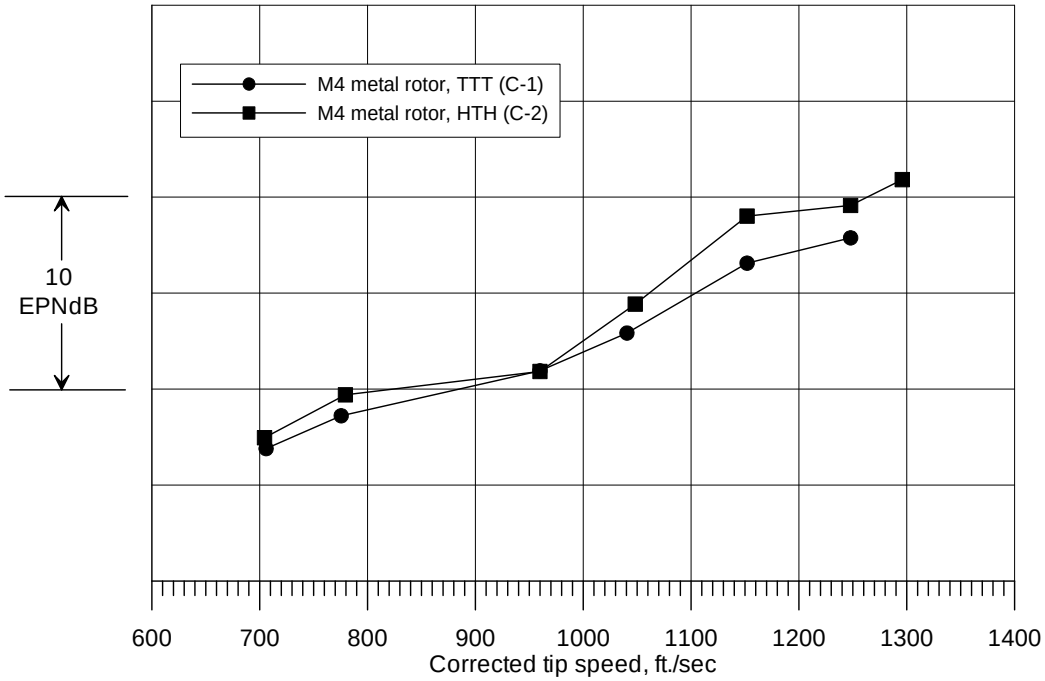

Figure 12.—Effect of rotor bypass duct acoustic treatment for the baseline M4 metal rotor. (EPNL calculated from 9×15 LSWT sideline data, 0° AOA, 5.6 scale factor, 304.8-m (1000-ft) flyover).

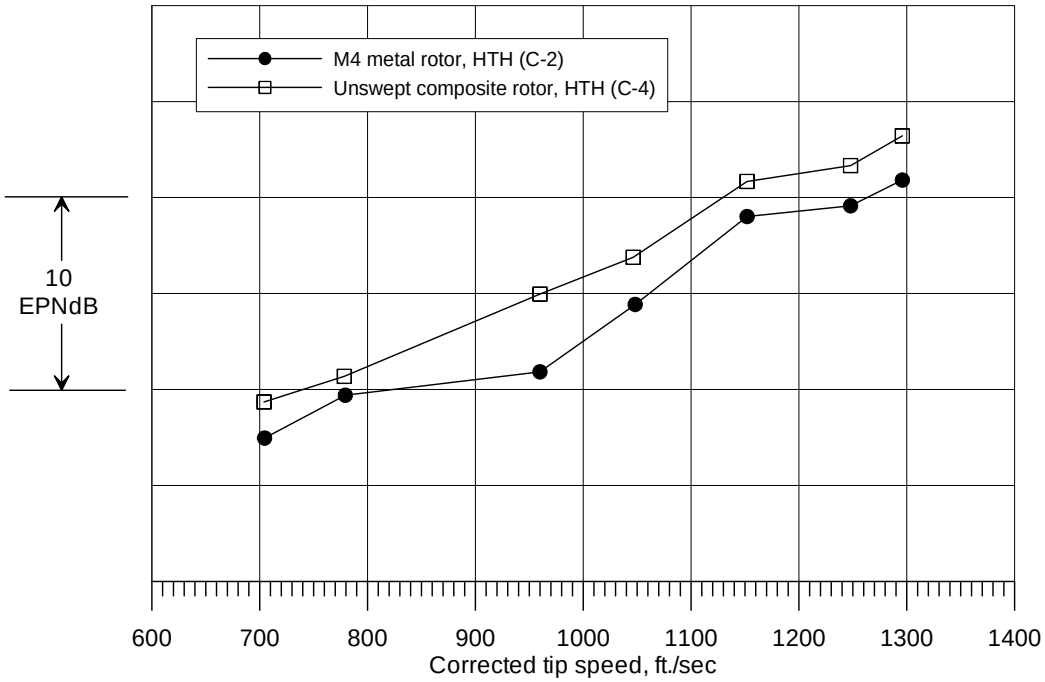

Figure 13.—Comparison of unswept metal M4 and composite rotors (HTH).

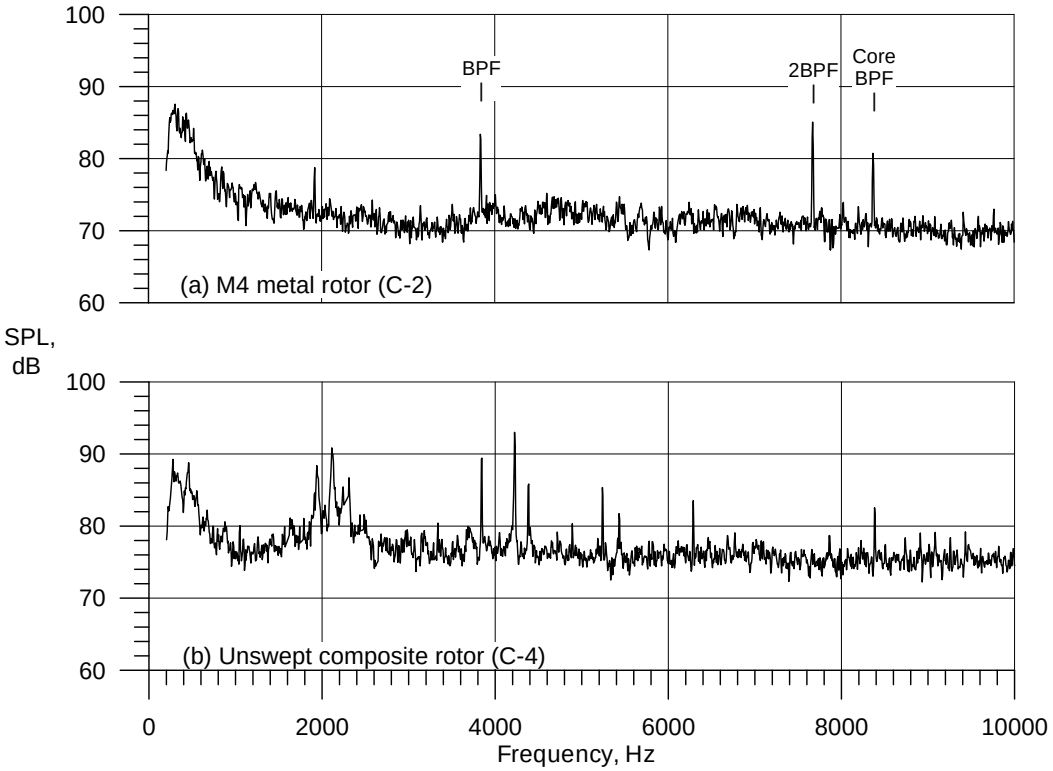

Figure 14.—Comparison of constant (6 Hz) bandwidth spectra for the unswept metal M4 and composite rotors at 10 k rpm_c (47° sideline emission angle, HTH).

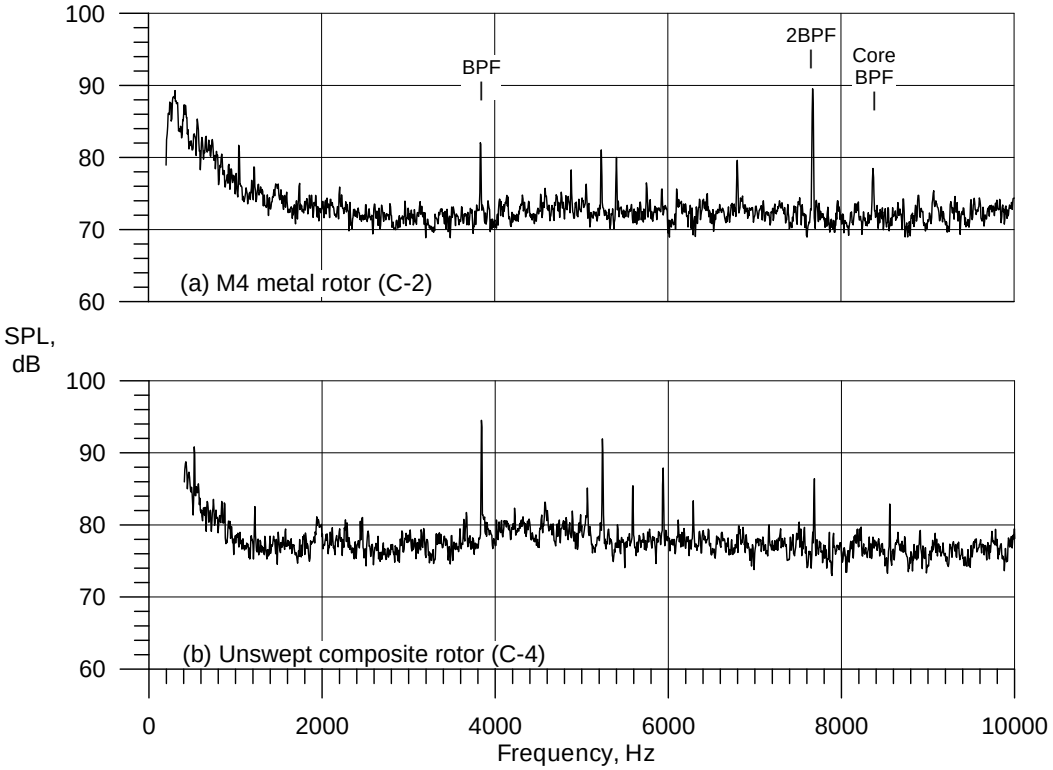

Figure 15.—Comparison of constant (6 Hz) bandwidth spectra for the unswept metal M4 and composite rotors at 10 k rpm_c (102° sideline emission angle, HTH).

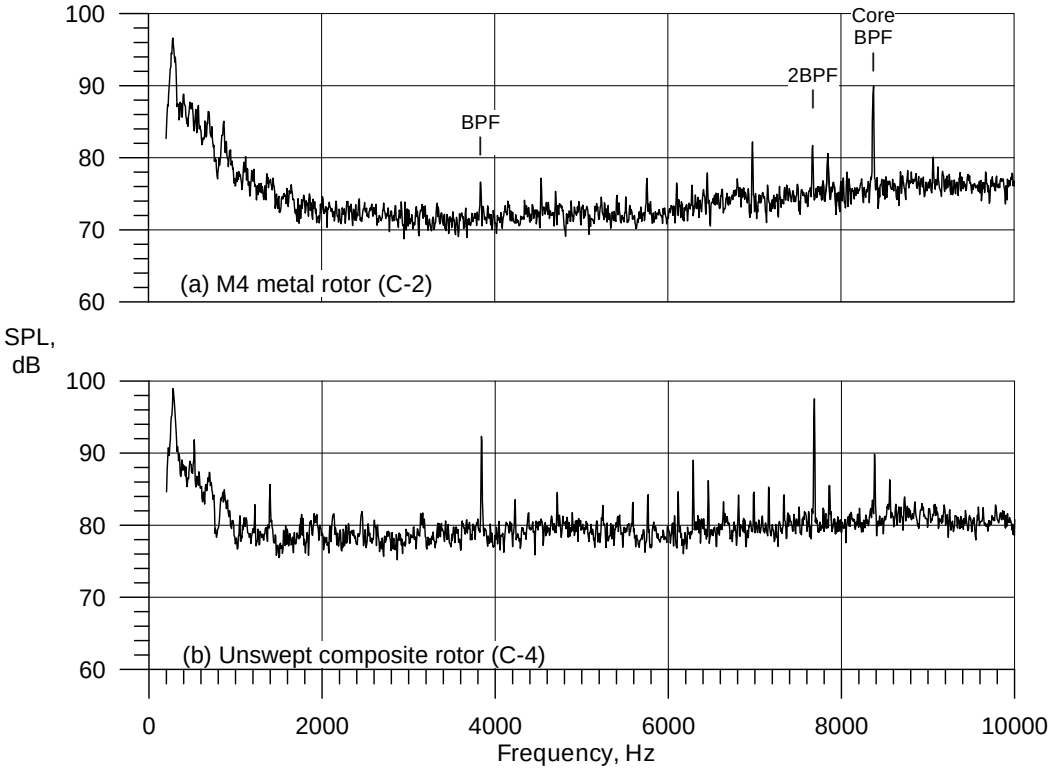

Figure 16.—Comparison of constant (6 Hz) bandwidth spectra for the unswept metal M4 and composite rotors at 10 k rpm_c (130° sideline emission angle, HTH).

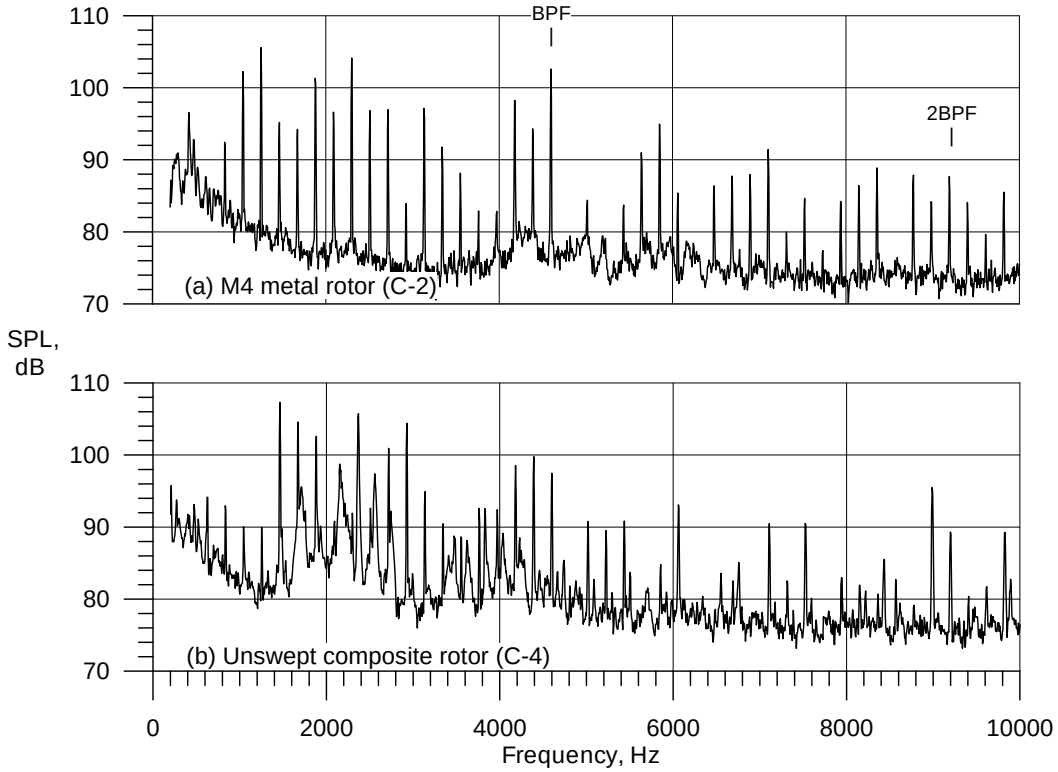

Figure 17.—Comparison of constant (6 Hz) bandwidth spectra for the unswept metal M4 and composite rotors at 12 k rpm_c (47° sideline emission angle, HTH).

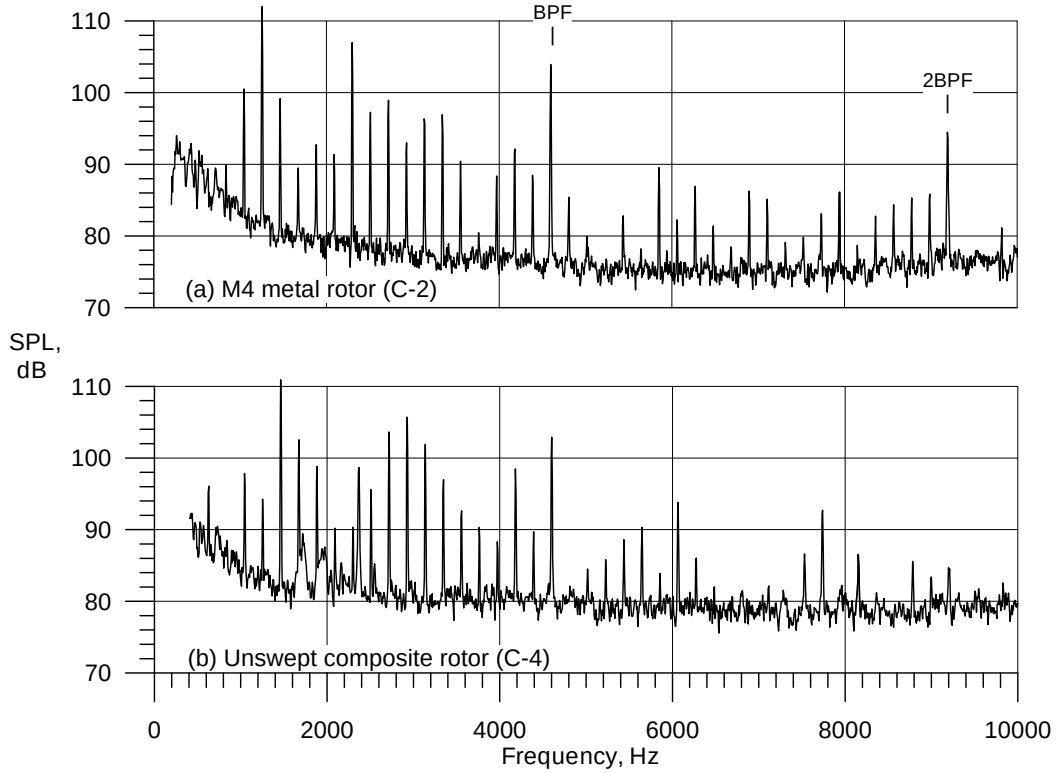

Figure 18.—Comparison of constant (6 Hz) bandwidth spectra for the unswept metal M4 and composite rotors at 12 k rpm_c (102° sideline emission angle, HTH).

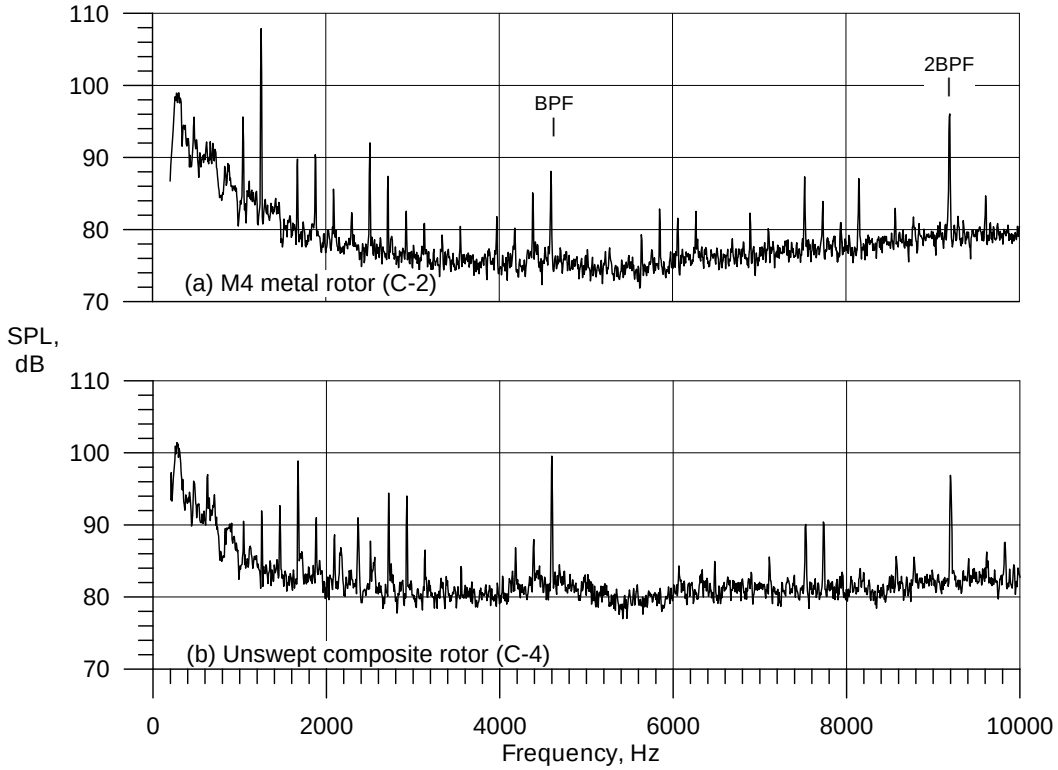

Figure 19.—Comparison of constant (6 Hz) bandwidth spectra for the unswept metal M4 and composite rotors at 12 k rpm_c (130° sideline emission angle, HTH).

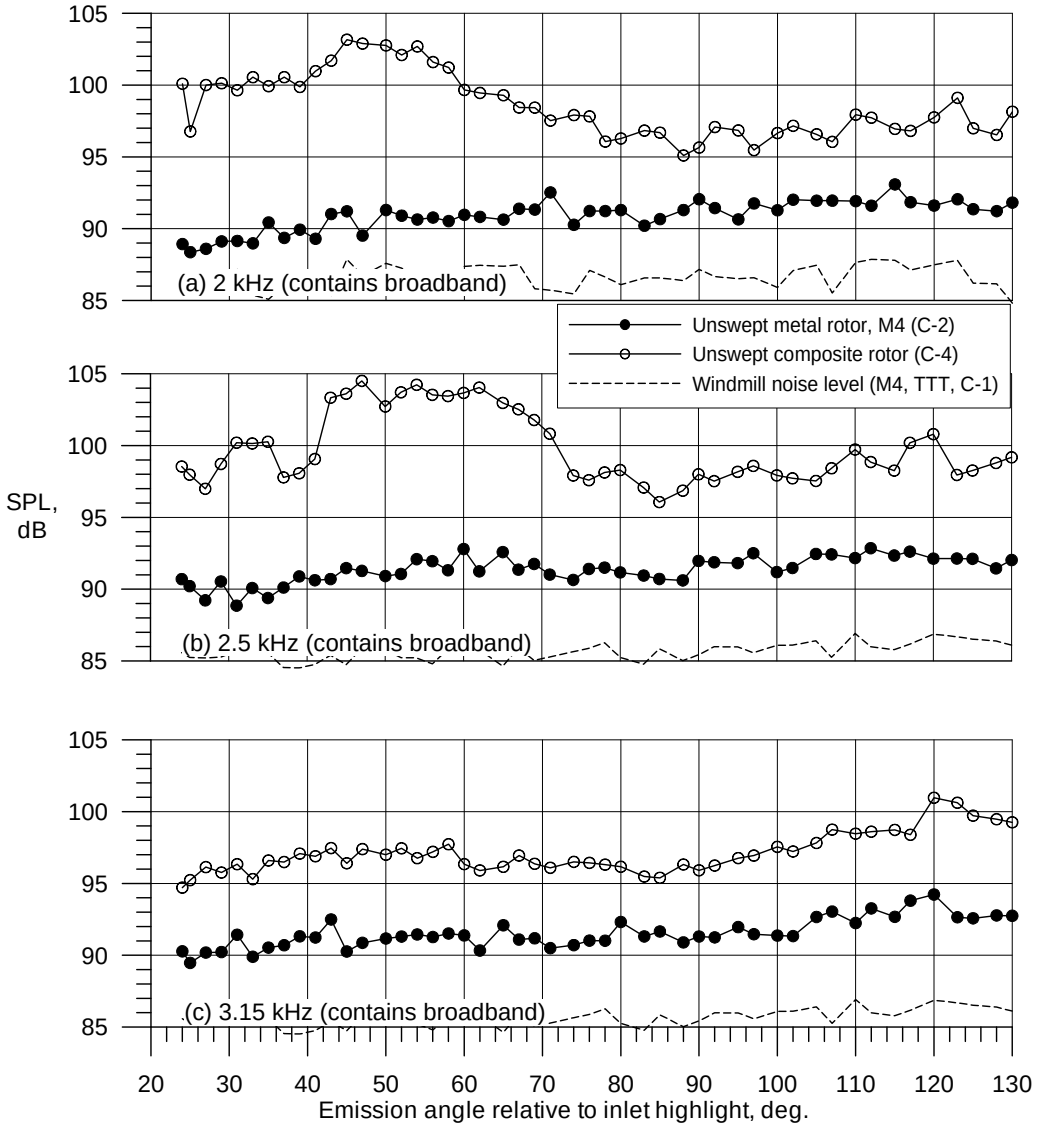

Figure 20.—Comparison of 1/3rd octave directivities for the M4 unswept metal and unswept composite rotors at 10 k rpm_c (HTH).

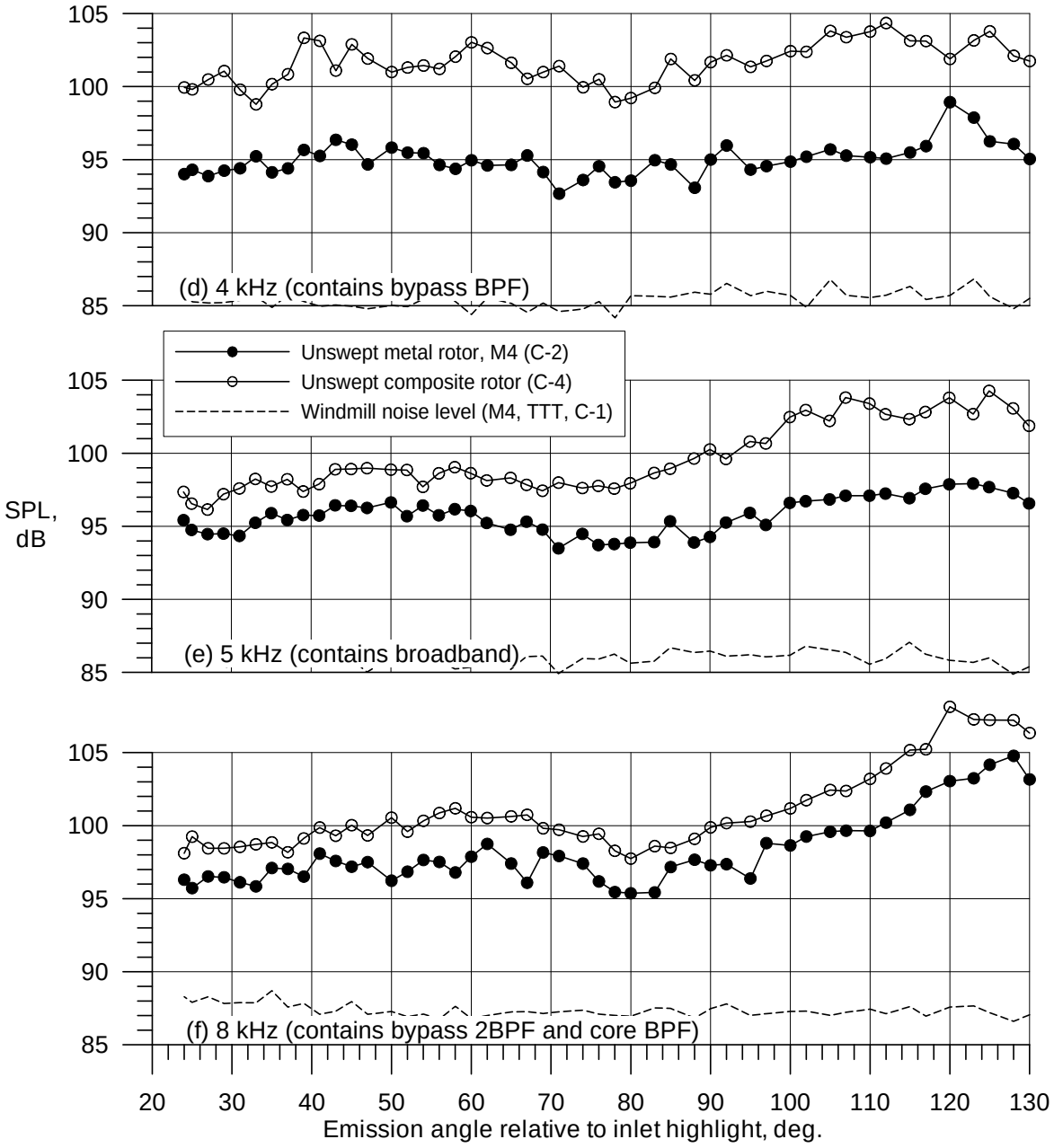

Figure 20.—Concluded.

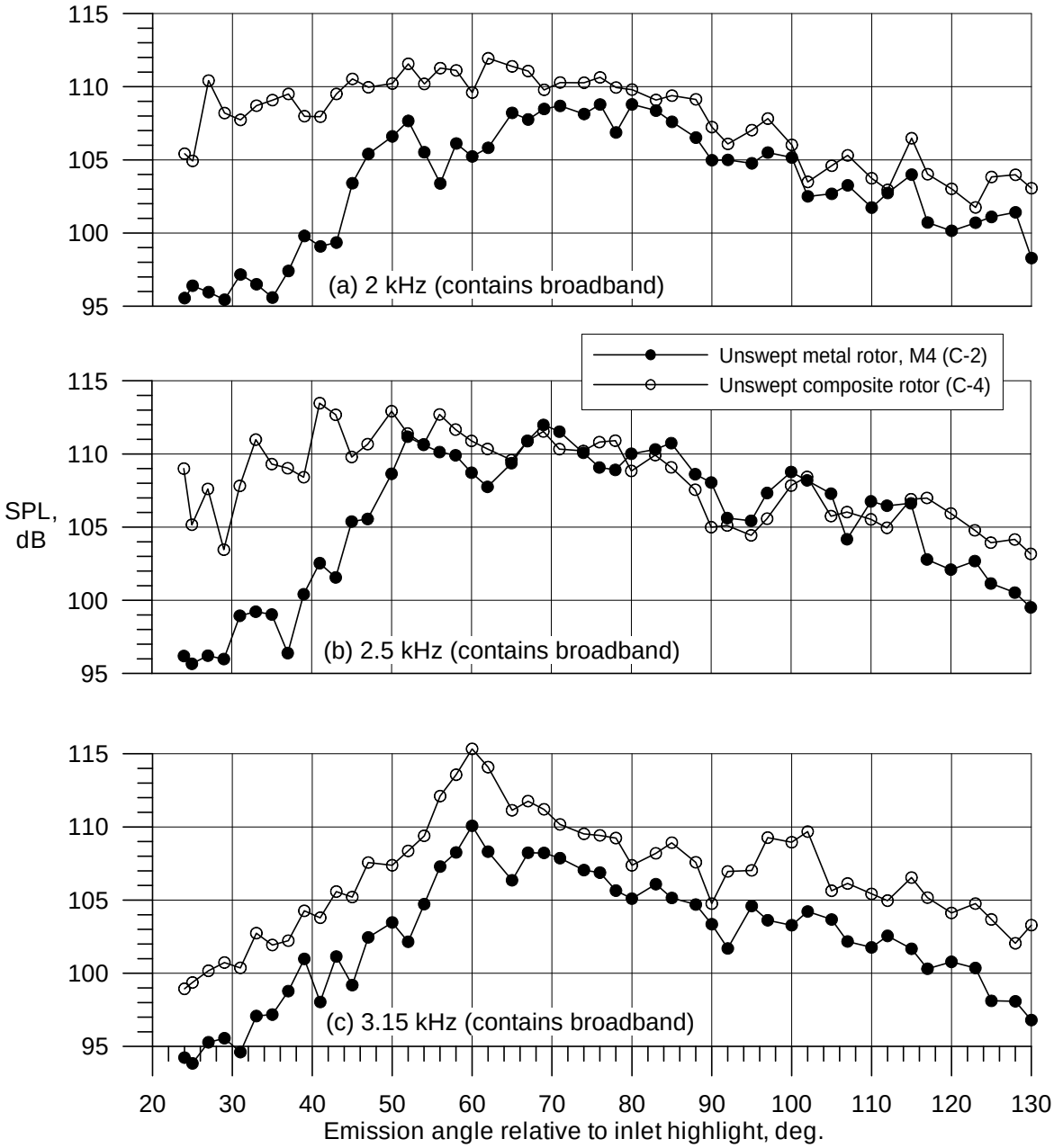

Figure 21.—Comparison of 1/3rd octave directivities for the M4 unswept metal and unswept composite rotors at 12 k rpm_c (HTH).

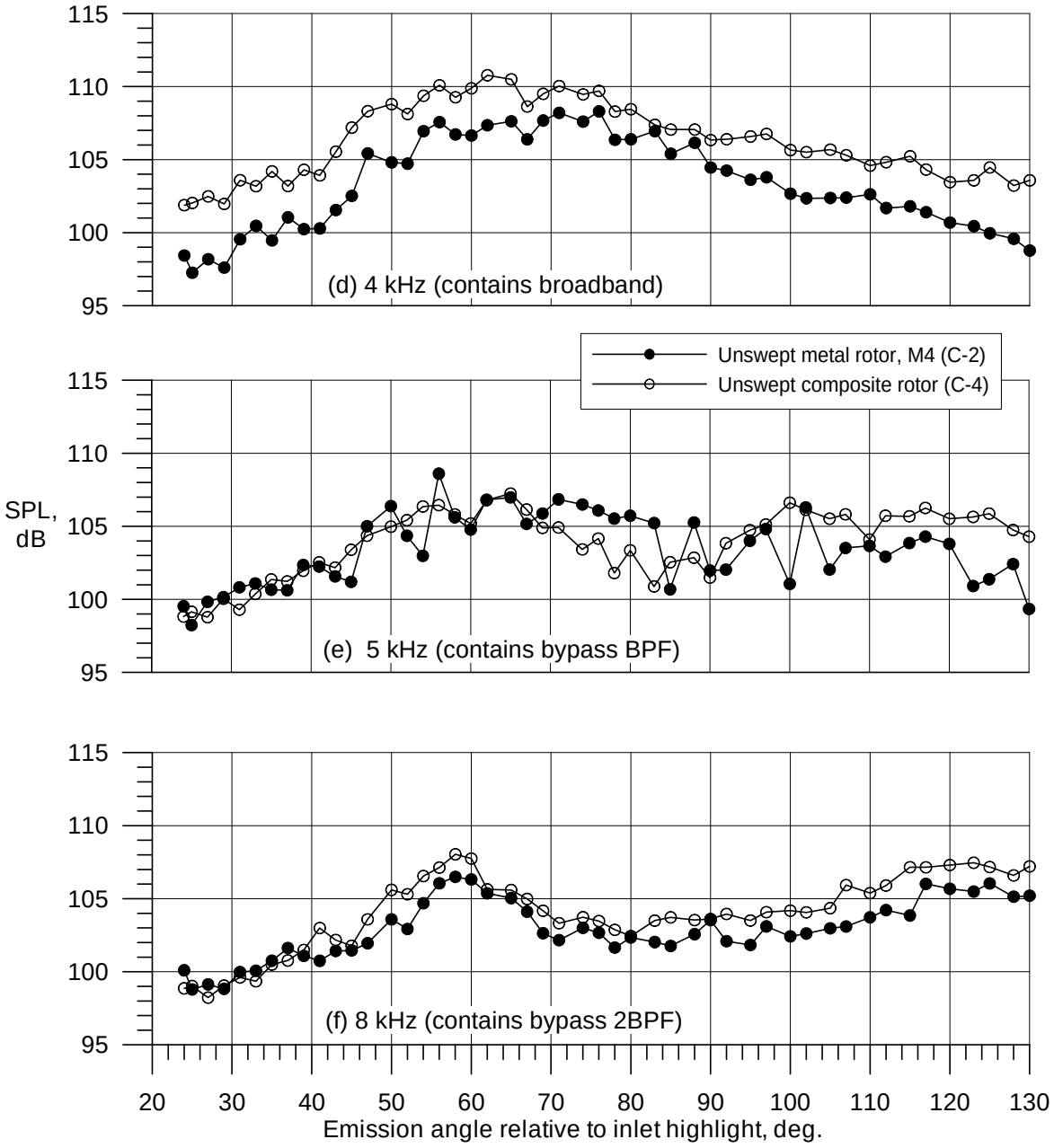

Figure 21.—Concluded.

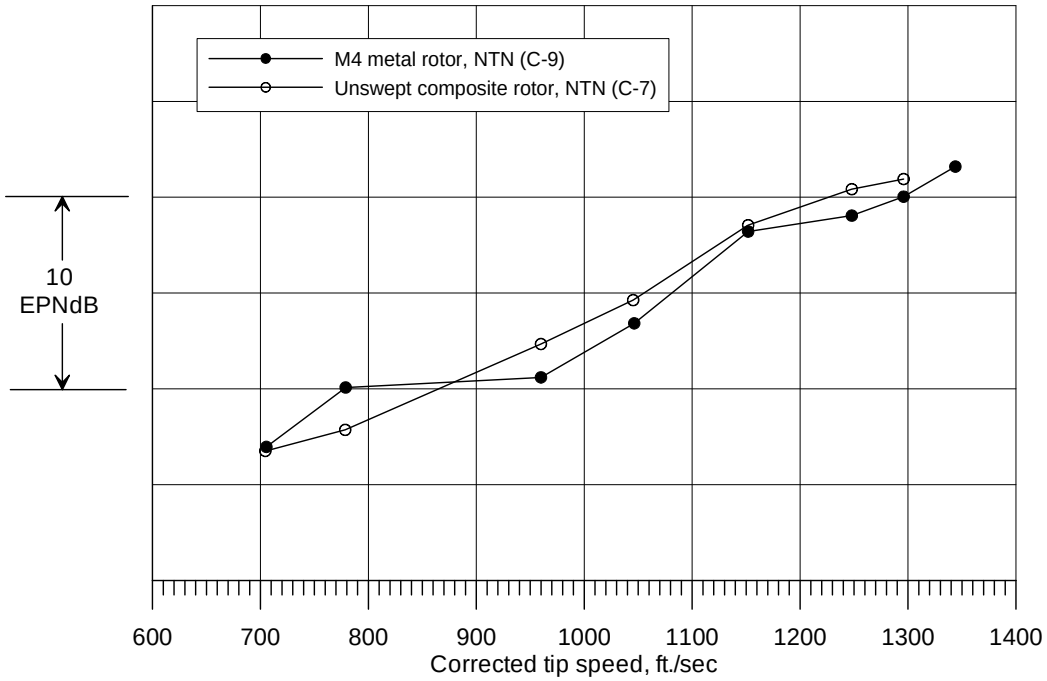

Figure 22.—Comparison of unswept metal M4 and composite rotors (NTN).

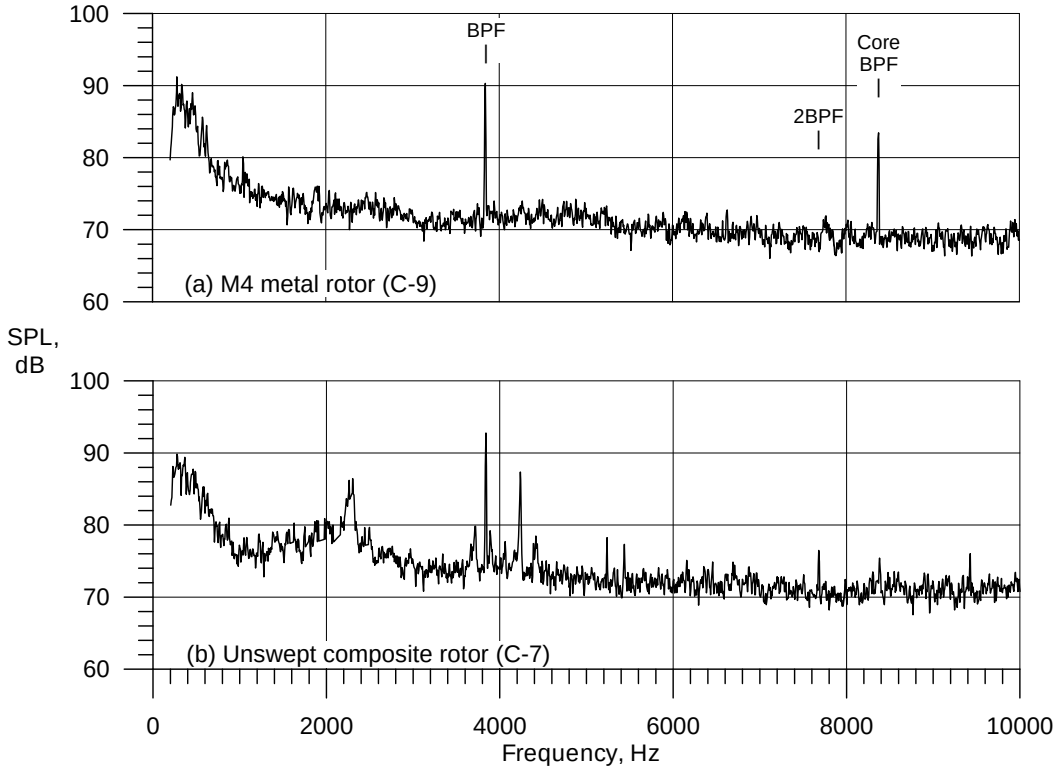

Figure 23.—Comparison of constant (6 Hz) bandwidth spectra for the unswept metal M4 and composite rotors at 10 k rpm_c (47° sideline emission angle, NTN).

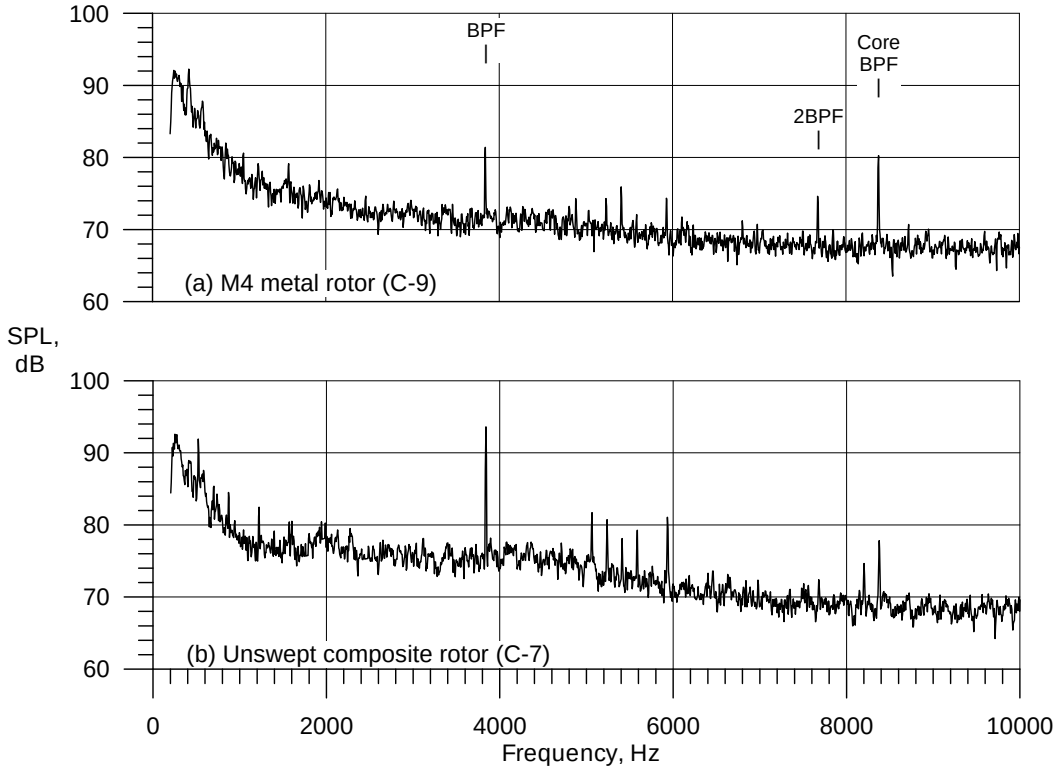

Figure 24.—Comparison of constant (6 Hz) bandwidth spectra for the unswept metal M4 and composite rotors at 10 k rpm_c (102° sideline emission angle, NTN).

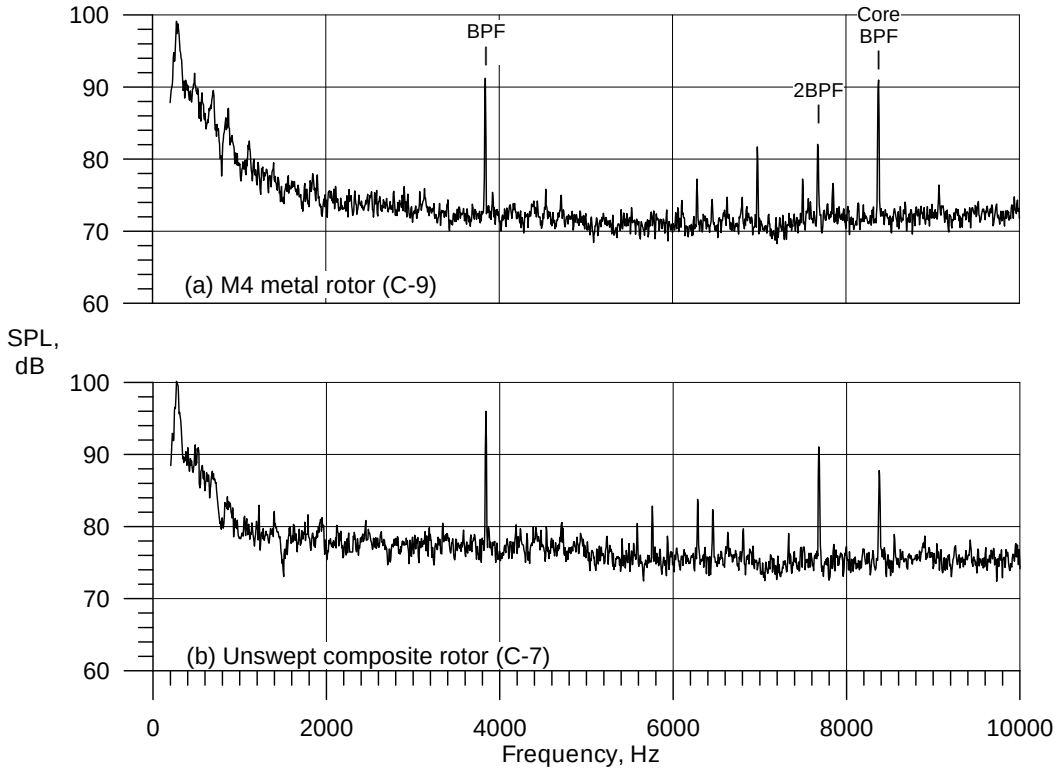

Figure 25.—Comparison of constant (6 Hz) bandwidth spectra for the unswept metal M4 and composite rotors at 10 k rpm_c (130° sideline emission angle, NTN).

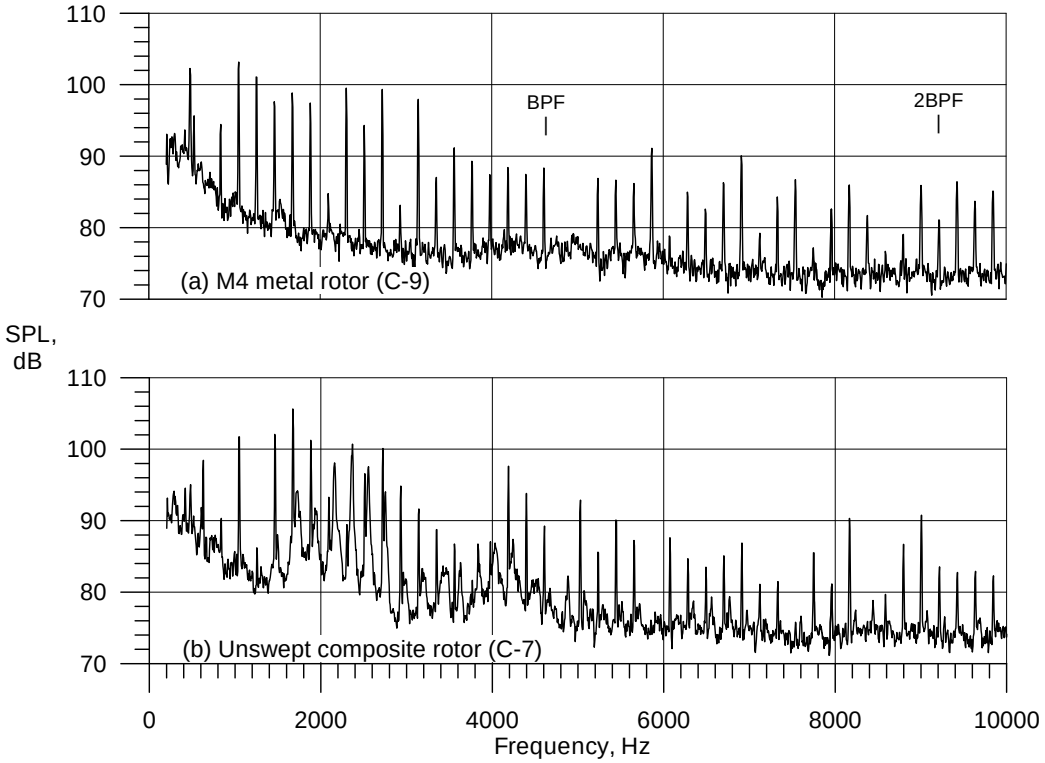

Figure 26.—Comparison of constant (6 Hz) bandwidth spectra for the unswept metal M4 and composite rotors at 12 k rpm_c (47° sideline emission angle, NTN).

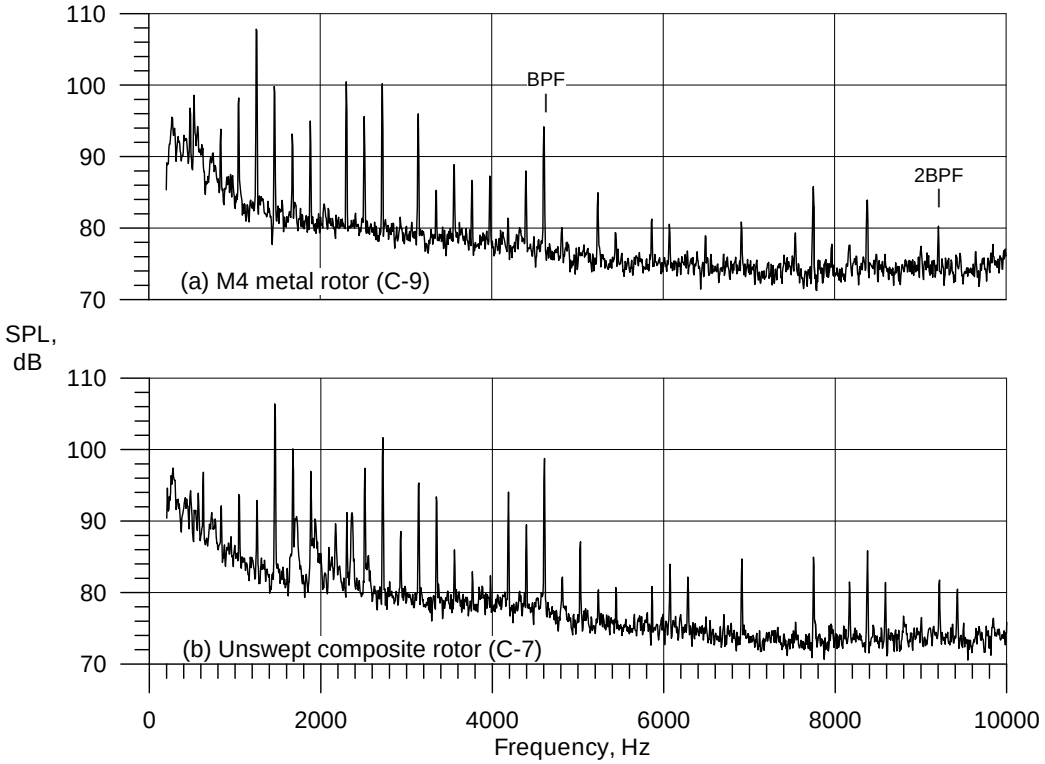

Figure 27.—Comparison of constant (6 Hz) bandwidth spectra for the unswept metal M4 and composite rotors at 12 k rpm_c (102° sideline emission angle, NTN).

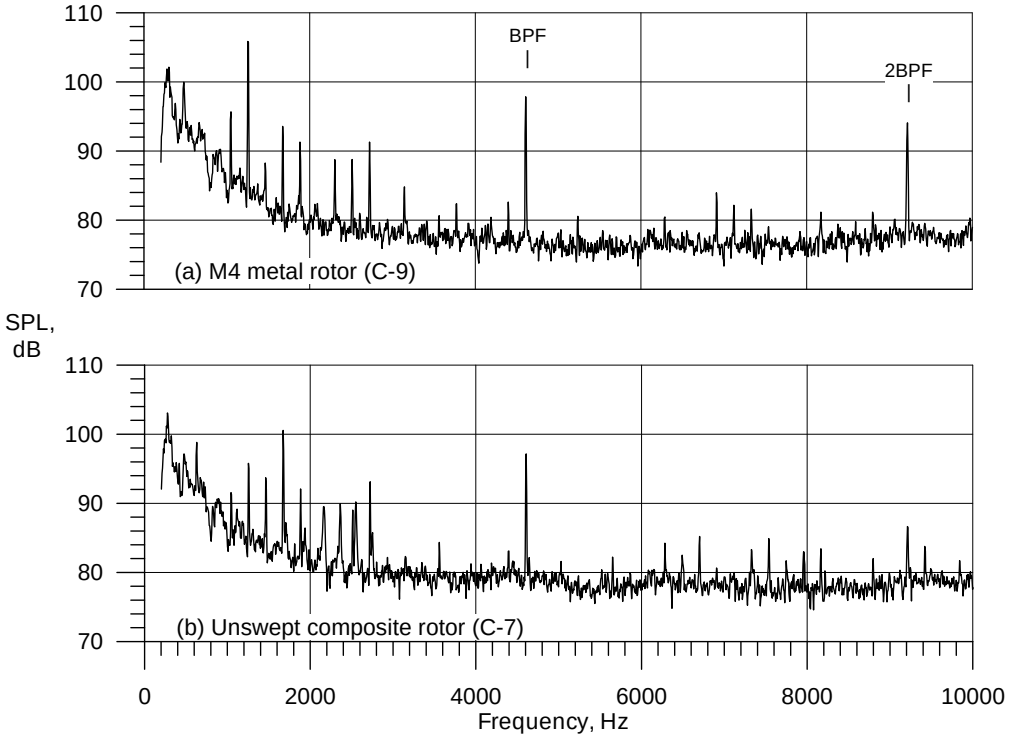

Figure 28.—Comparison of constant (6 Hz) bandwidth spectra for the unswept metal M4 and composite rotors at 12 k rpm_c (130° sideline emission angle, NTN).

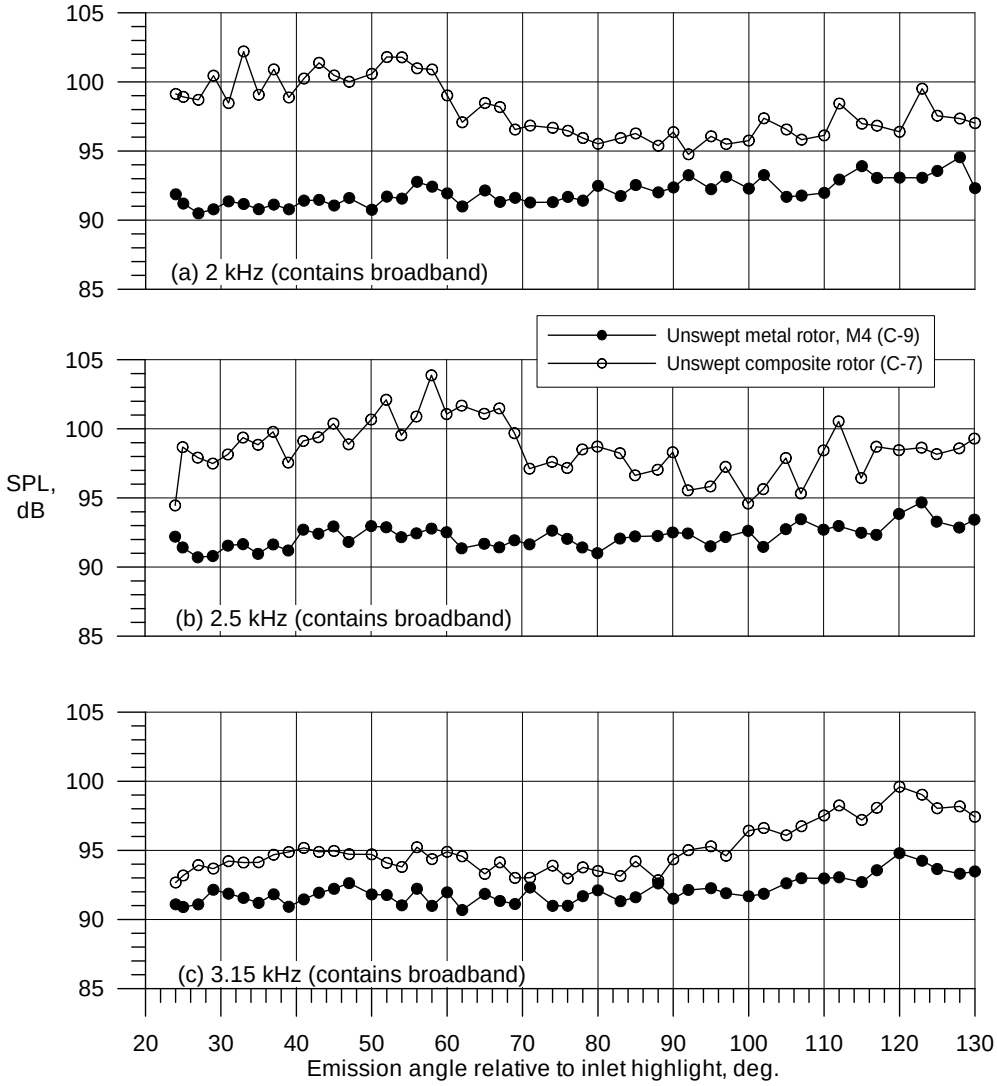

Figure 29.—Comparison of 1/3rd octave directivities for the M4 unswept metal rotor and unswept composite rotors at 10 k rpm_c (NTN).

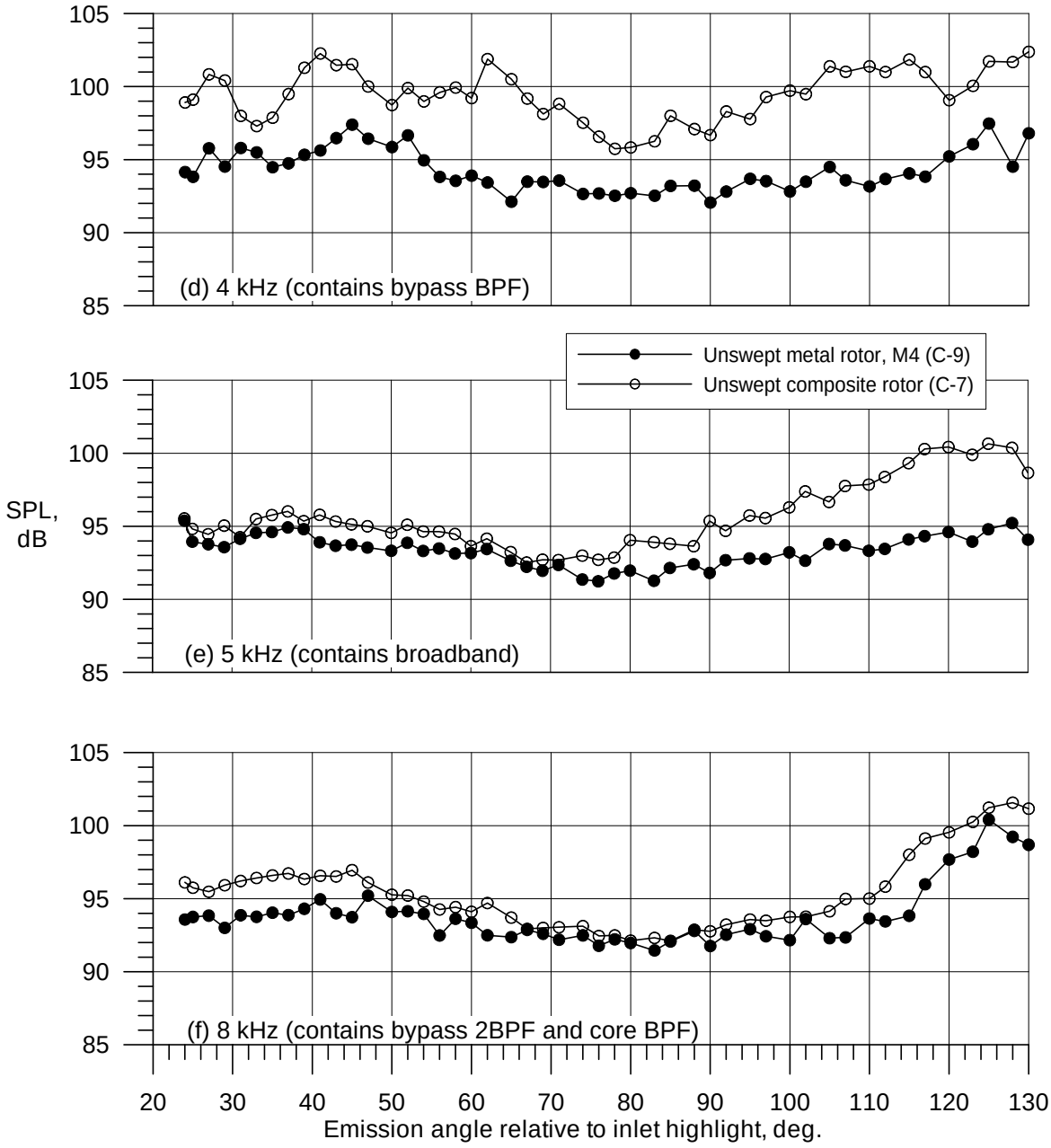

Figure 29.—Concluded.

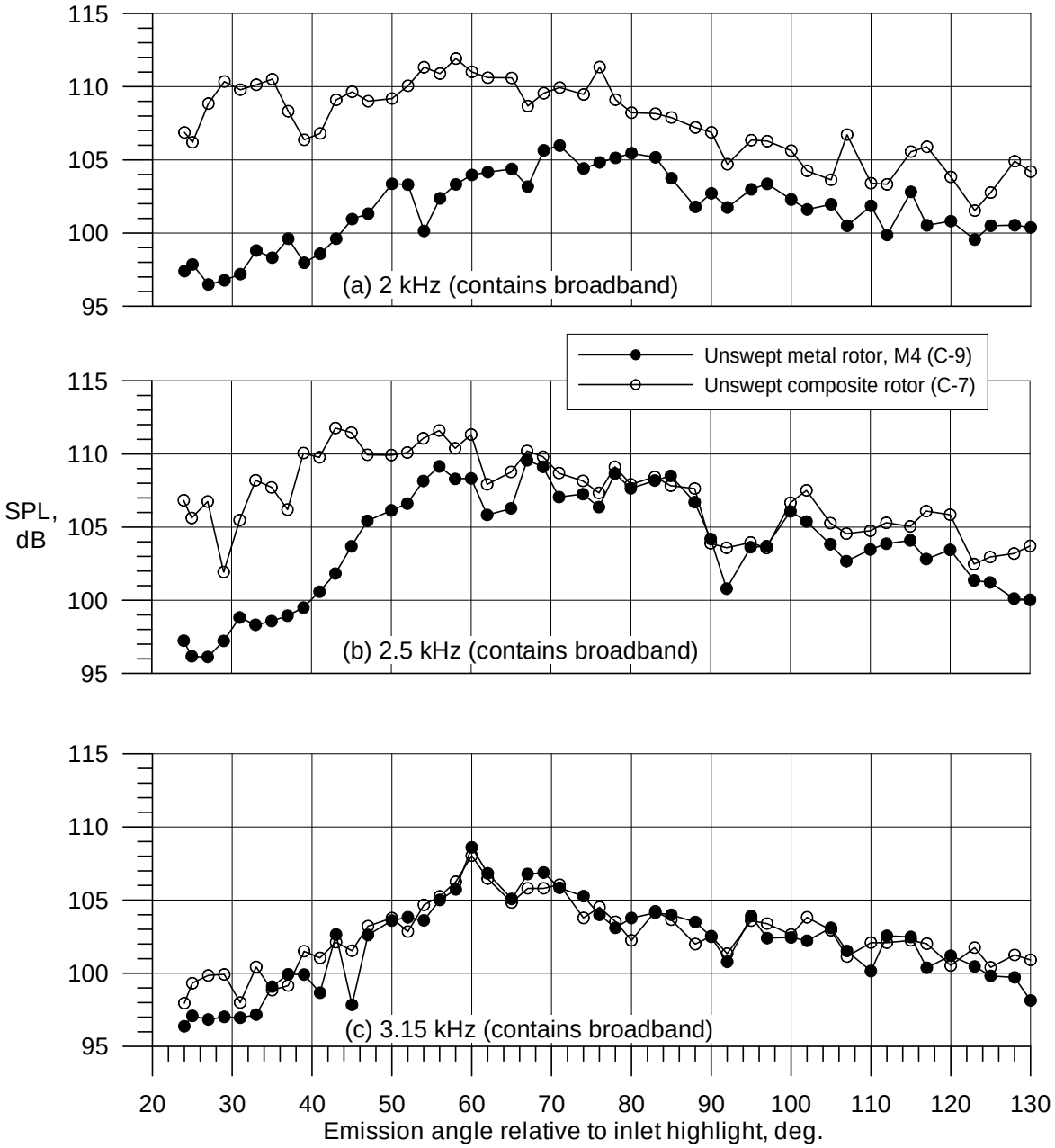

Figure 30.—Comparison of 1/3rd octave directivities for the M4 unswept metal rotor and unswept composite rotors at 12 k rpm_c (NTN).

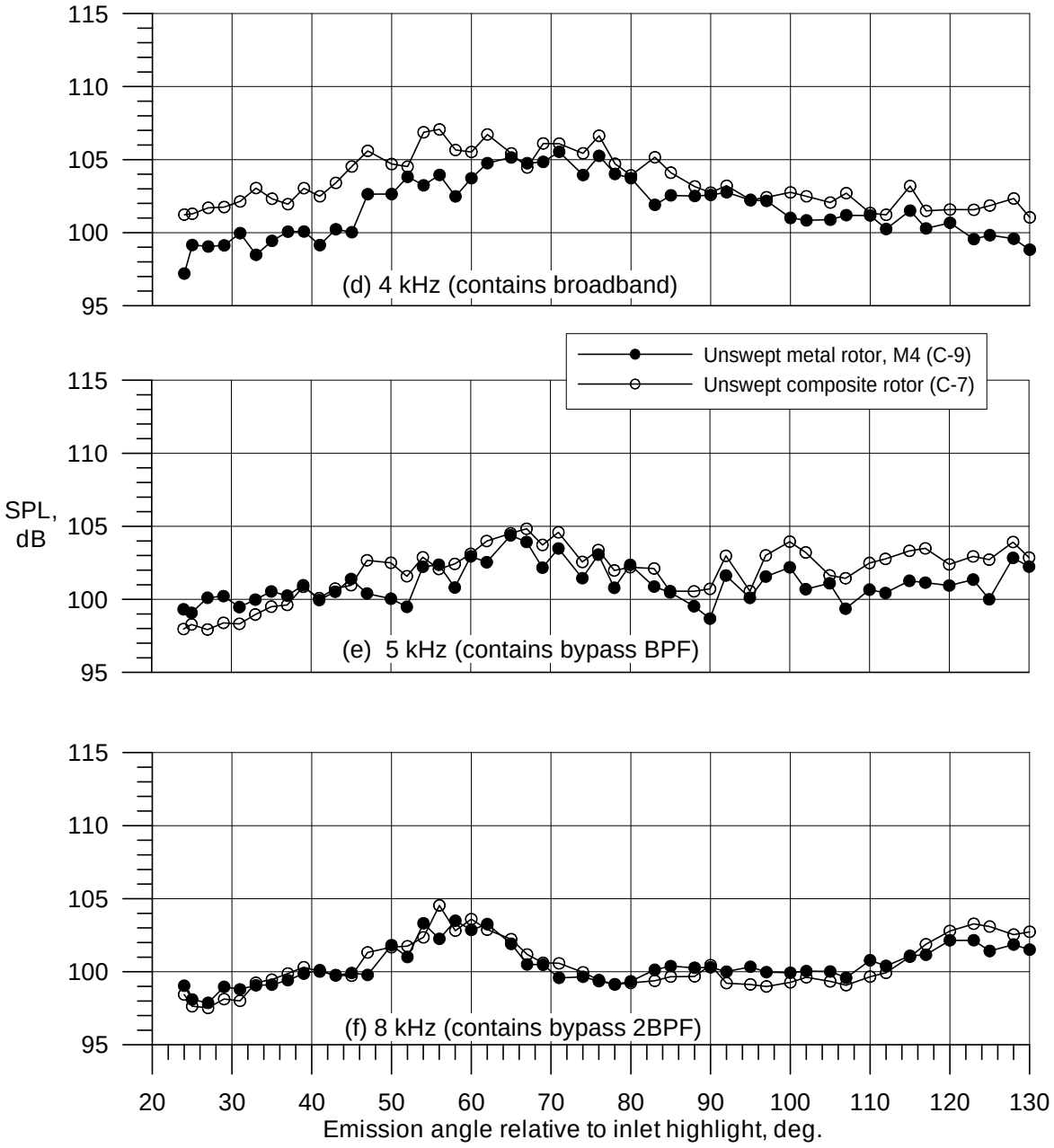

Figure 30.—Concluded.

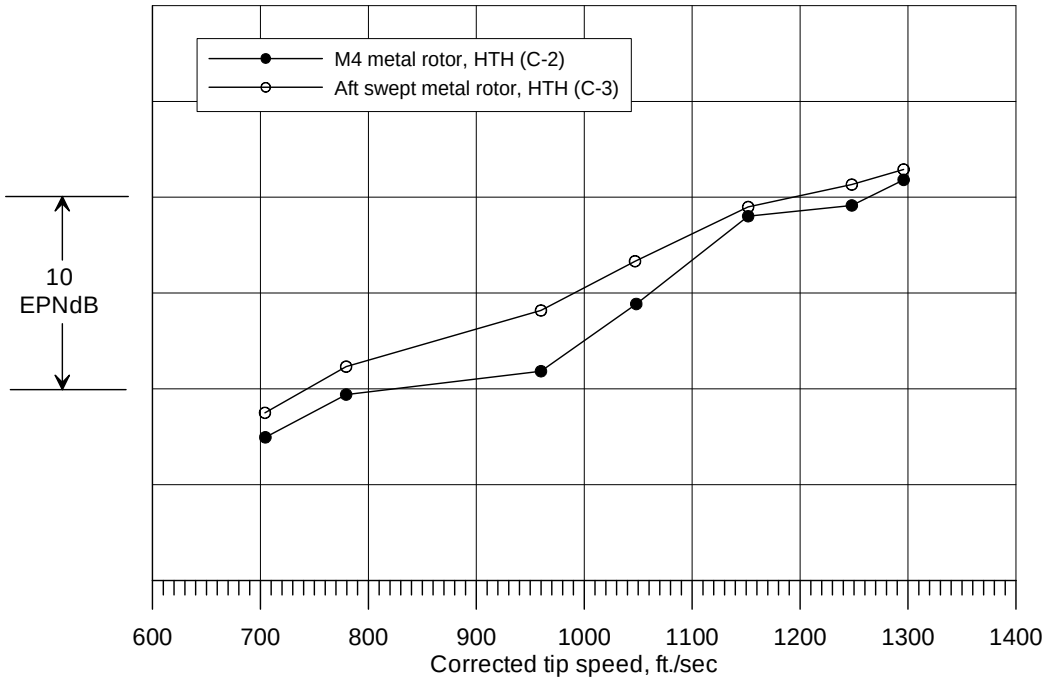

Figure 31.—Comparison of unswept M4 and aft-swept metal rotors (HTH).

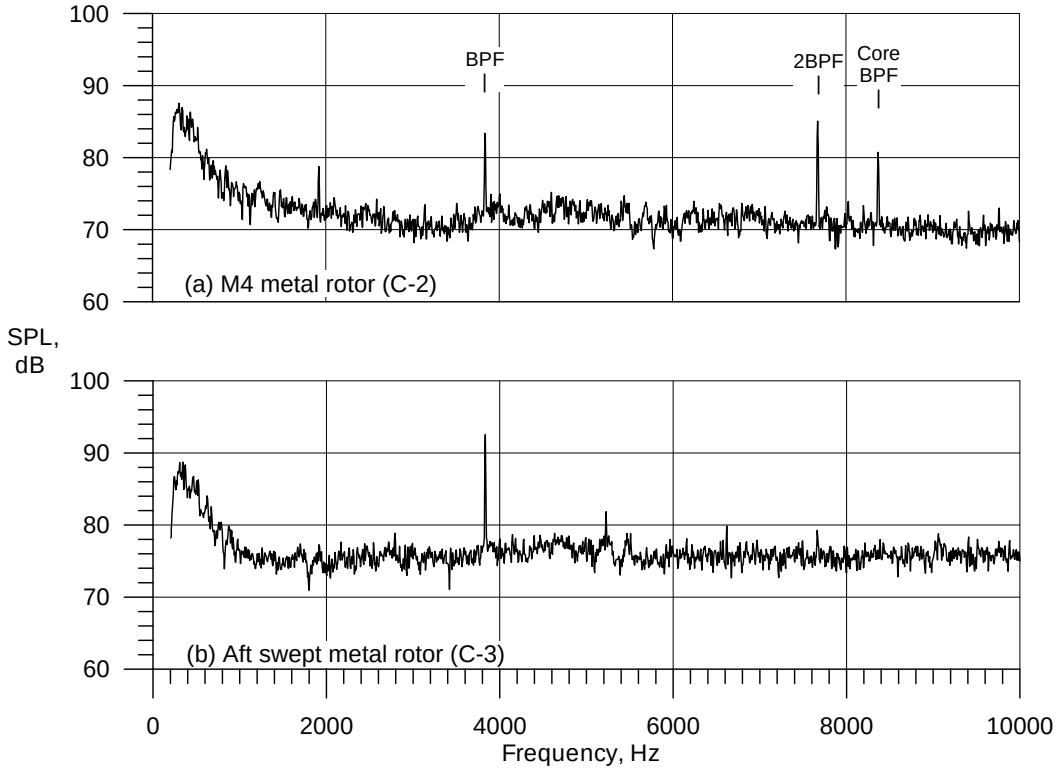

Figure 32.—Comparison of constant (6 Hz) bandwidth spectra for the unswept and aft-swept metal rotors at 10 k rpm_c (47° sideline emission angle, HTH).

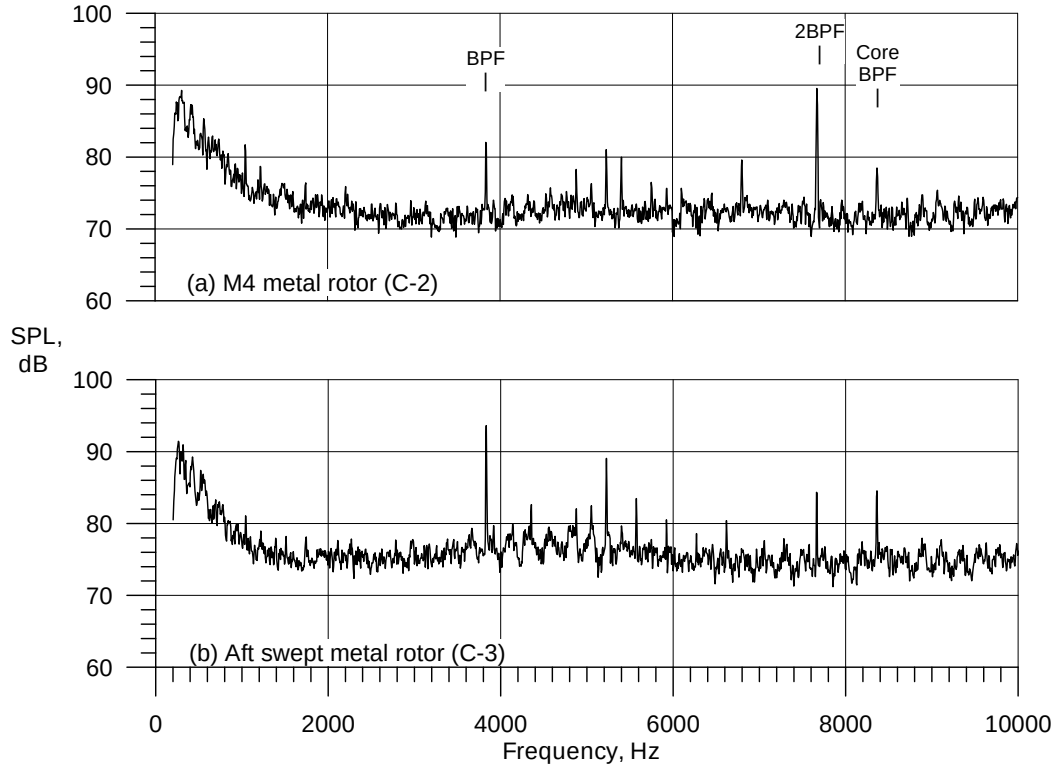

Figure 33.—Comparison of constant (6 Hz) bandwidth spectra for the unswept and aft-swept metal rotors at 10 k rpm_c (102° sideline emission angle, HTH).

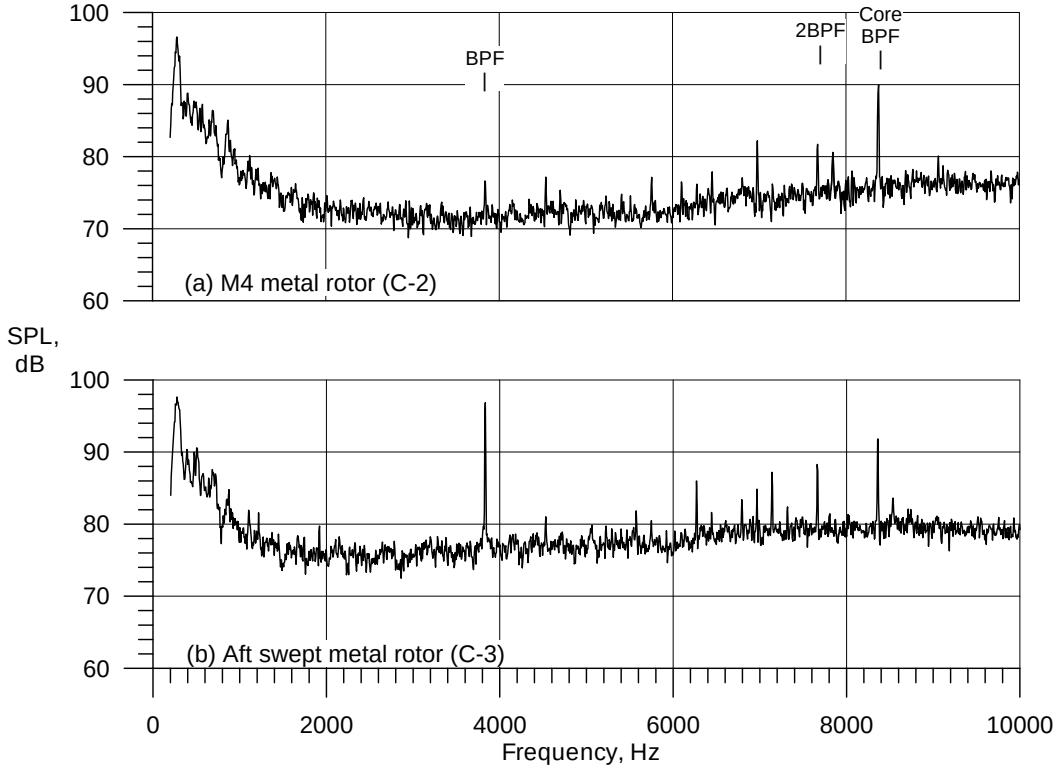

Figure 34.—Comparison of constant (6 Hz) bandwidth spectra for the unswept and aft-swept metal rotors at 10 k rpm_c (130° sideline emission angle, HTH).

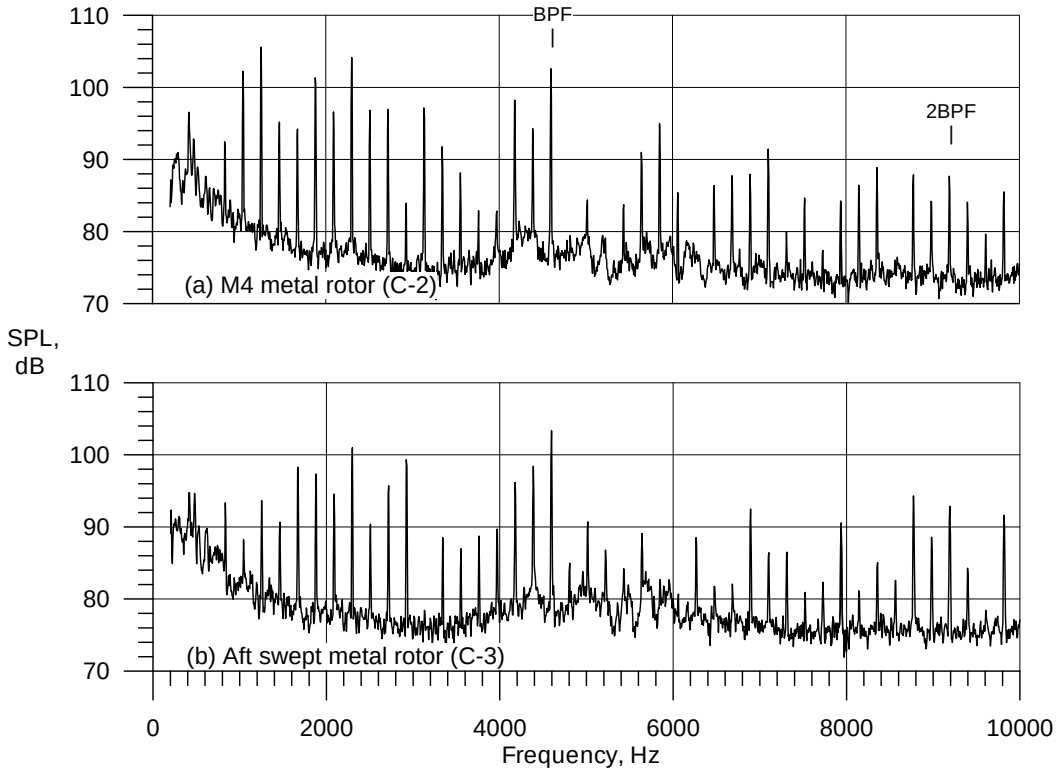

Figure 35.—Comparison of constant (6 Hz) bandwidth spectra for the unswept and aft-swept metal rotors at 12 k rpm_c (47° sideline emission angle, HTH).

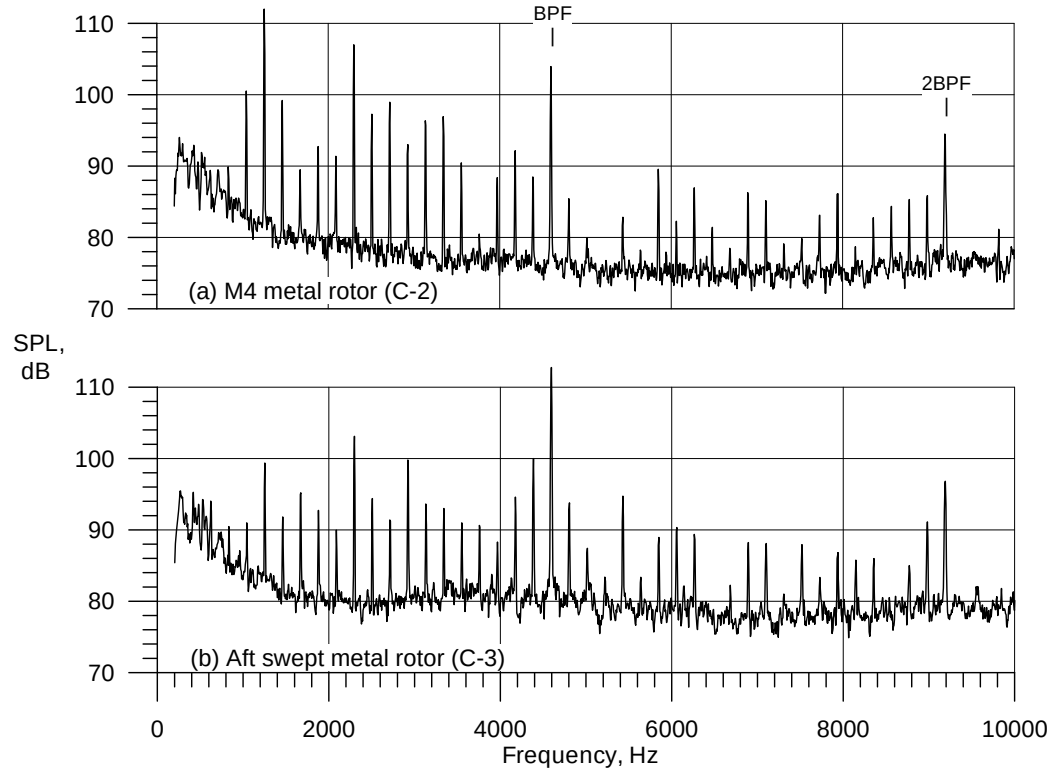

Figure 36.—Comparison of constant (6 Hz) bandwidth spectra for the unswept and aft-swept metal rotors at 12 k rpm_c (102° sideline emission angle, HTH).

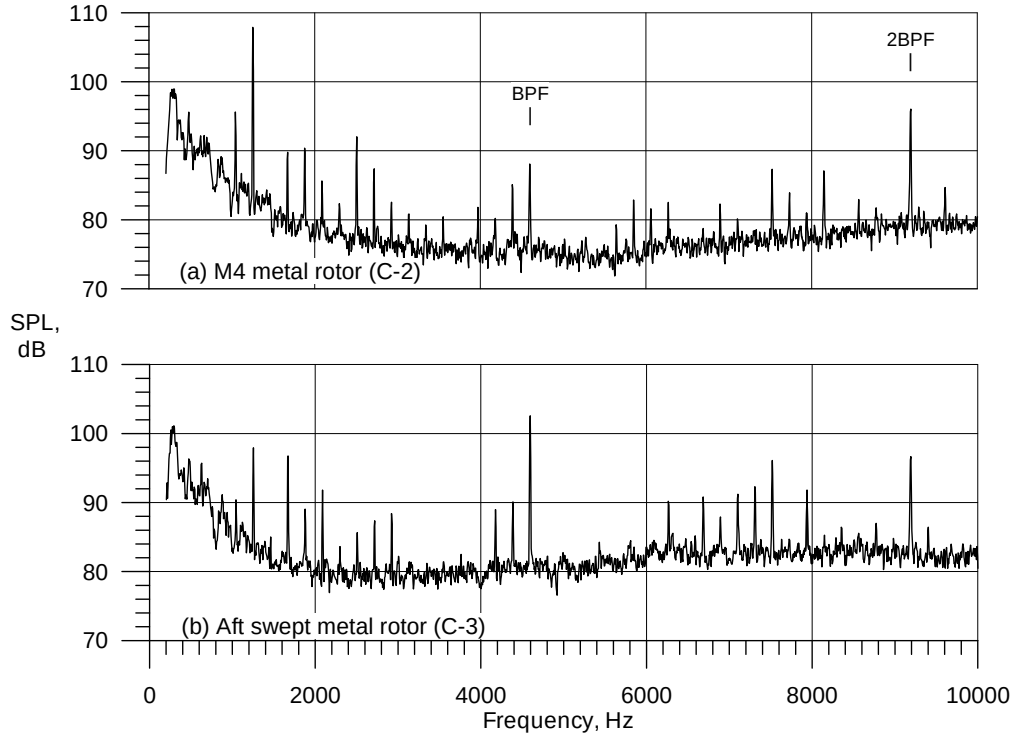

Figure 37.—Comparison of constant (6 Hz) bandwidth spectra for the unswept and aft-swept metal rotors at 12 k rpm_c (130° sideline emission angle, HTH).

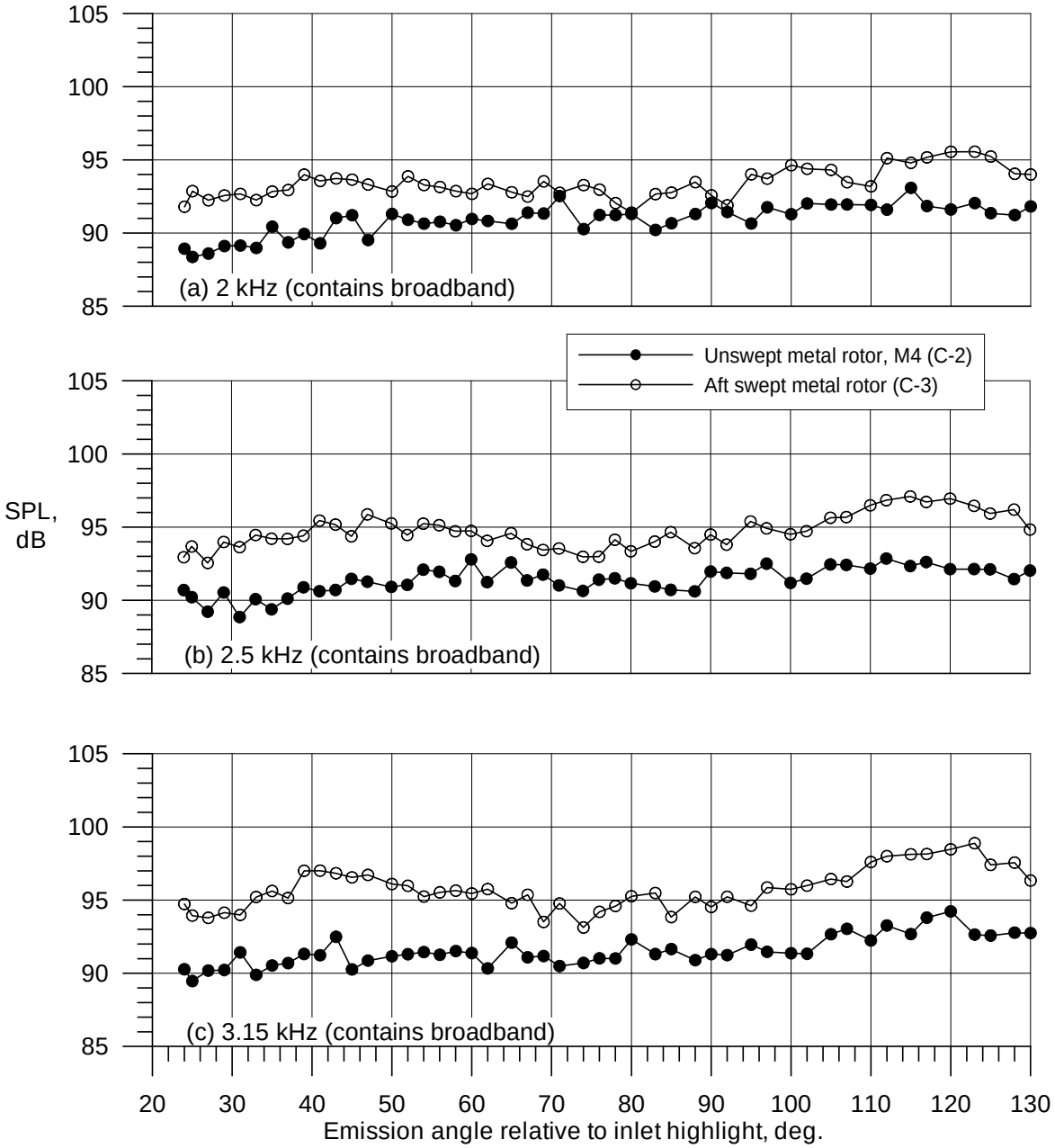

Figure 38.—Comparison of 1/3rd octave directivities for the unswept M4 and aft-swept metal rotors at 10 k rpm_c (HTH).

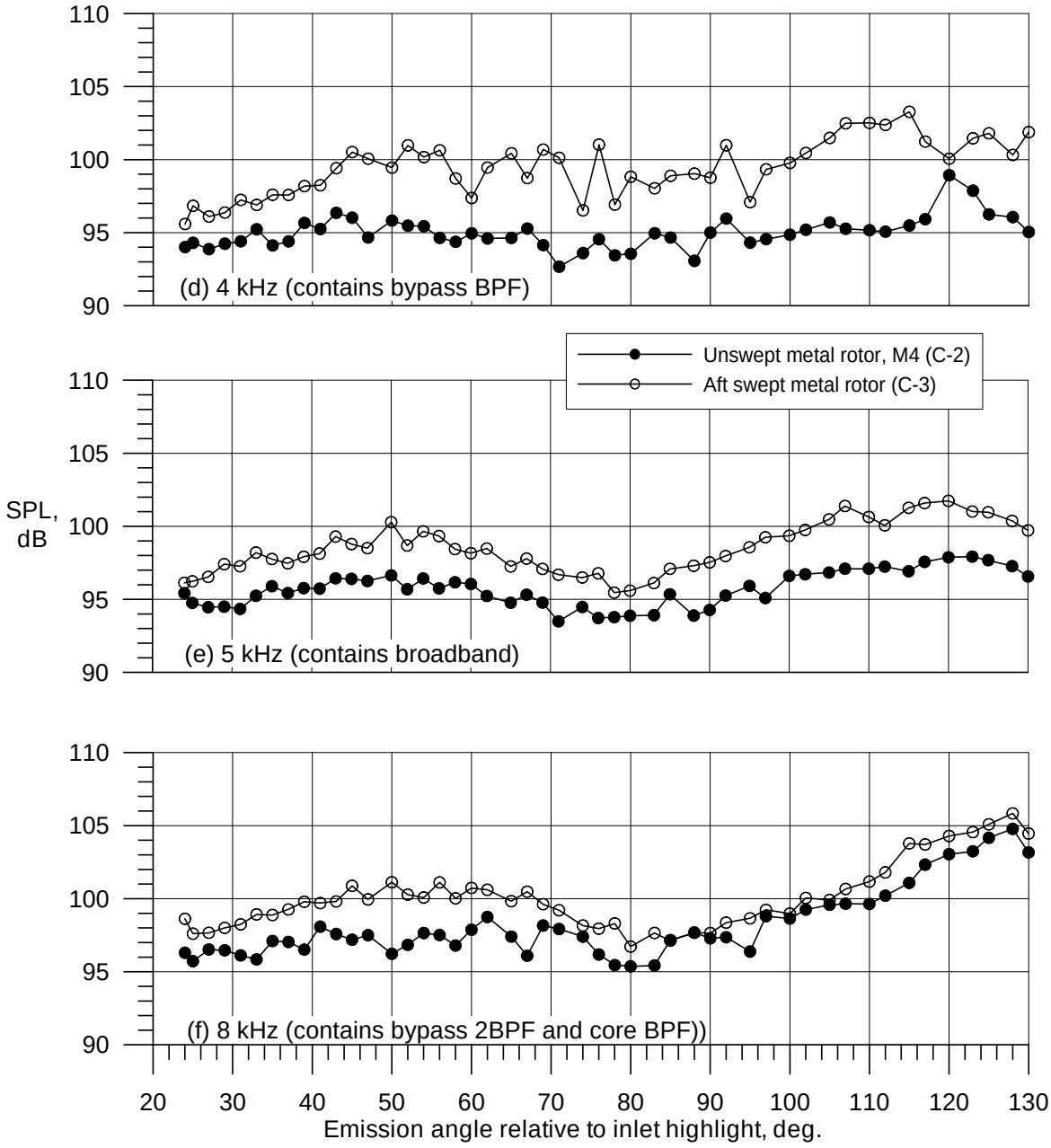

Figure 38.—Concluded.

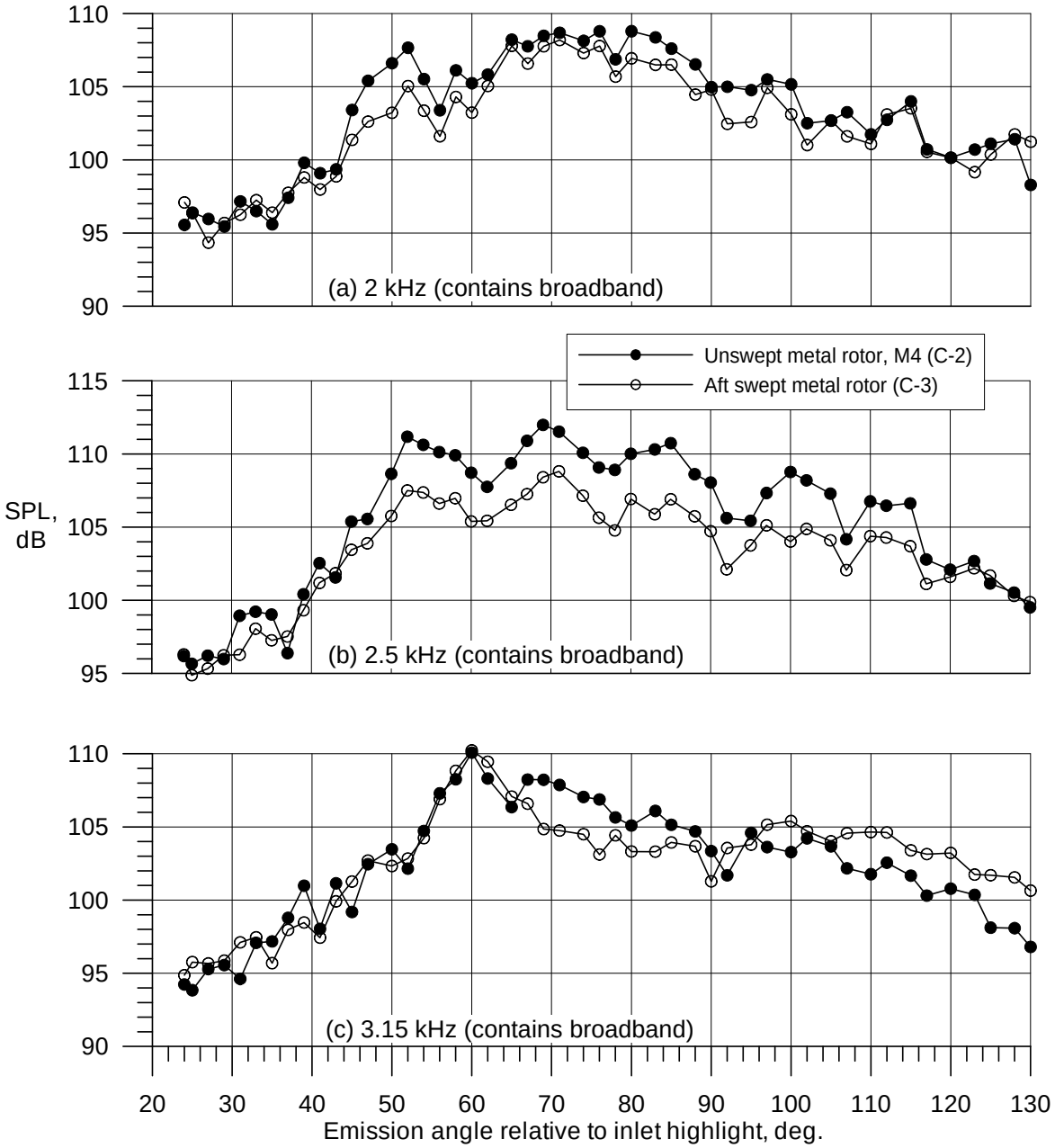

Figure 39.—Comparison of 1/3rd octave directivities for the unswept M4 and aft-swept metal rotors at 12 k rpm_c (HTH).

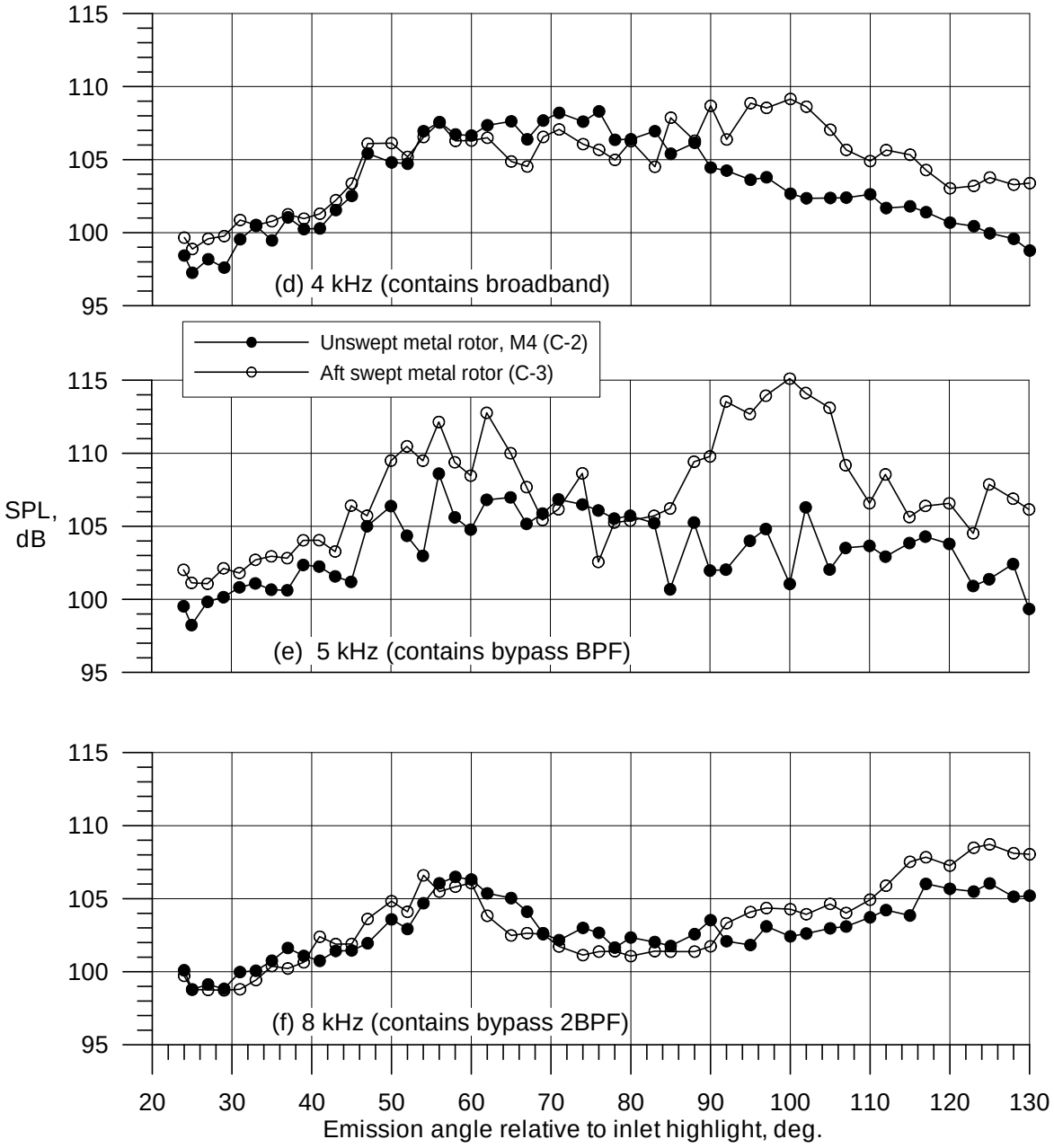

Figure 39.—Concluded.

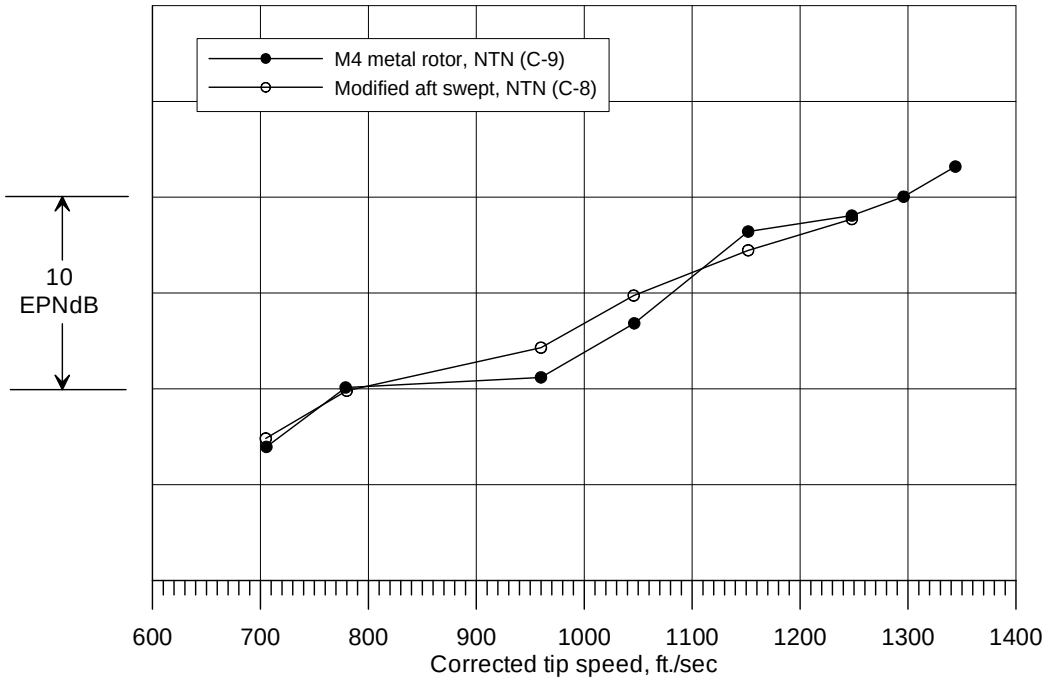

Figure 40.—Comparison of unswept M4 and aft-swept metal rotors (NTN).

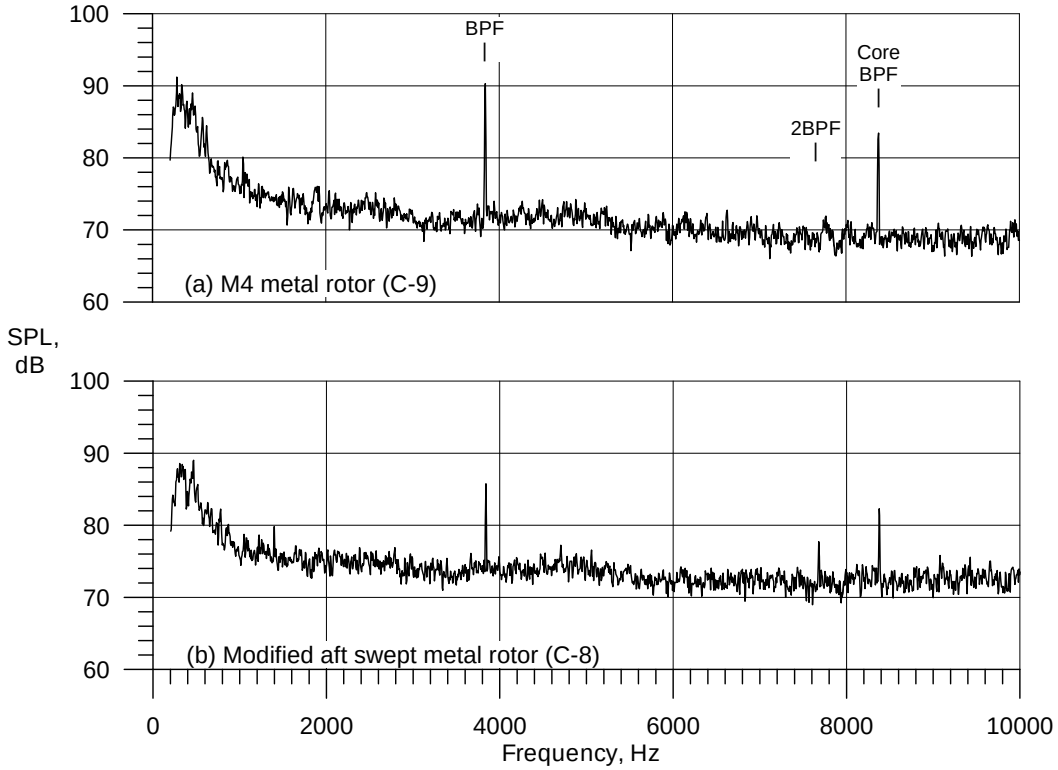

Figure 41.—Comparison of constant (6 Hz) broadband spectra for the unswept metal M4 and modified aft-swept metal rotors at 10 k rpm_c (47° emission angle, NTN).

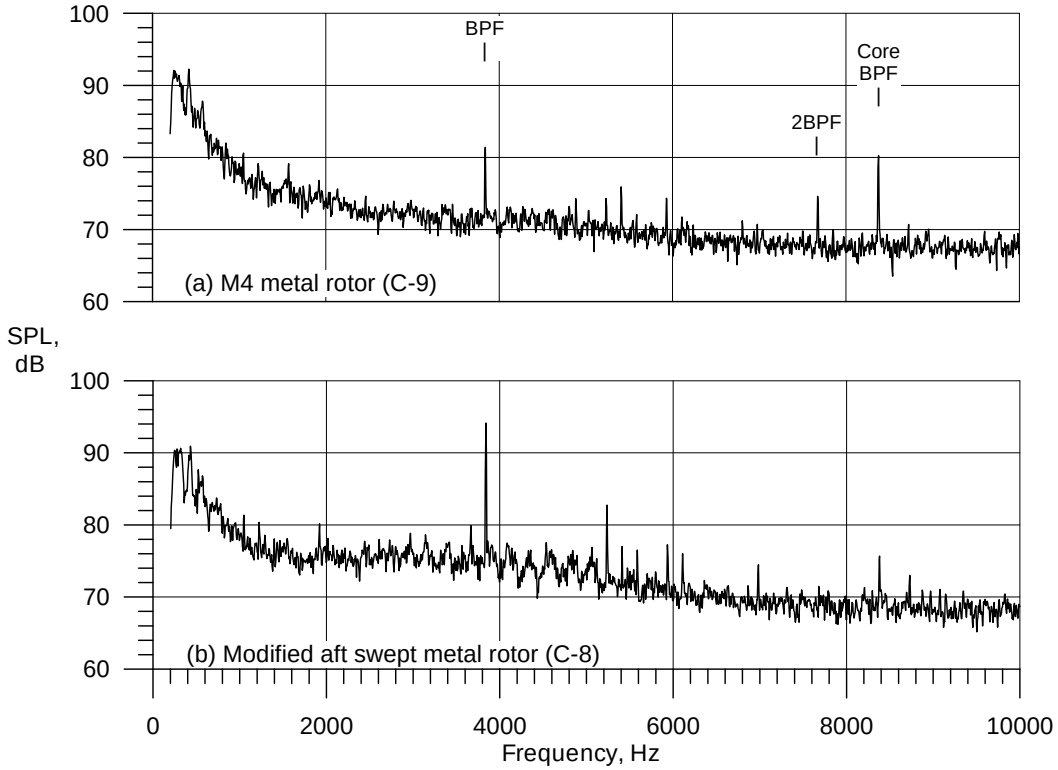

Figure 42.—Comparison of constant (6 Hz) broadband spectra for the unswept metal M4 and modified aft-swept metal rotors at 10 k rpm_c (102° emission angle, NTN).

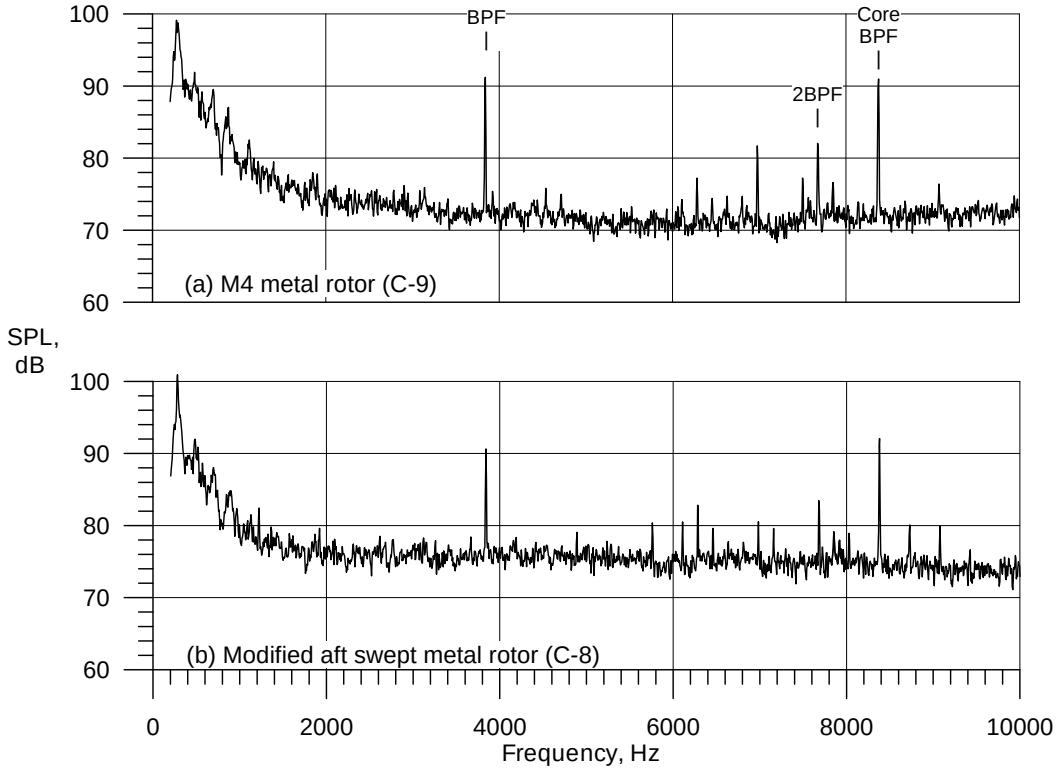

Figure 43.—Comparison of constant (6 Hz) broadband spectra for the unswept metal M4 and modified aft-swept metal rotors at 10 k rpm_c (130° emission angle, NTN).

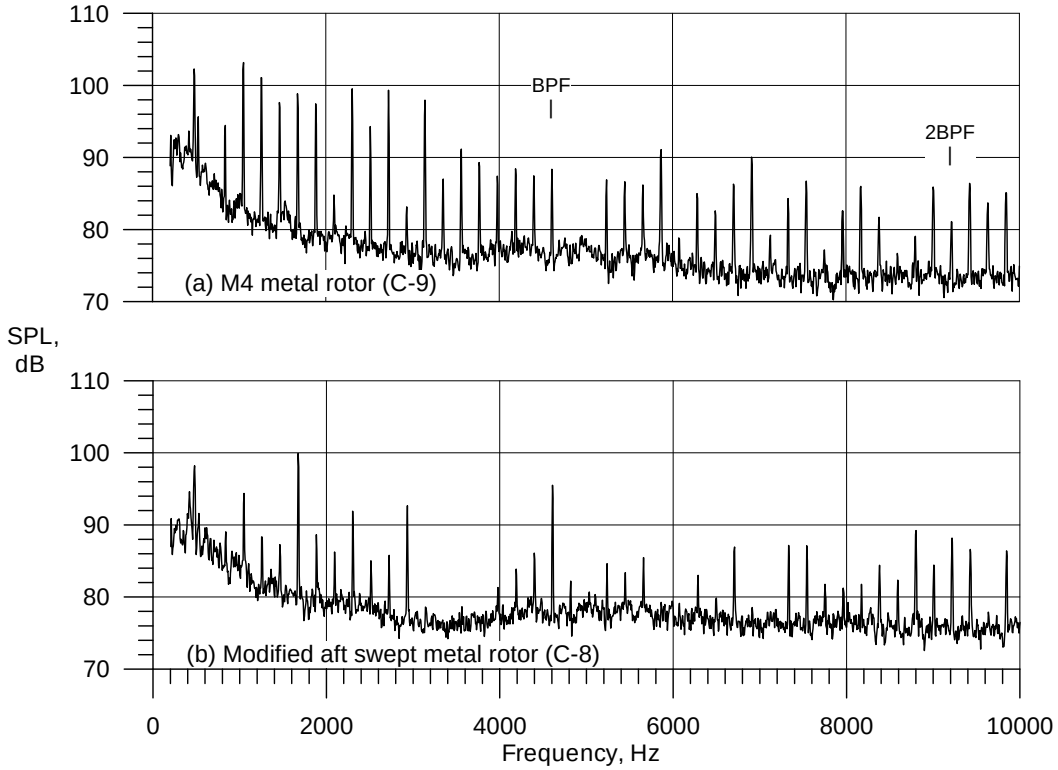

Figure 44.—Comparison of constant (6 Hz) broadband spectra for the unswept metal M4 and modified aft-swept metal rotors at 12 k rpm_c (47° emission angle, NTN).

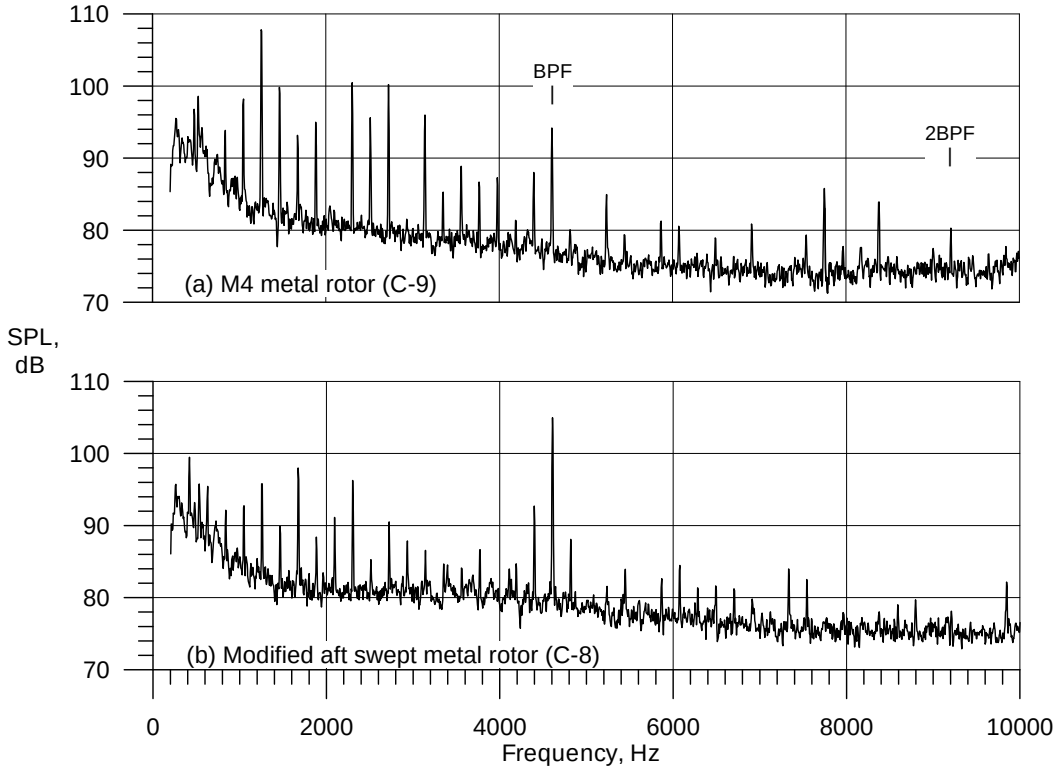

Figure 45.—Comparison of constant (6 Hz) broadband spectra for the unswept metal M4 and modified aft-swept metal rotors at 12 k rpm_c (102° emission angle, NTN).

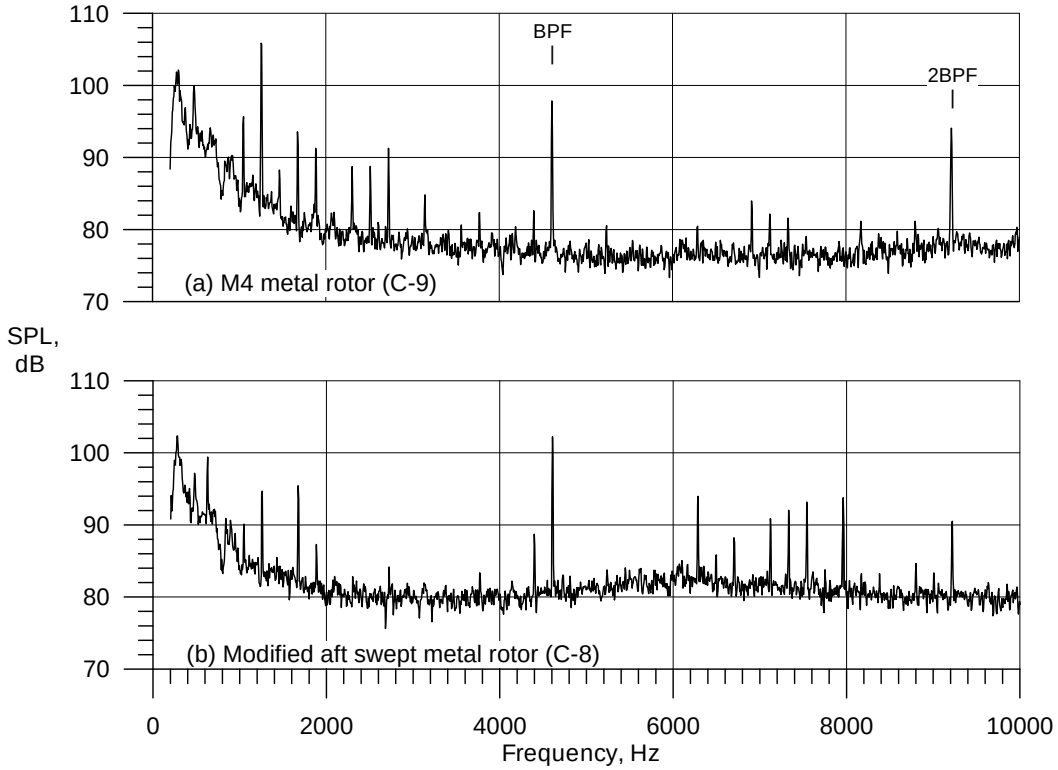

Figure 46.—Comparison of constant (6 Hz) broadband spectra for the unswept metal M4 and modified aft-swept metal rotors at 12 k rpm_c (130° emission angle, NTN).

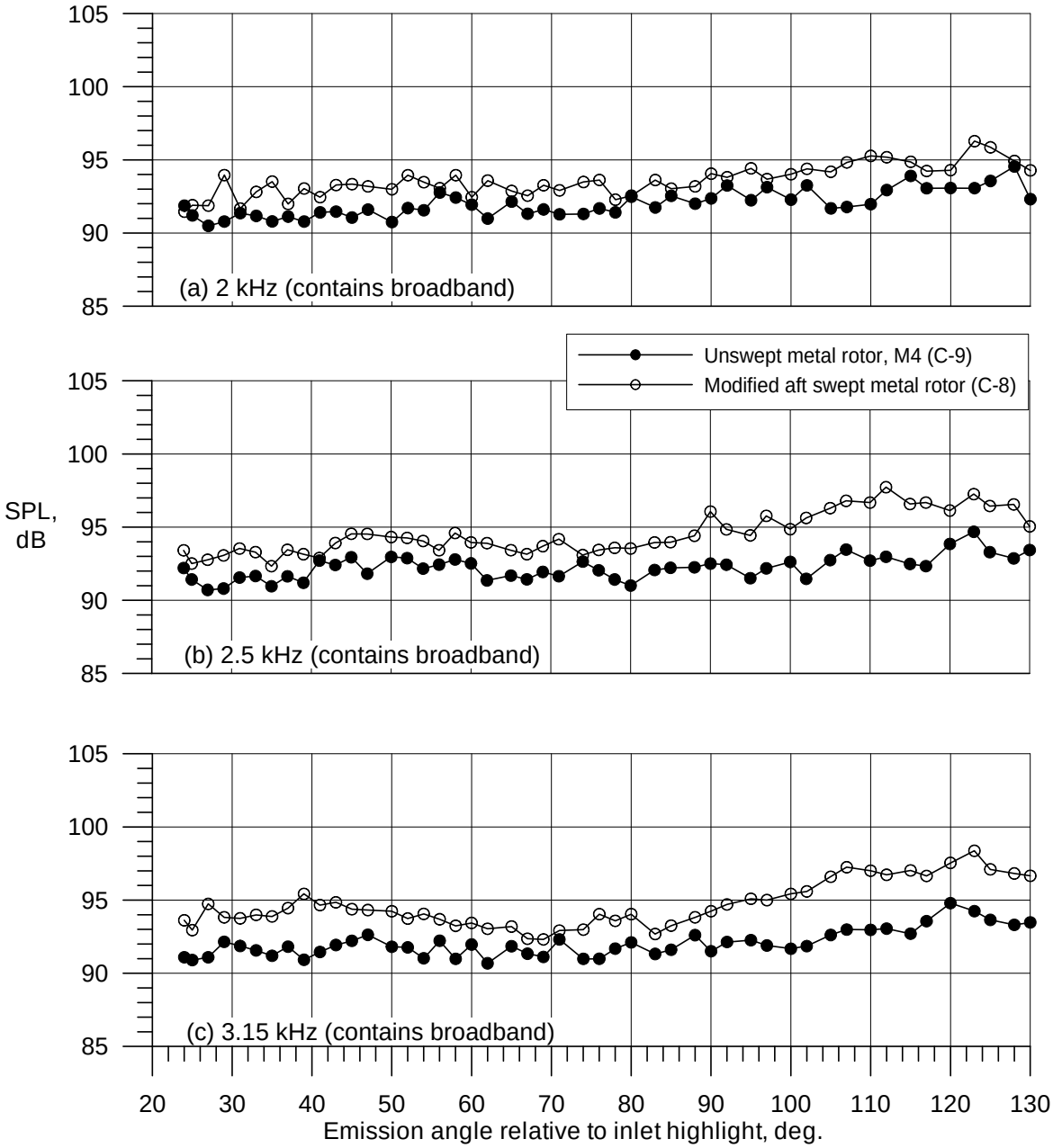

Figure 47.—Comparison of 1/3rd octave directivities for the M4 unswept and modified aft-swept metal rotors at 10 k rpm_c (NTN).

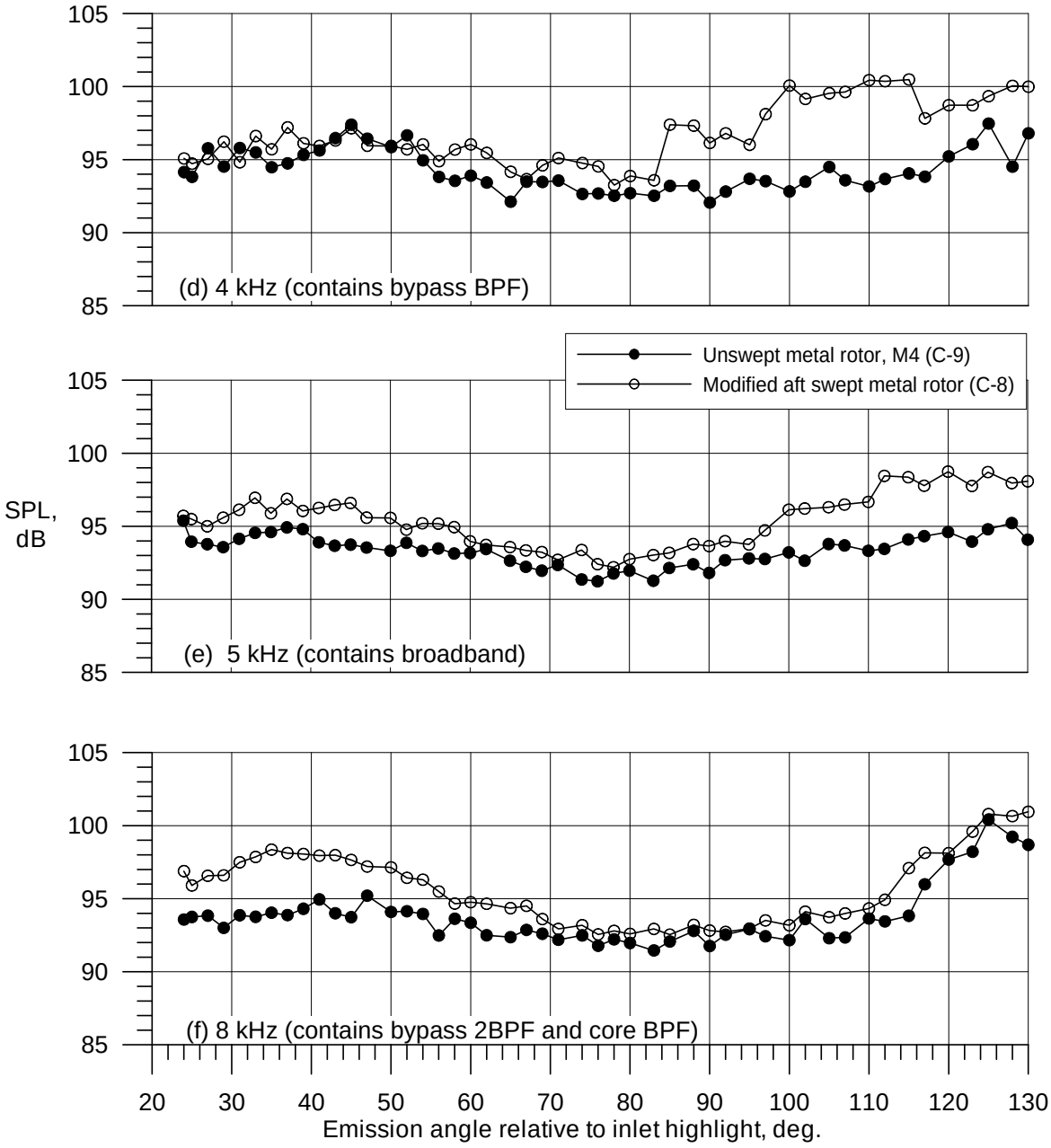

Figure 47.—Concluded.

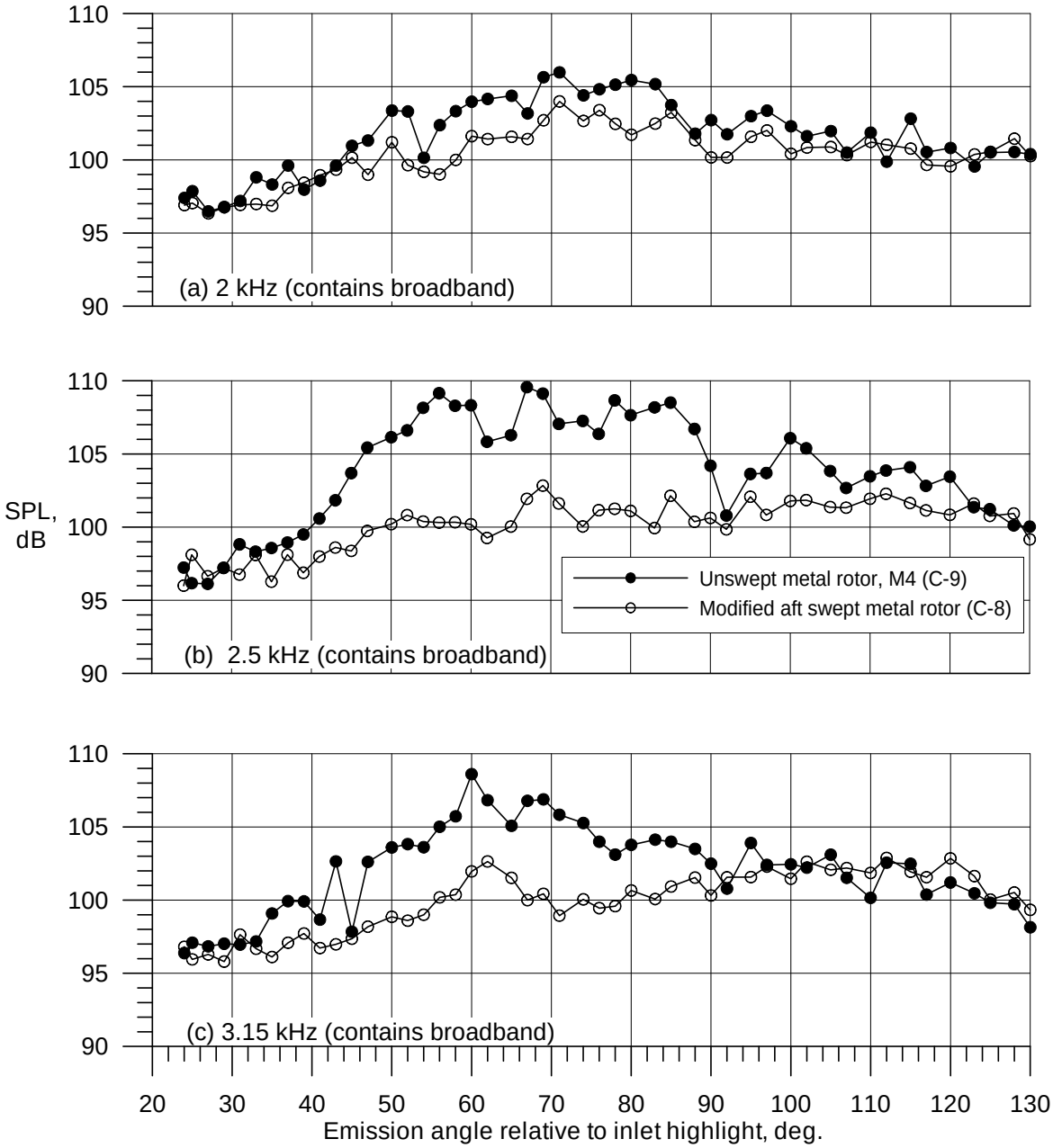

Figure 48.—Comparison of 1/3rd octave directivities for the M4 unswept and modified aft-swept metal rotors at 12 k rpm_c (NTN).

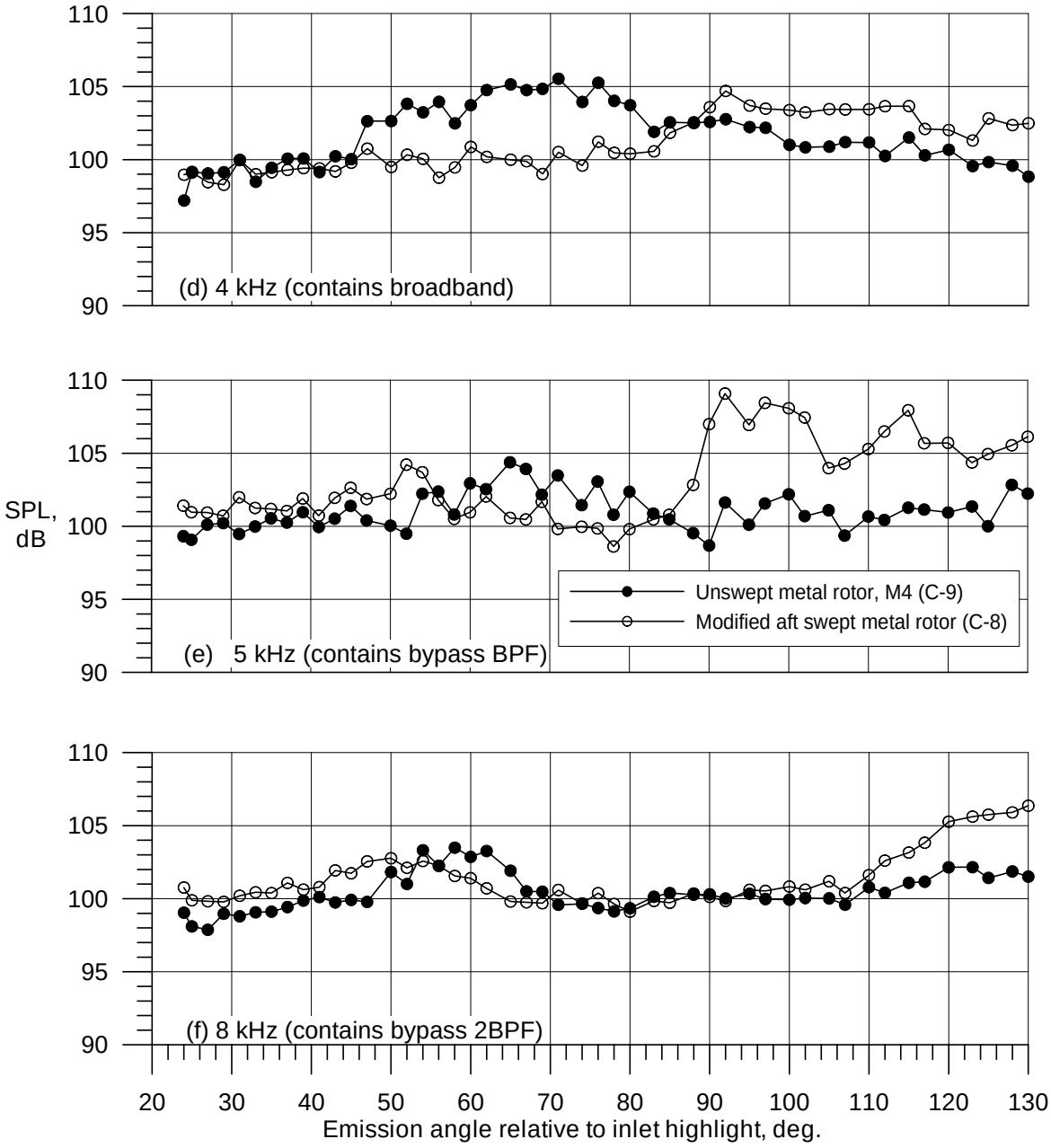

Figure 48.—Concluded.

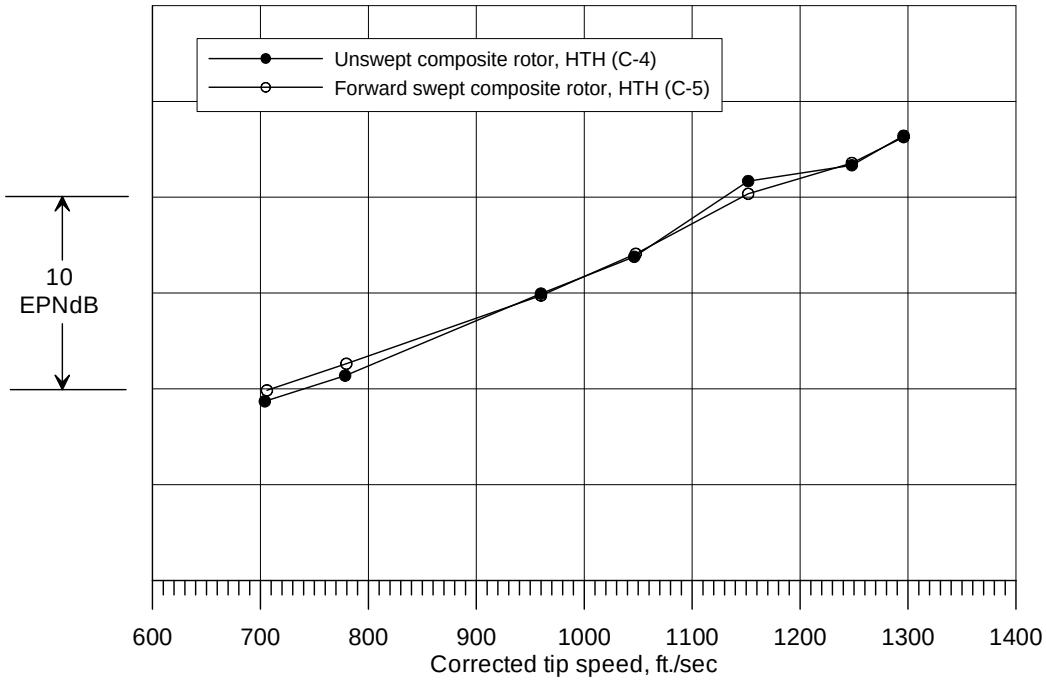

Figure 49.—Comparison of unswept and forward-swept composite rotors (HTH).

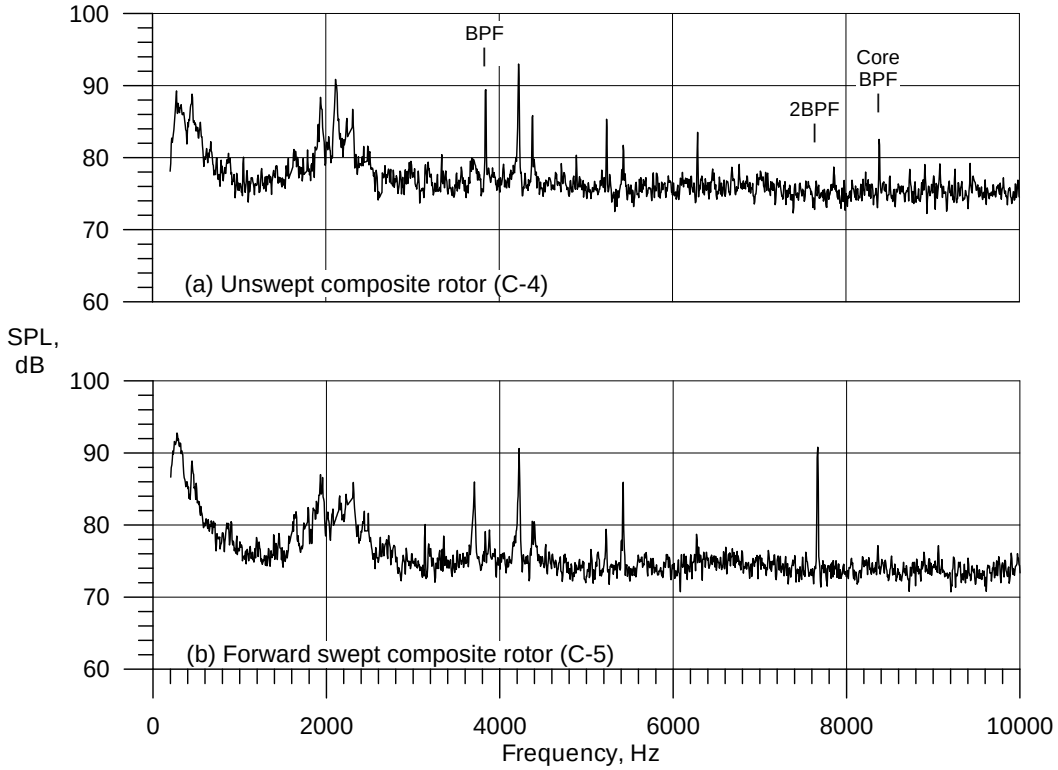

Figure 50.—Comparison of constant (6 Hz) bandwidth spectra for the unswept and forward-swept composite rotors at 10 k rpm_c (47° sideline emission angle, HTH).

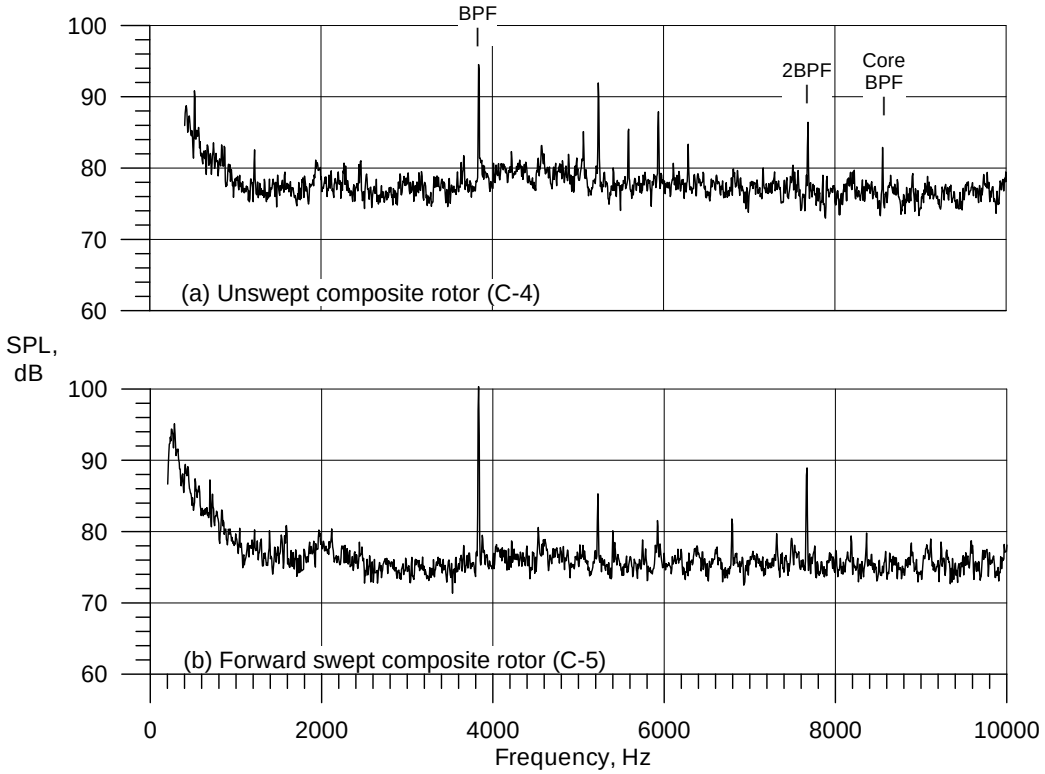

Figure 51.—Comparison of constant (6 Hz) bandwidth spectra for the unswept and forward-swept composite rotors at 10 k rpm_c (102° sideline emission angle, HTH).

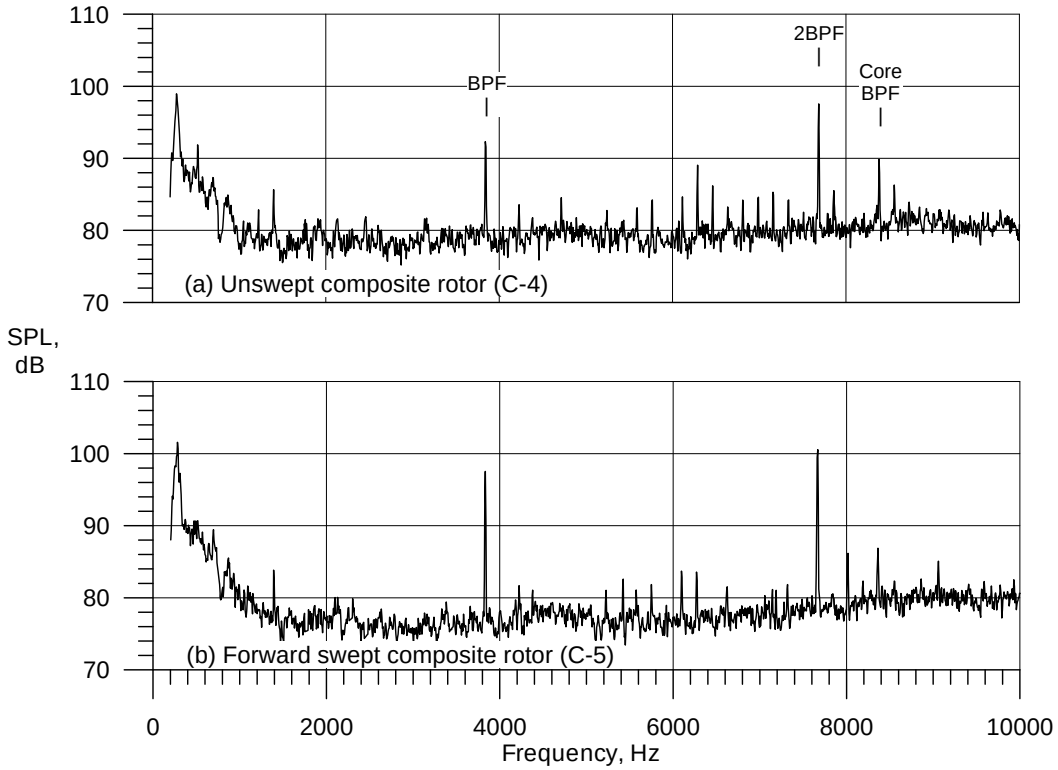

Figure 52.—Comparison of constant (6 Hz) bandwidth spectra for the unswept and forward-swept composite rotors at 10 k rpm_c (130° sideline emission angle, HTH).

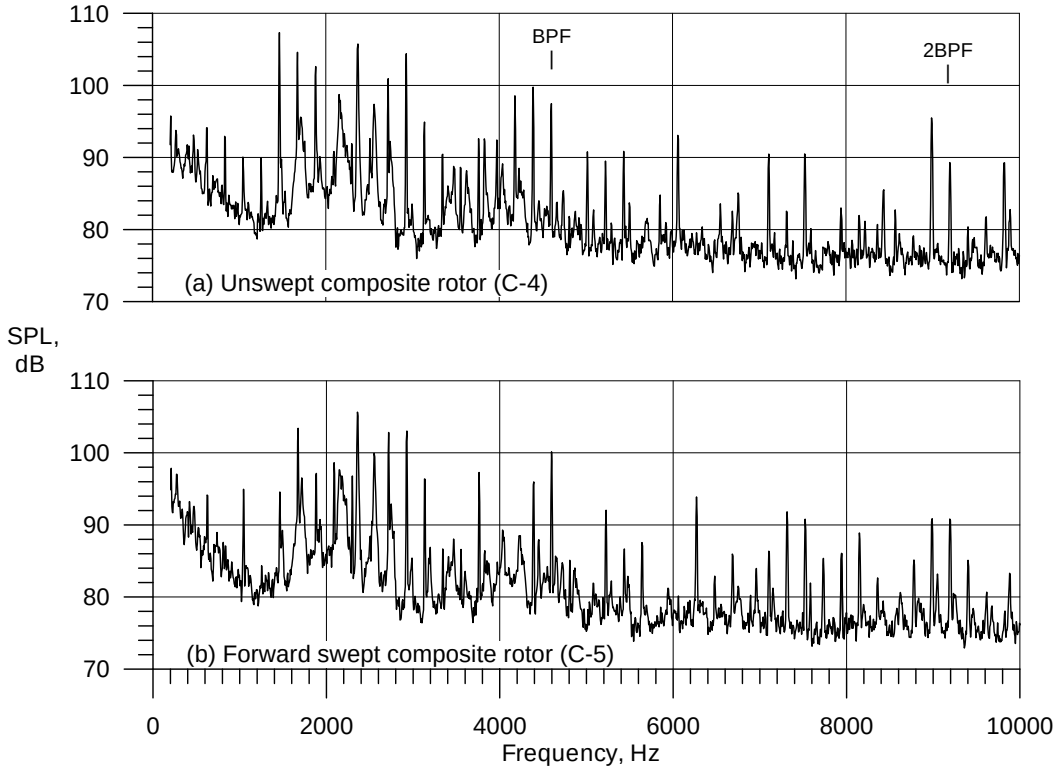

Figure 53.—Comparison of constant (6 Hz) bandwidth spectra for the unswept and forward-swept composite rotors at 12 k rpm_c (47° sideline emission angle, HTH).

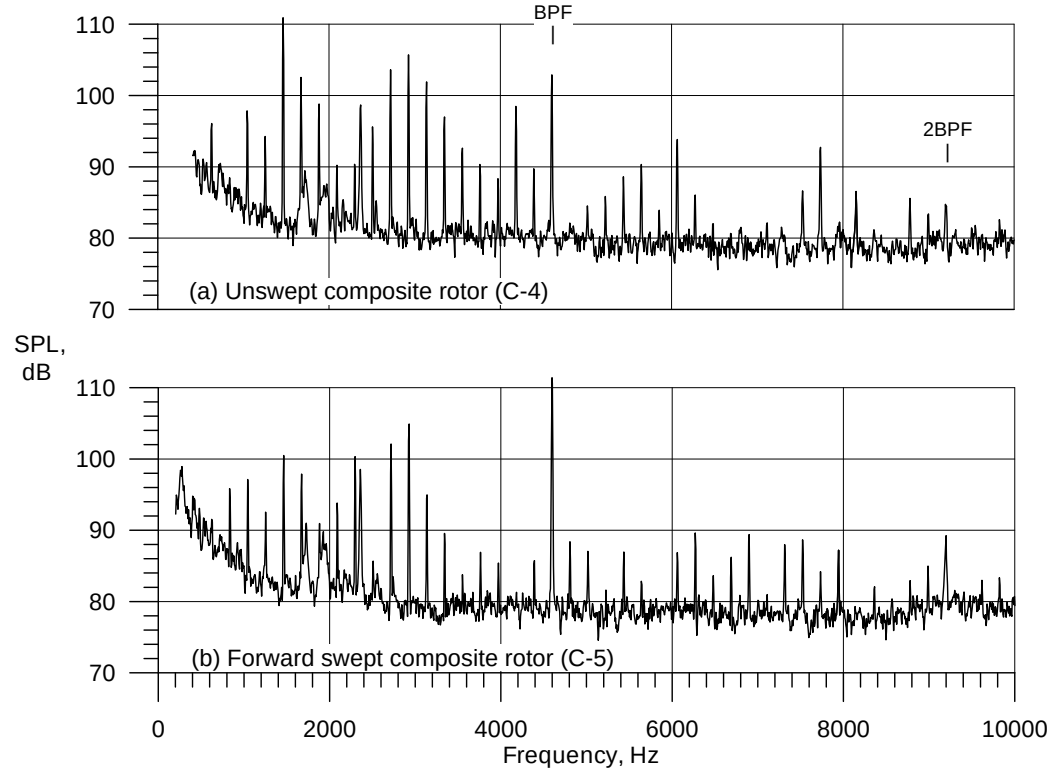

Figure 54.—Comparison of constant (6 Hz) bandwidth spectra for the unswept and forward-swept composite rotors at 12 k rpm_c (102° sideline emission angle, HTH).

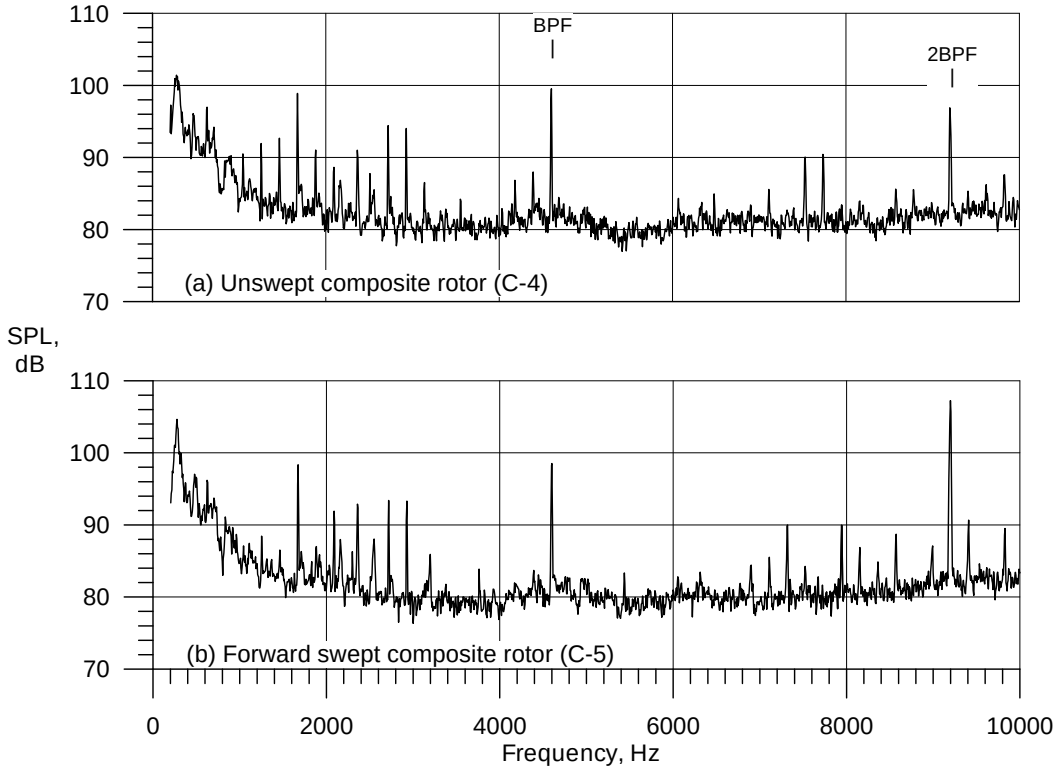

Figure 55.—Comparison of constant (6 Hz) bandwidth spectra for the unswept and forward-swept composite rotors at 12 k rpm_c (130° sideline emission angle, HTH).

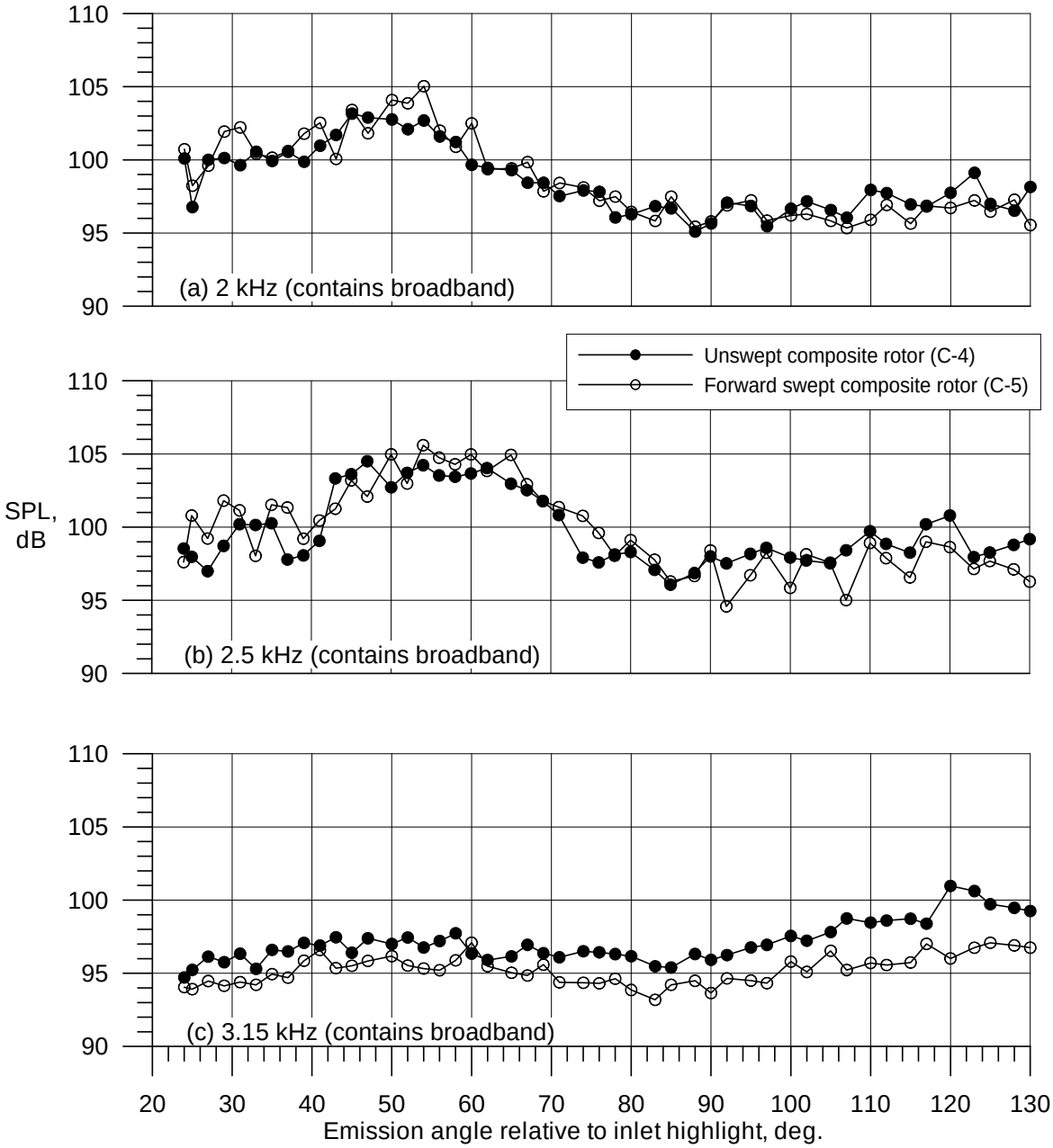

Figure 56.—Comparison of 1/3rd octave directivities for the unswept and forward-swept composite rotors at 10 k rpm_c (HTH).

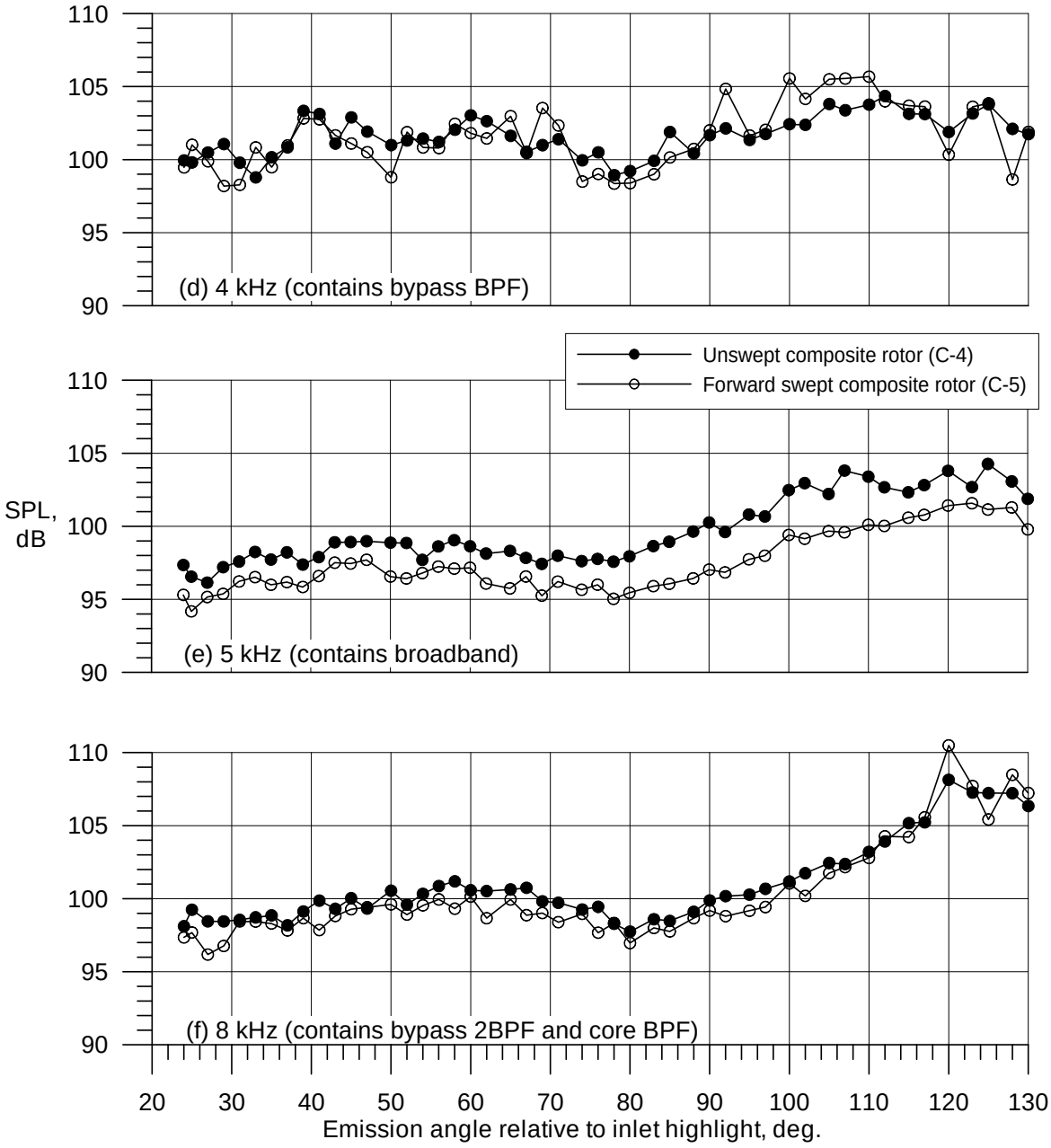

Figure 56.—Concluded.

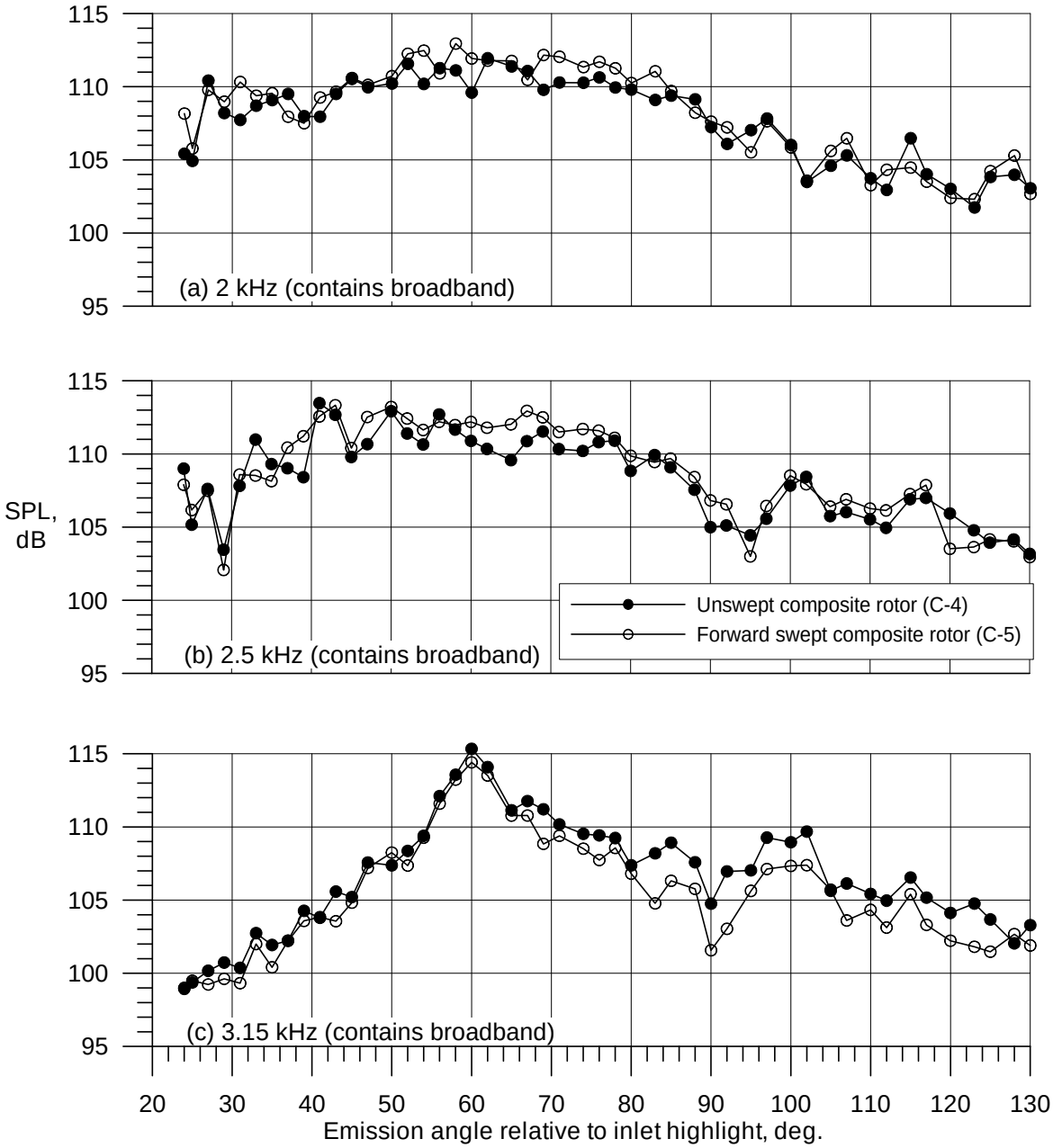

Figure 57.—Comparison of 1/3rd octave directivities for the unswept and forward-swept composite rotors at 12 k rpm_c (HTH).

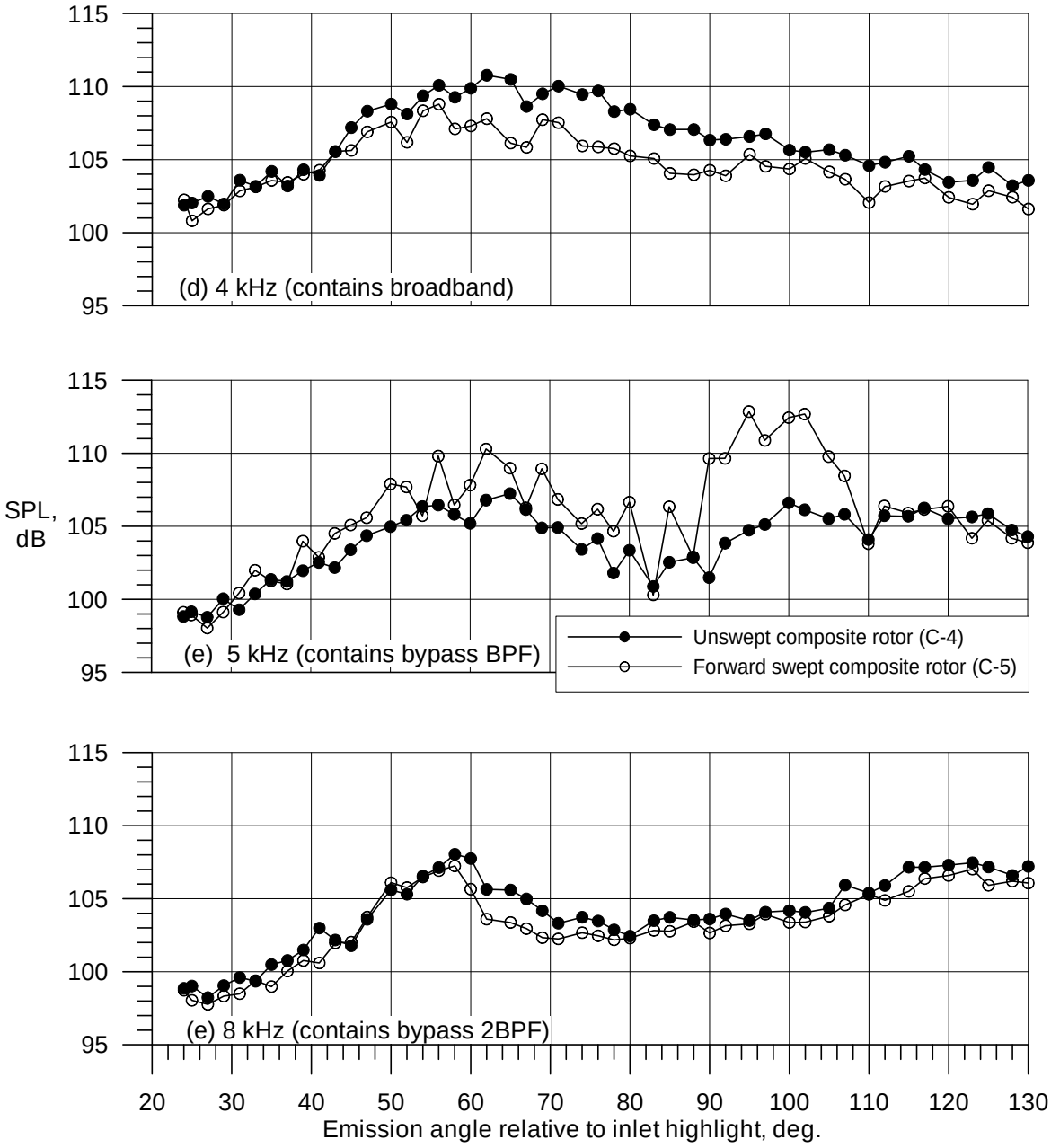

Figure 57.—Concluded.

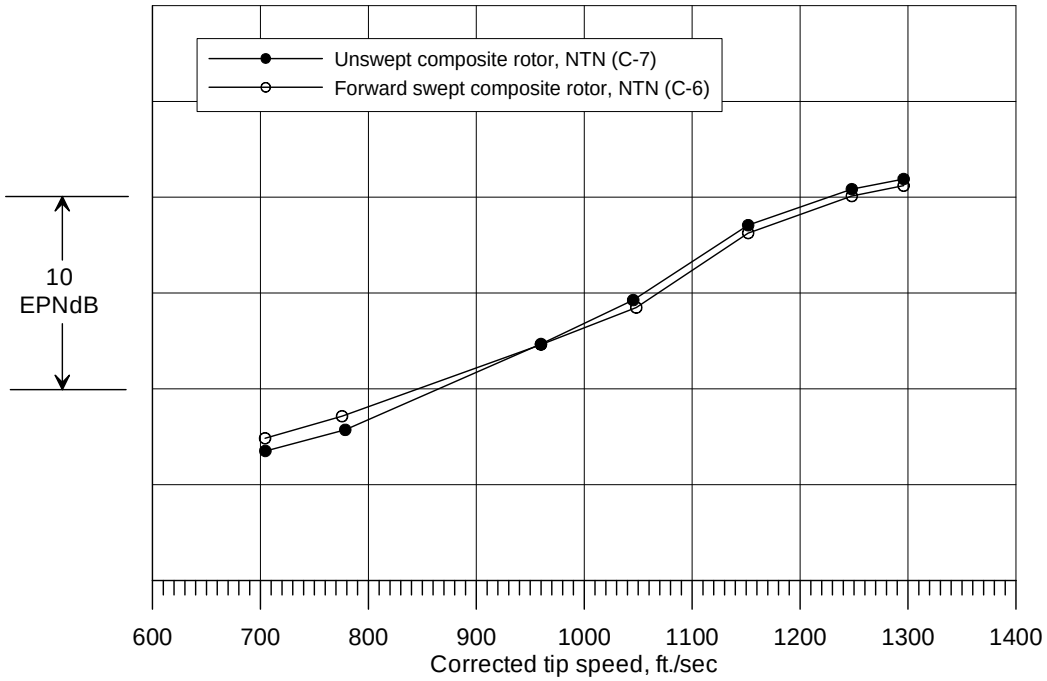

Figure 58.—Comparison of unswept and forward-swept composite rotors (NTN).

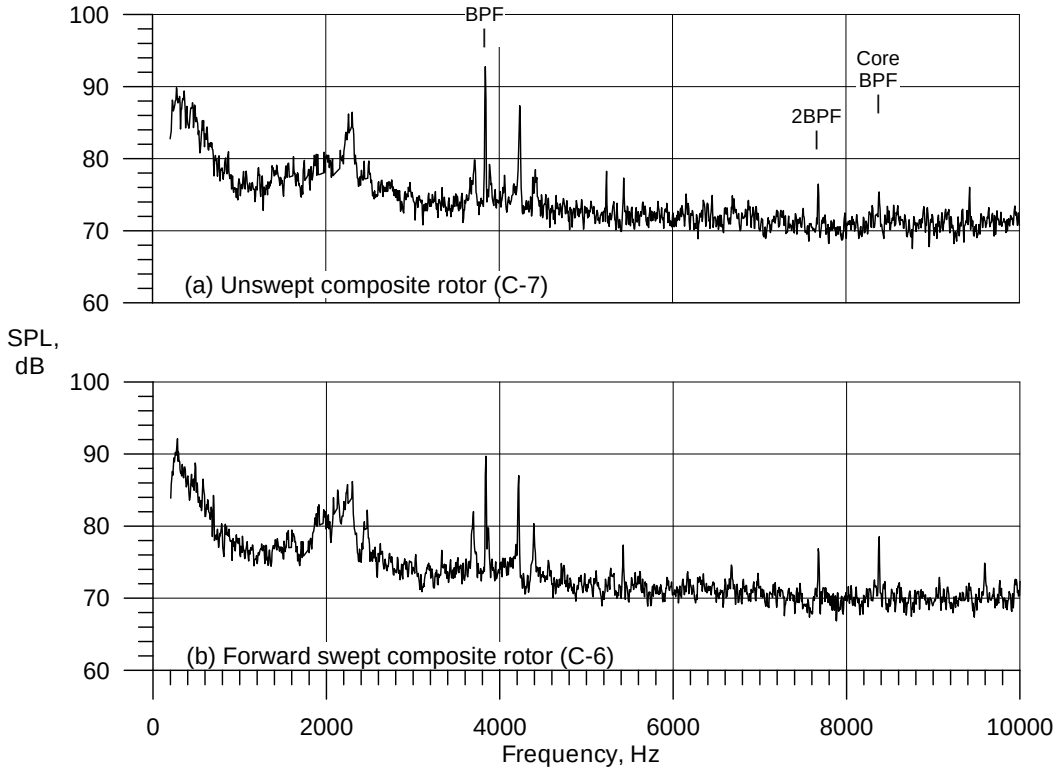

Figure 59.—Comparison of constant (6 Hz) bandwidth spectra for the unswept and forward-swept composite rotors at 10 k rpm_c (47° sideline emission angle, NTN).

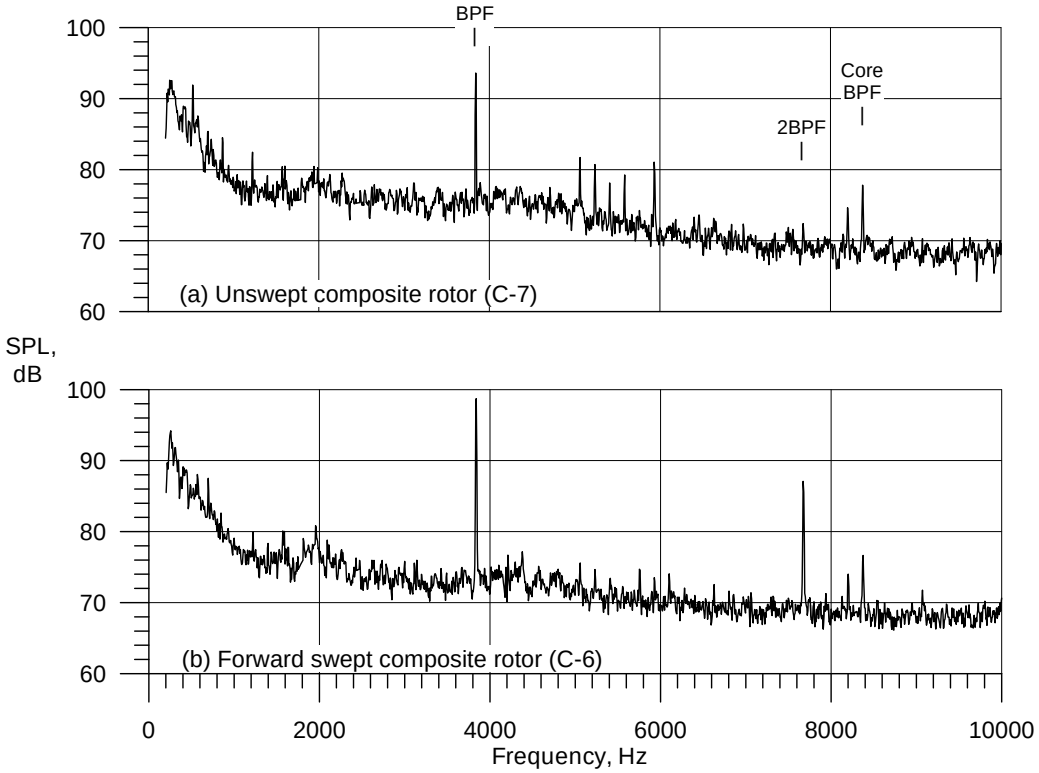

Figure 60.—Comparison of constant (6 Hz) bandwidth spectra for the unswept and forward-swept composite rotors at 10 k rpm_c (102° sideline emission angle, NTN).

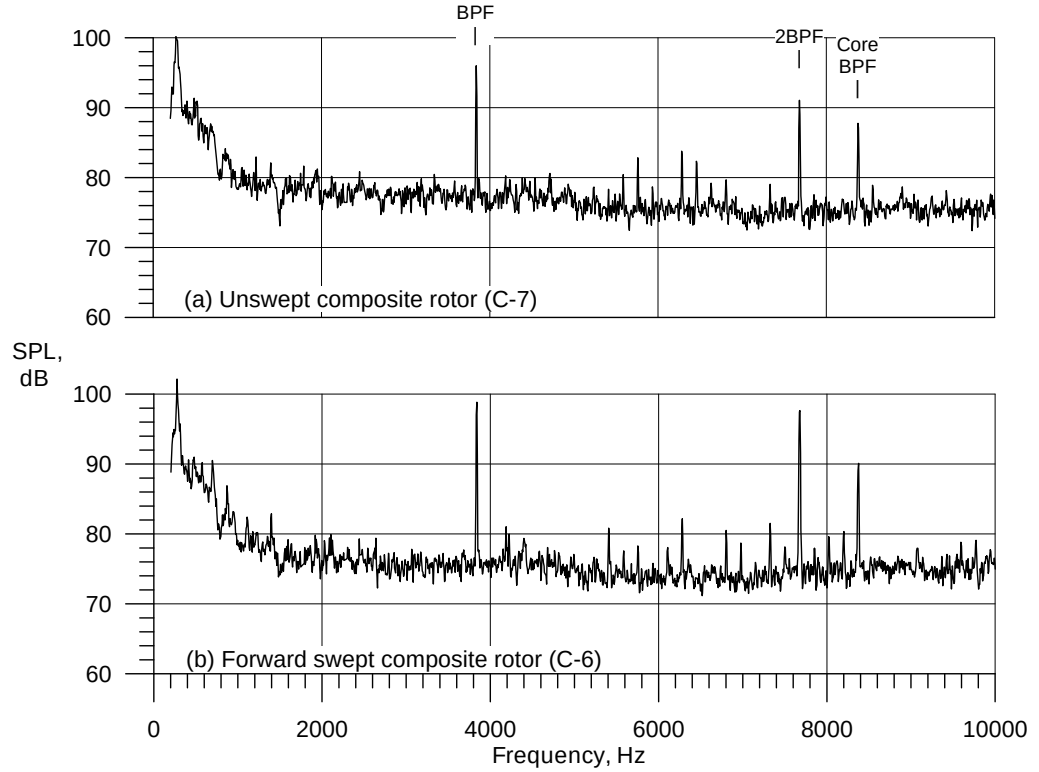

Figure 61.—Comparison of constant (6 Hz) bandwidth spectra for the unswept and forward-swept composite rotors at 10 k rpm_c (130° sideline emission angle, NTN).

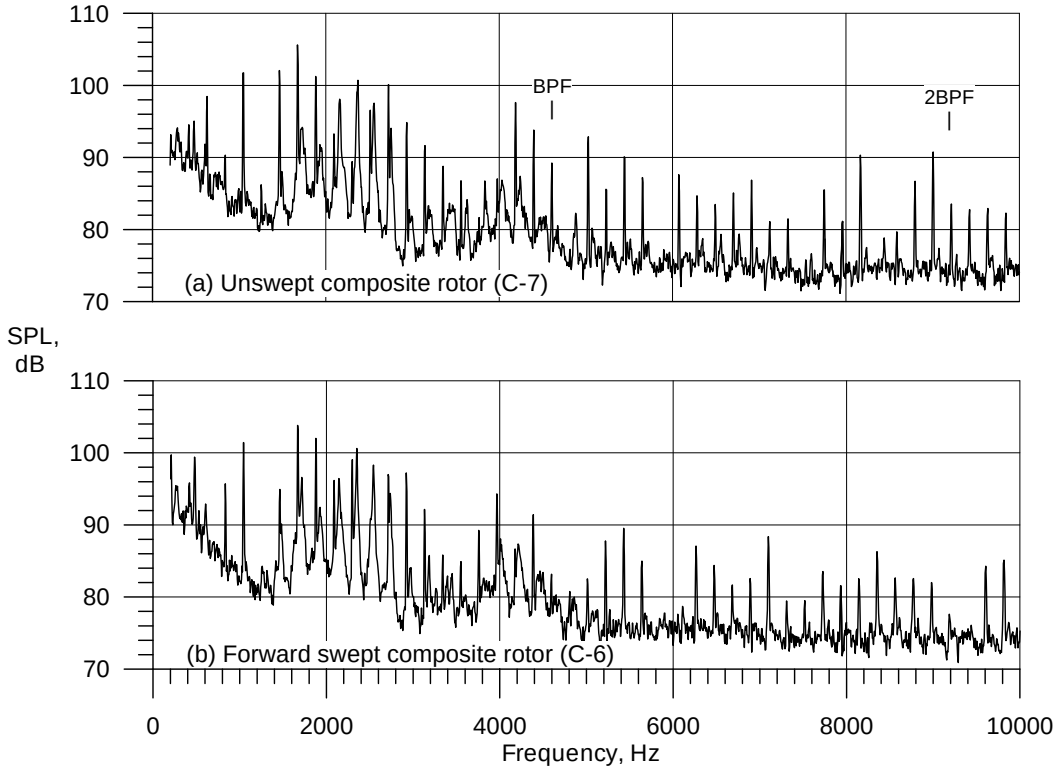

Figure 62.—Comparison of constant (6 Hz) bandwidth spectra for the unswept and forward-swept composite rotors at 12 k rpm_c (47° sideline emission angle, NTN).

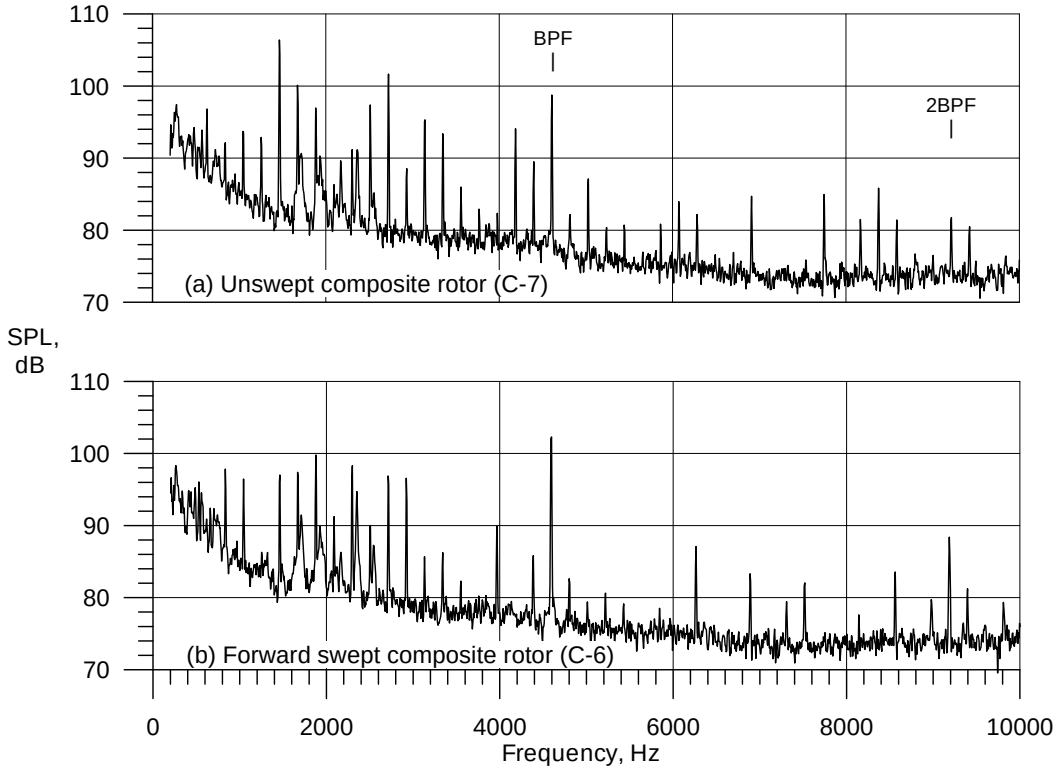

Figure 63.—Comparison of constant (6 Hz) bandwidth spectra for the unswept and forward-swept composite rotors at 12 k rpm_c (102° sideline emission angle, NTN).

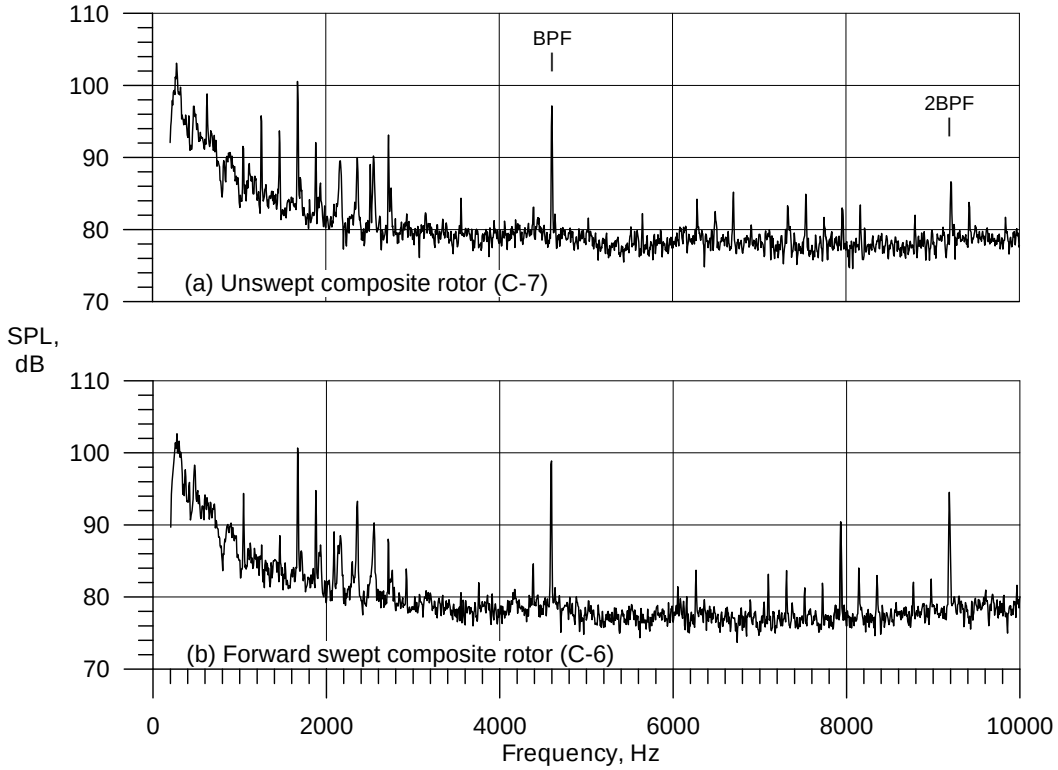

Figure 64.—Comparison of constant (6 Hz) bandwidth spectra for the unswept and forward-swept composite rotors at 12 k rpm_c (130° sideline emission angle, NTN).

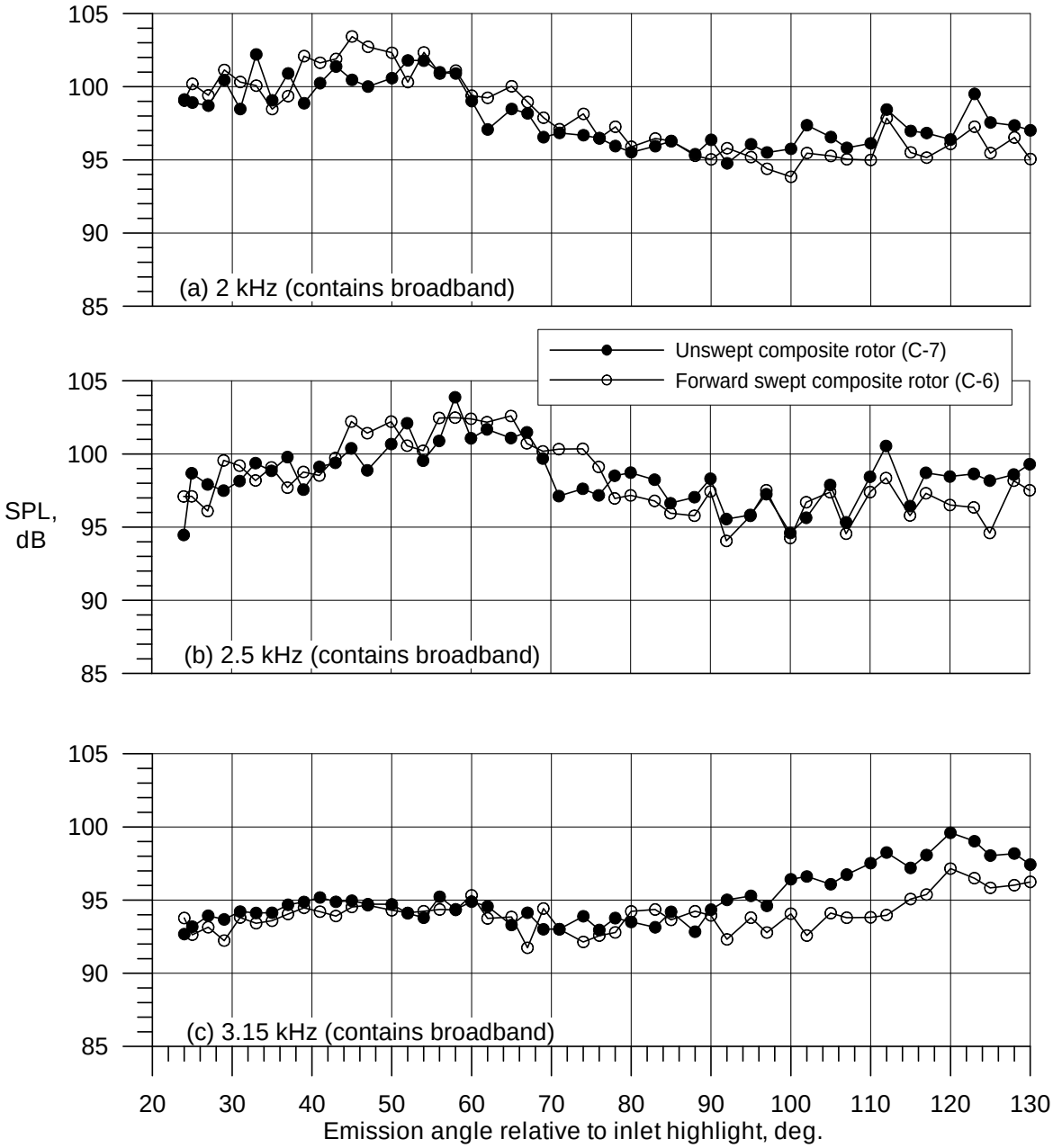

Figure 65.—Comparison of 1/3rd octave directivities for the unswept and forward-swept composite rotors at 10 k rpm_c (NTN).

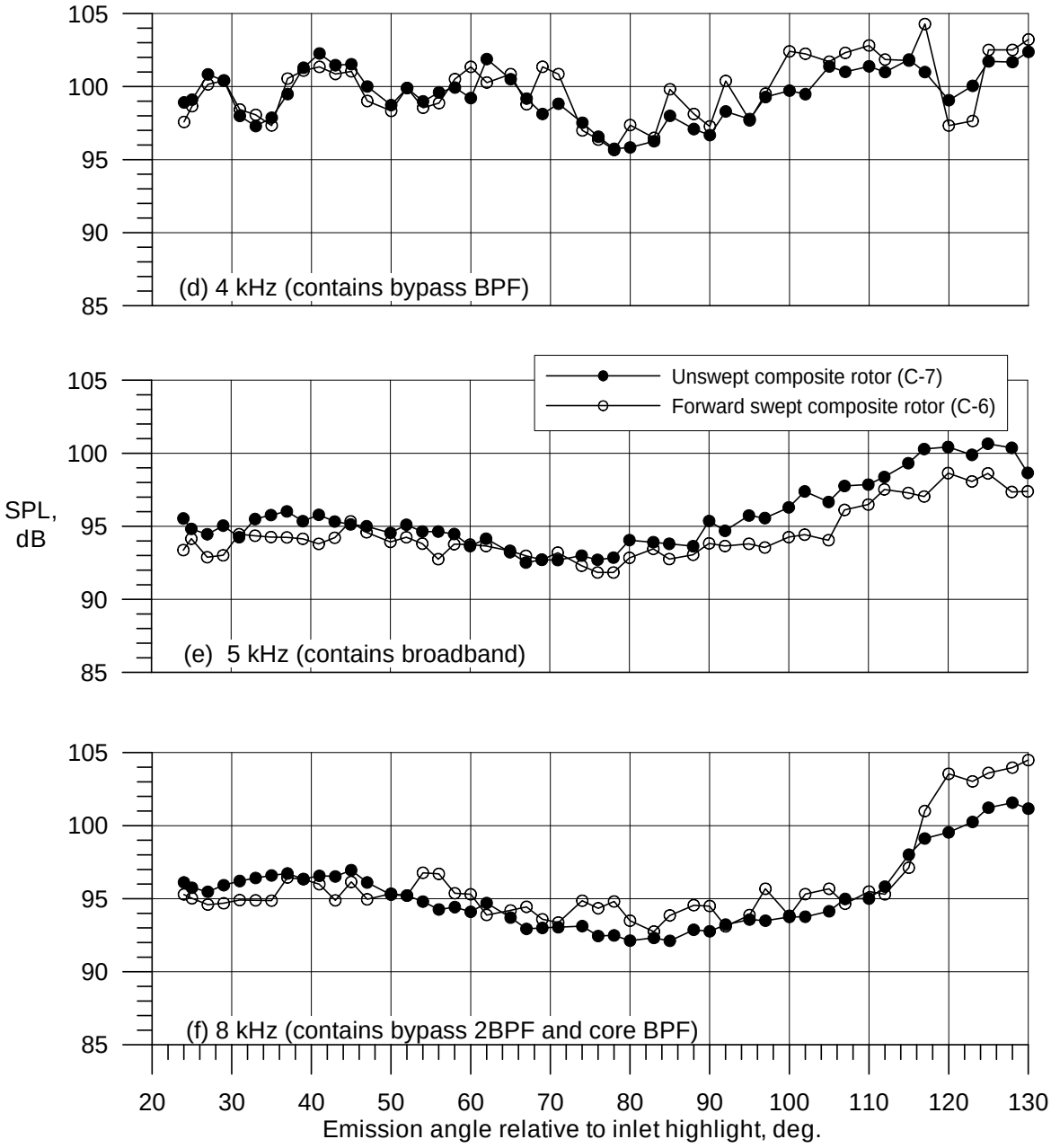

Figure 65.—Concluded.

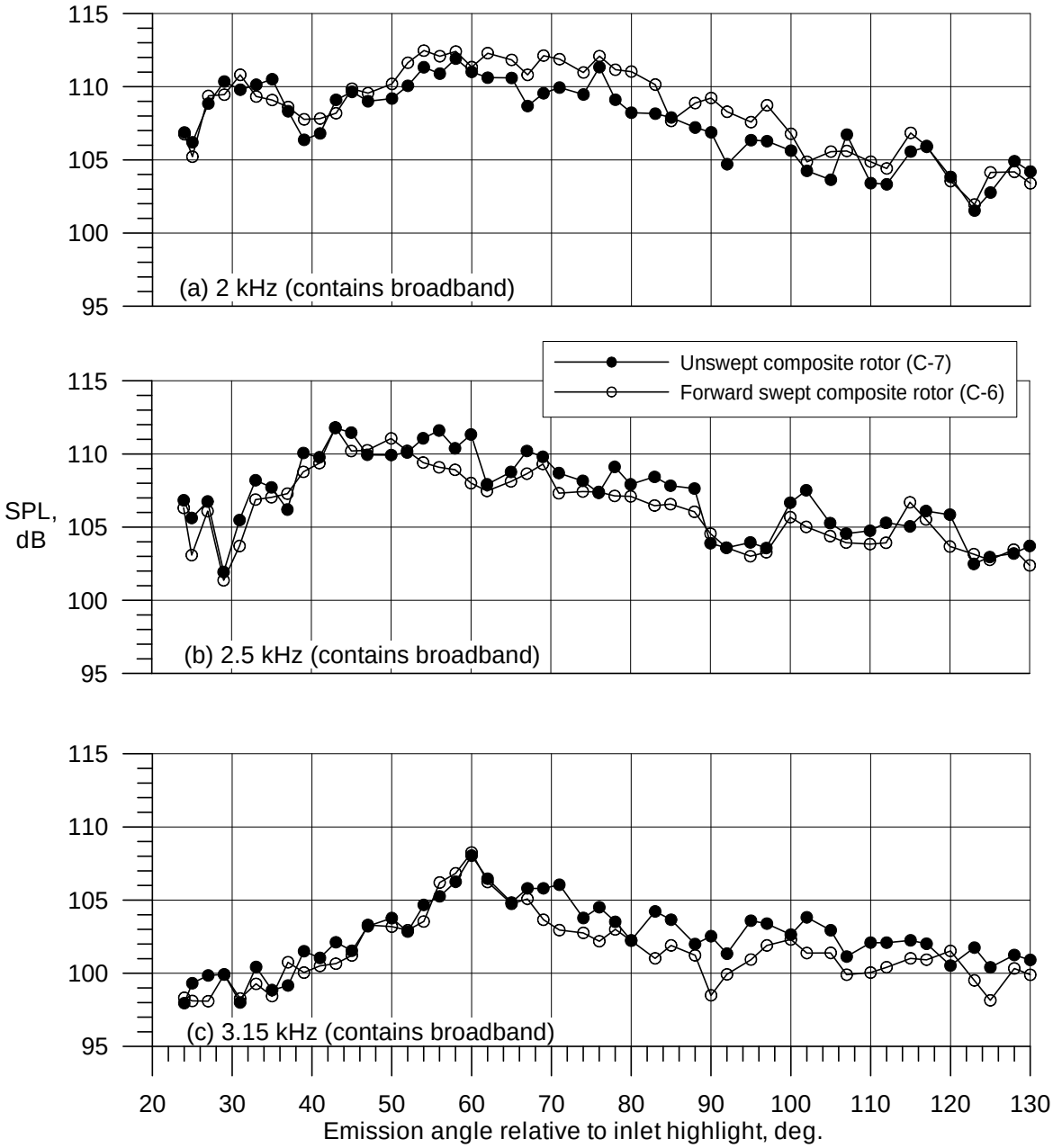

Figure 66.—Comparison of 1/3rd octave directivities for the unswept and forward-swept composite rotors at 12 k rpm_c (NTN).

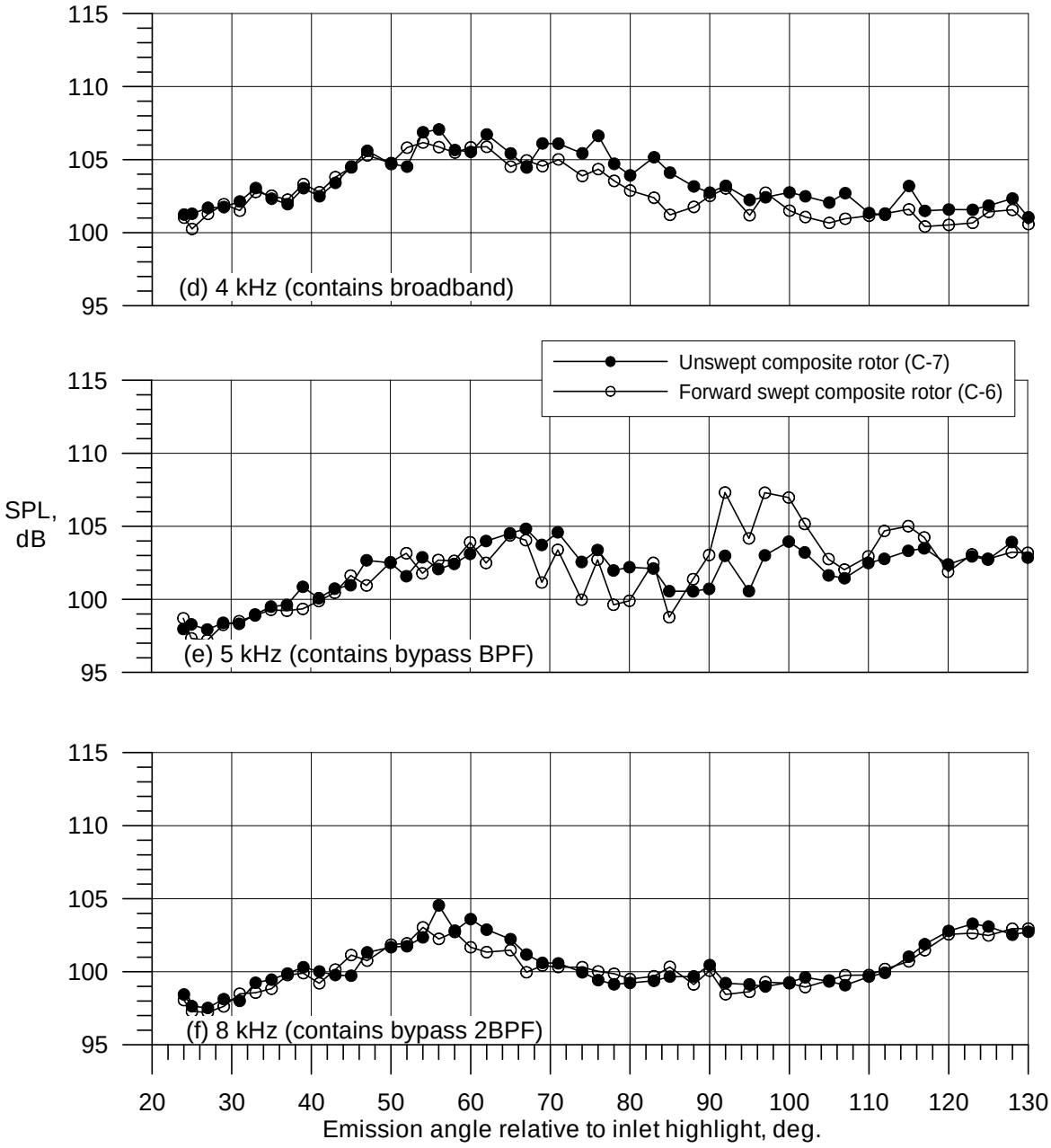

Figure 66.—Concluded.

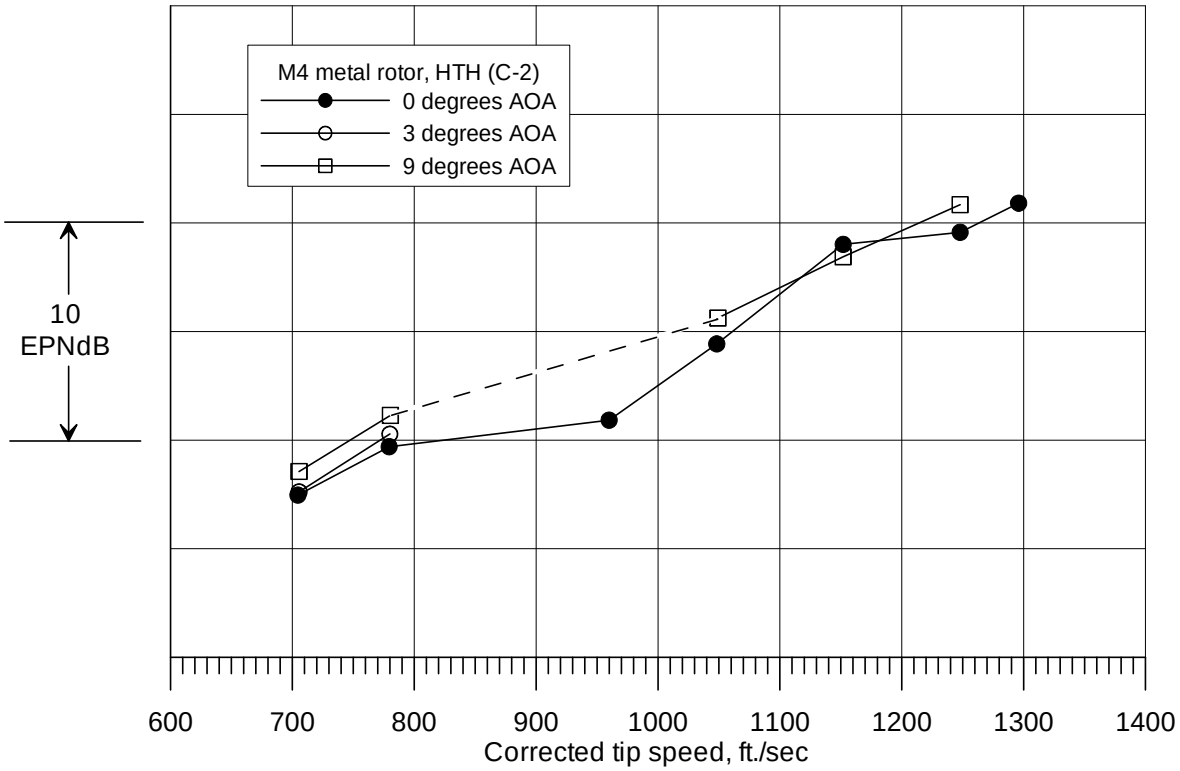

Figure 67.—Effect of fan axis angle-of-attack for the baseline M4 metal rotor, hardwall configuration (EPNL calculated from 9×15 LSWT sideline data, 5.6 scale factor, 304.8-m (1000-ft) flyover).

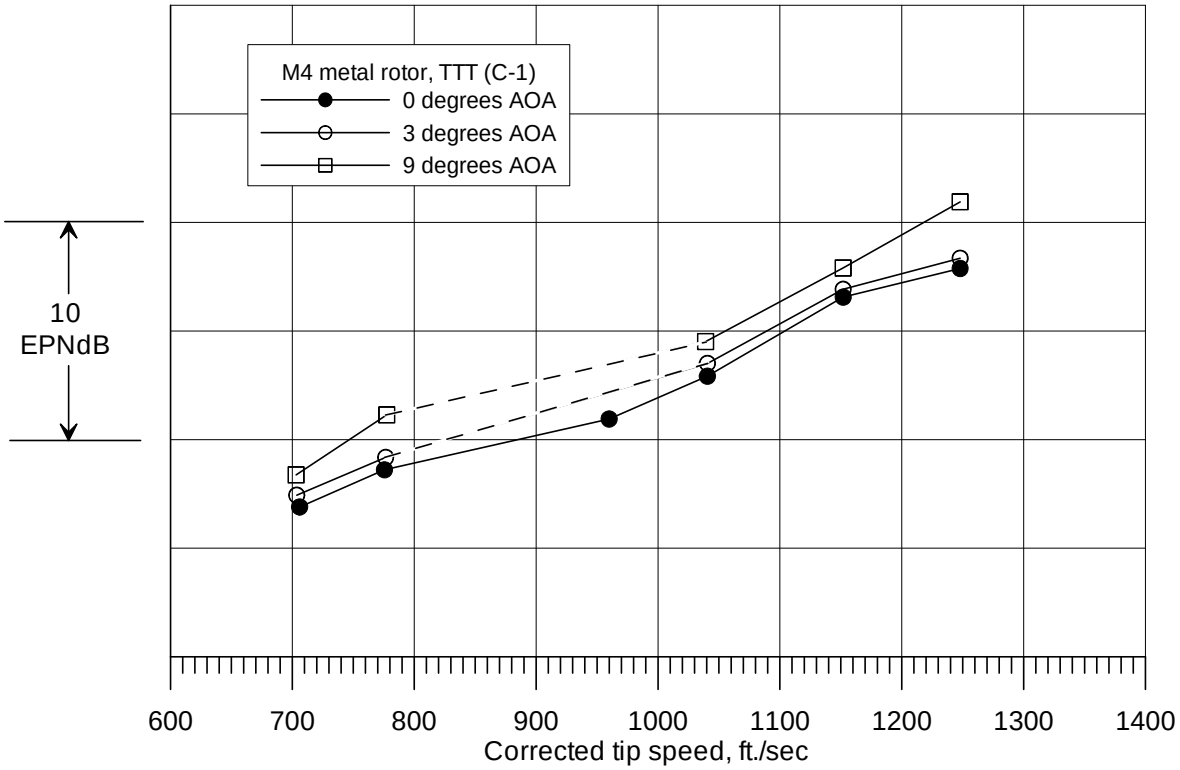

Figure 68.—Effect of fan axis angle-of-attack for the baseline M4 metal rotor, with acoustic treatment (EPNL calculated from 9×15 LSWT sideline data, 5.6 scale factor, 304.8-m (1000-ft) flyover).

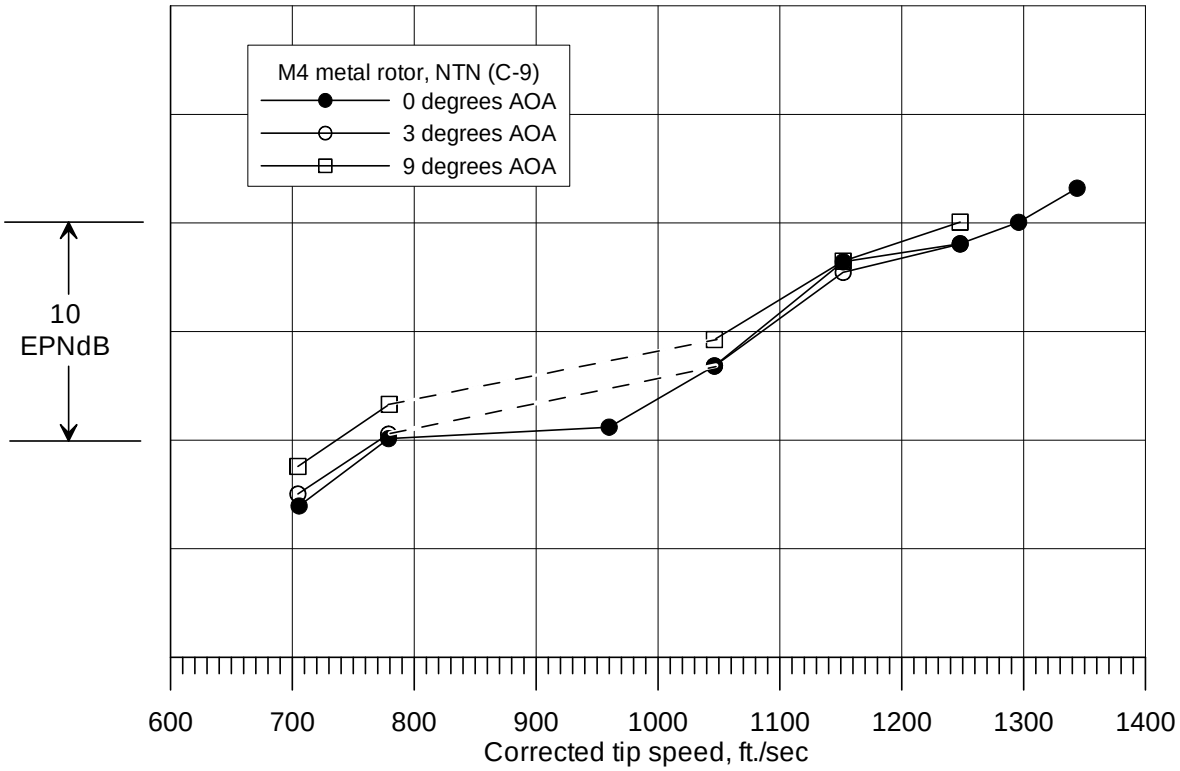

Figure 69.—Effect of fan axis angle-of-attack for the baseline M4 metal rotor, with “new” acoustic treatment (EPNL calculated from 9×15 LSWT sideline data, 5.6 scale factor, 304.8-m (1000-ft) flyover).

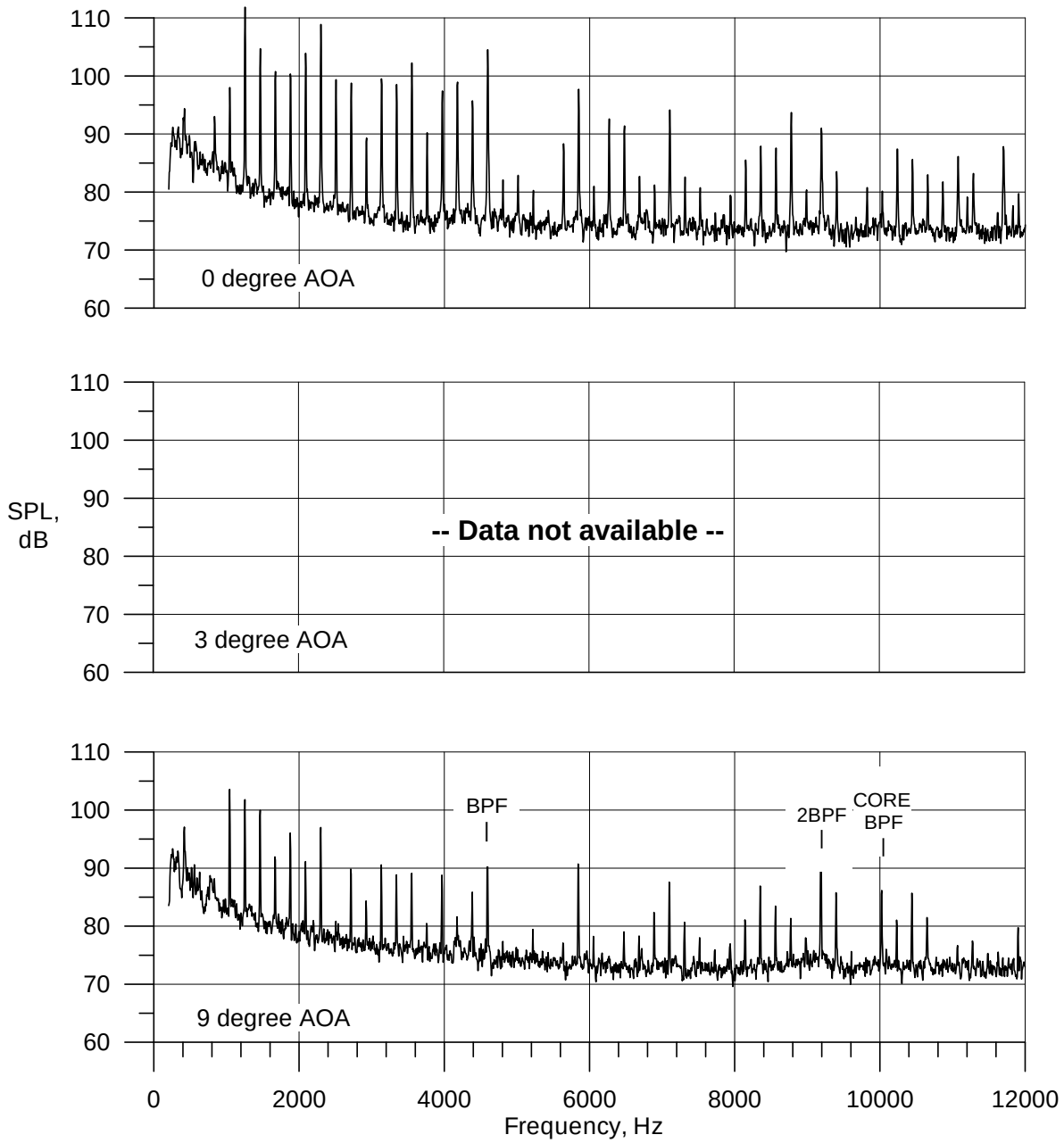

Figure 70.—Constant bandwidth (6 Hz) spectra. (M4 metal rotor, hardwall (HTH, C-2), 74° emission sideline angle on 89-in. sideline, 12 k rpm_c).

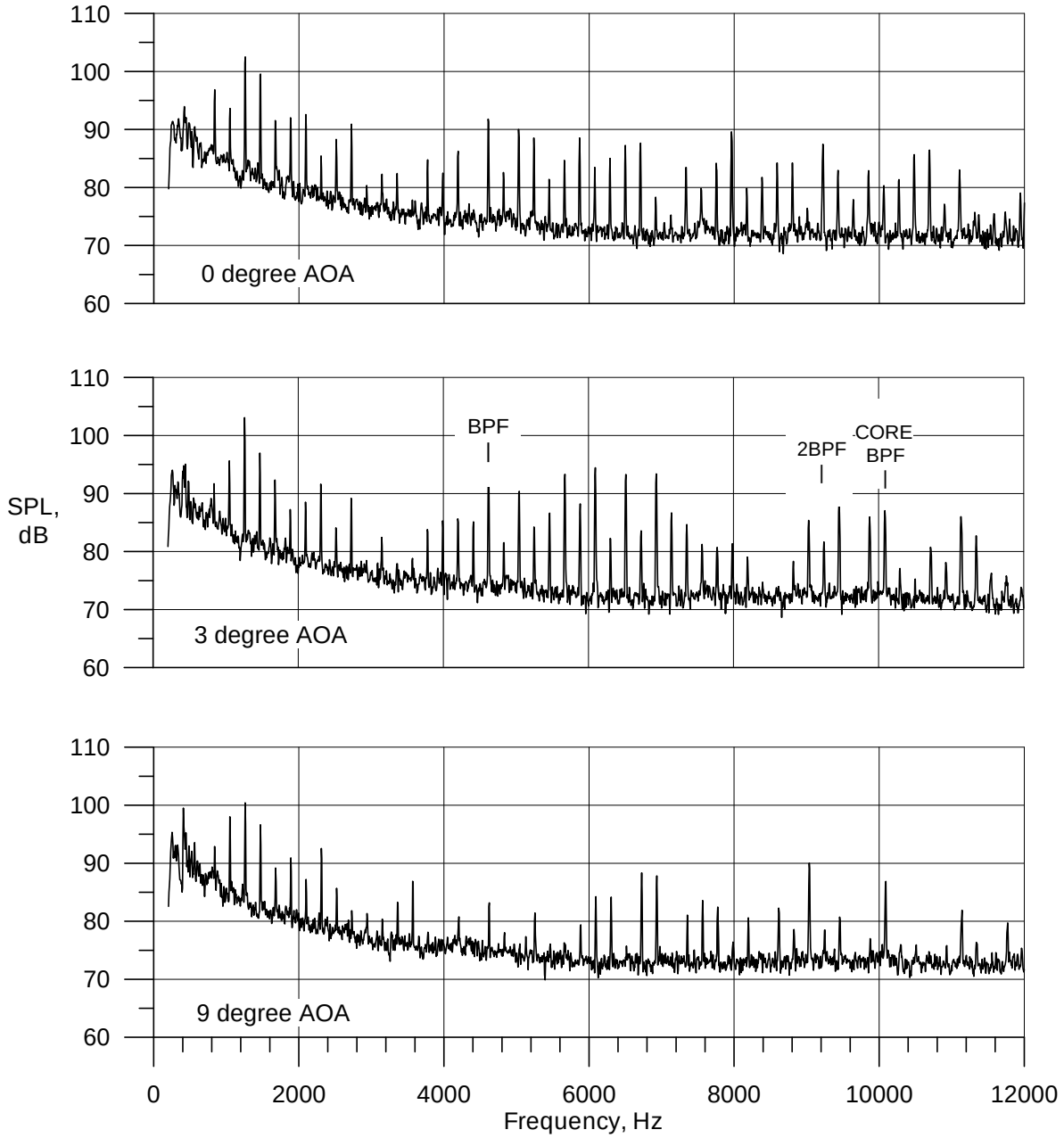

Figure 71.—Constant bandwidth (6 Hz) spectra. (M4 metal rotor, treated (TTT, C-1), 74° emission sideline angle on 89-in. sideline, 12 k rpm_c).

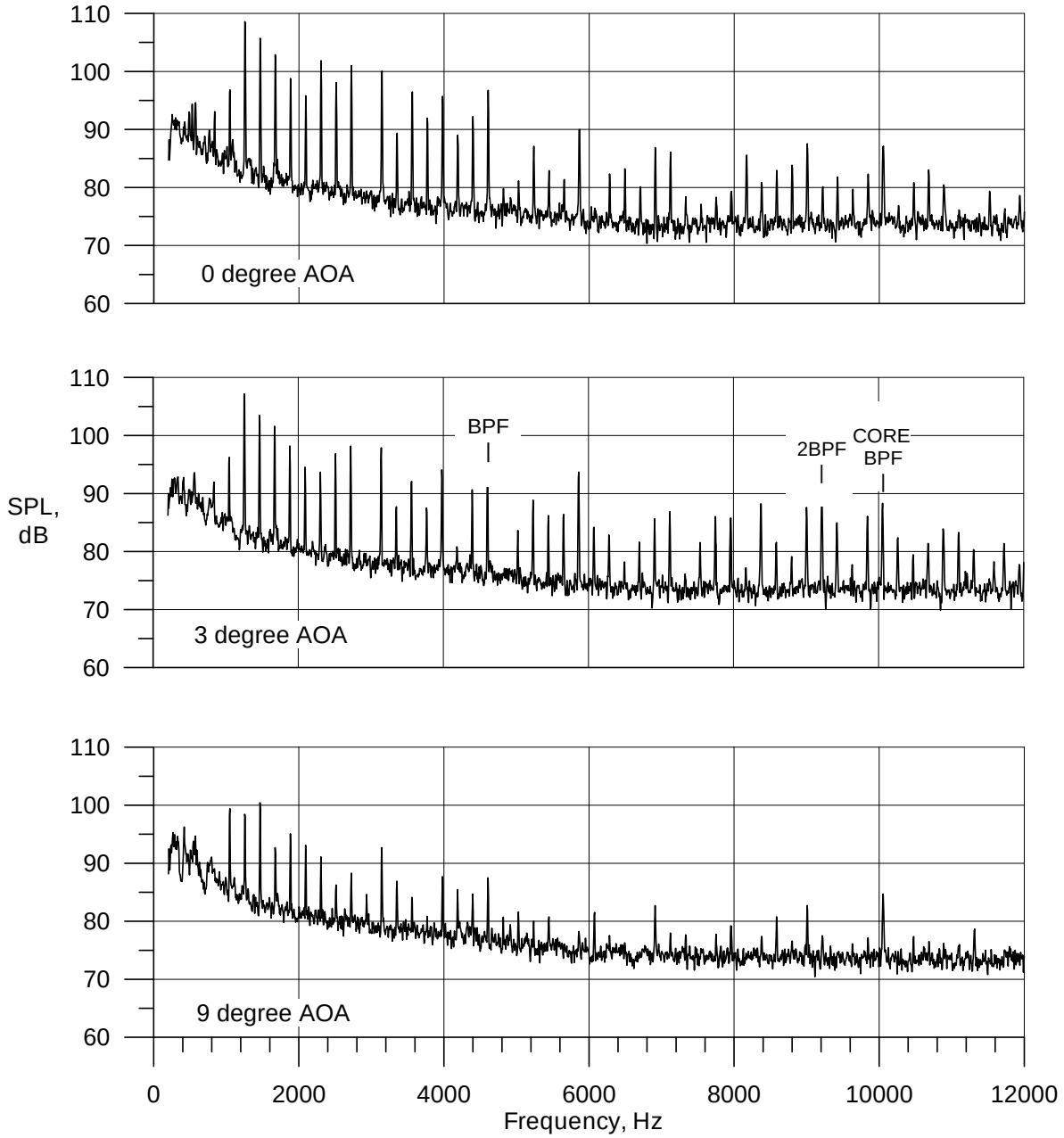

Figure 72.—Constant bandwidth (6 Hz) spectra. (M4 metal rotor, treated (NTN, C-9), 74° emission sideline angle on 89-in. sideline, 12 k rpm_c).

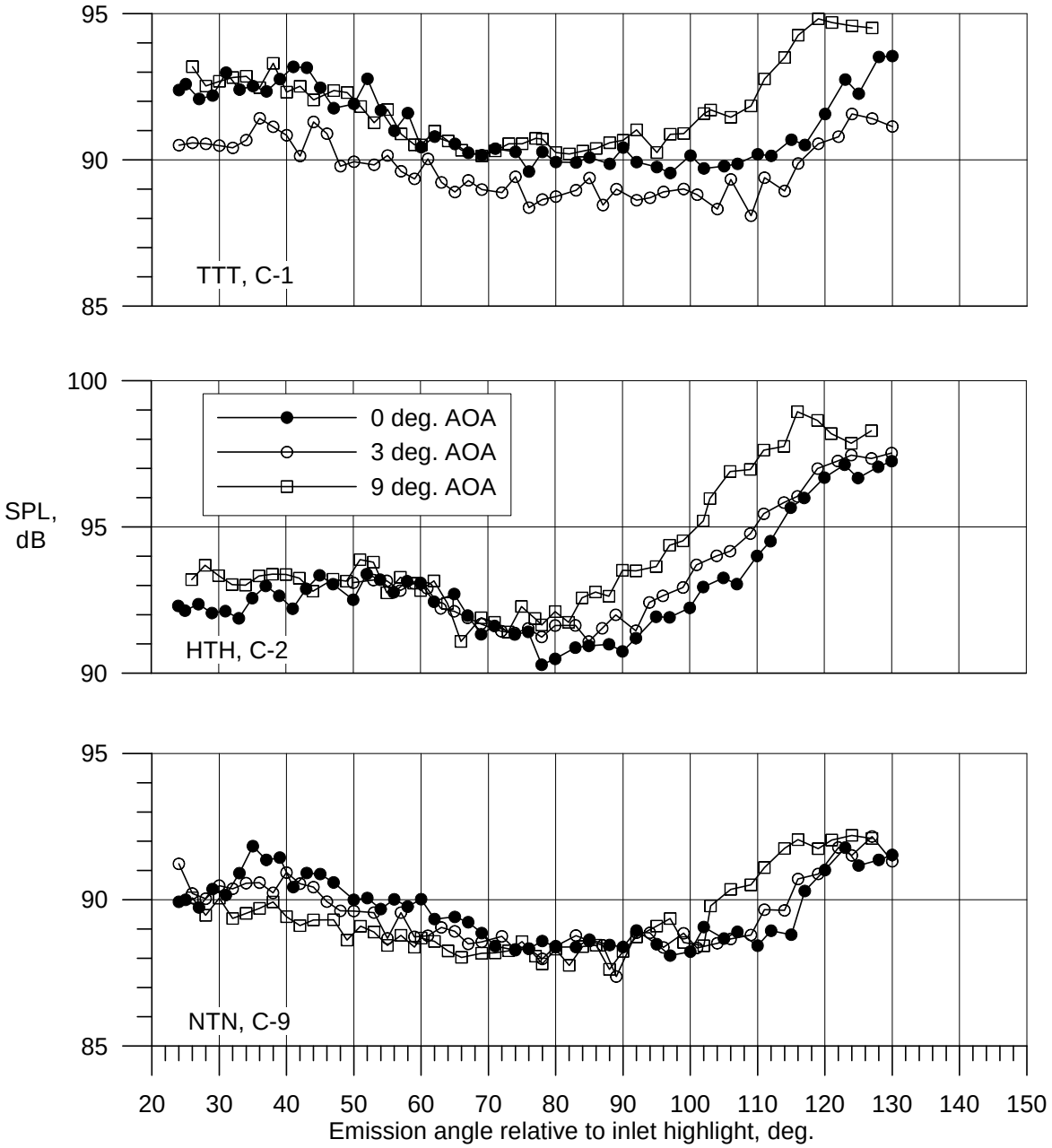

Figure 73.—1/3rd octave directivities at 8200 rpm_c showing fan axis angle-of-attack effects (Baseline M4 metal rotor, 8 kHz (broadband spectral region)).

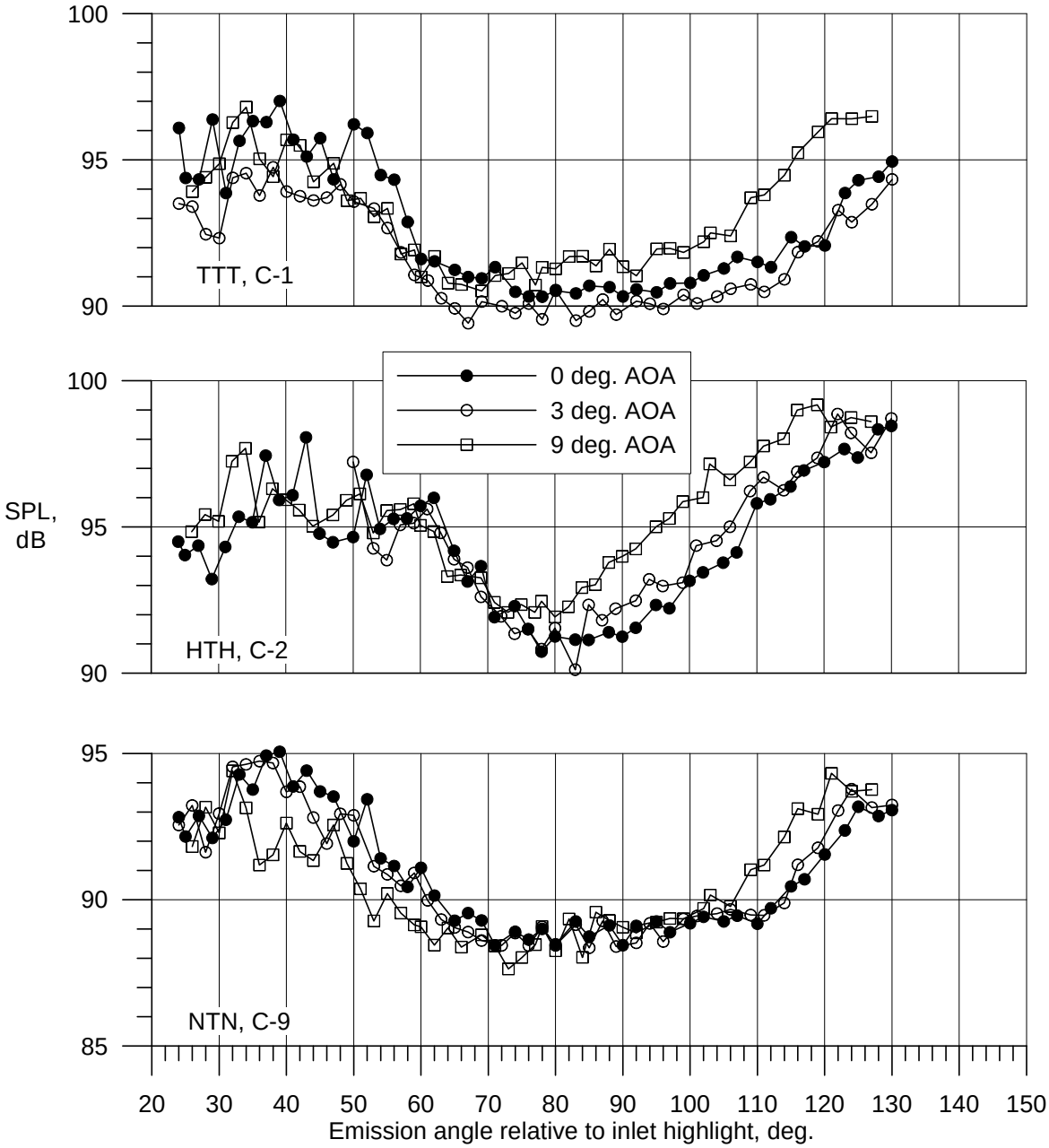

Figure 74.—1/3rd octave directivities at 8200 rpm_c showing fan axis angle-of-attack effects (Baseline M4 metal rotor, 10 kHz (1/3rd octave band contains bypass 3BPF tone)).

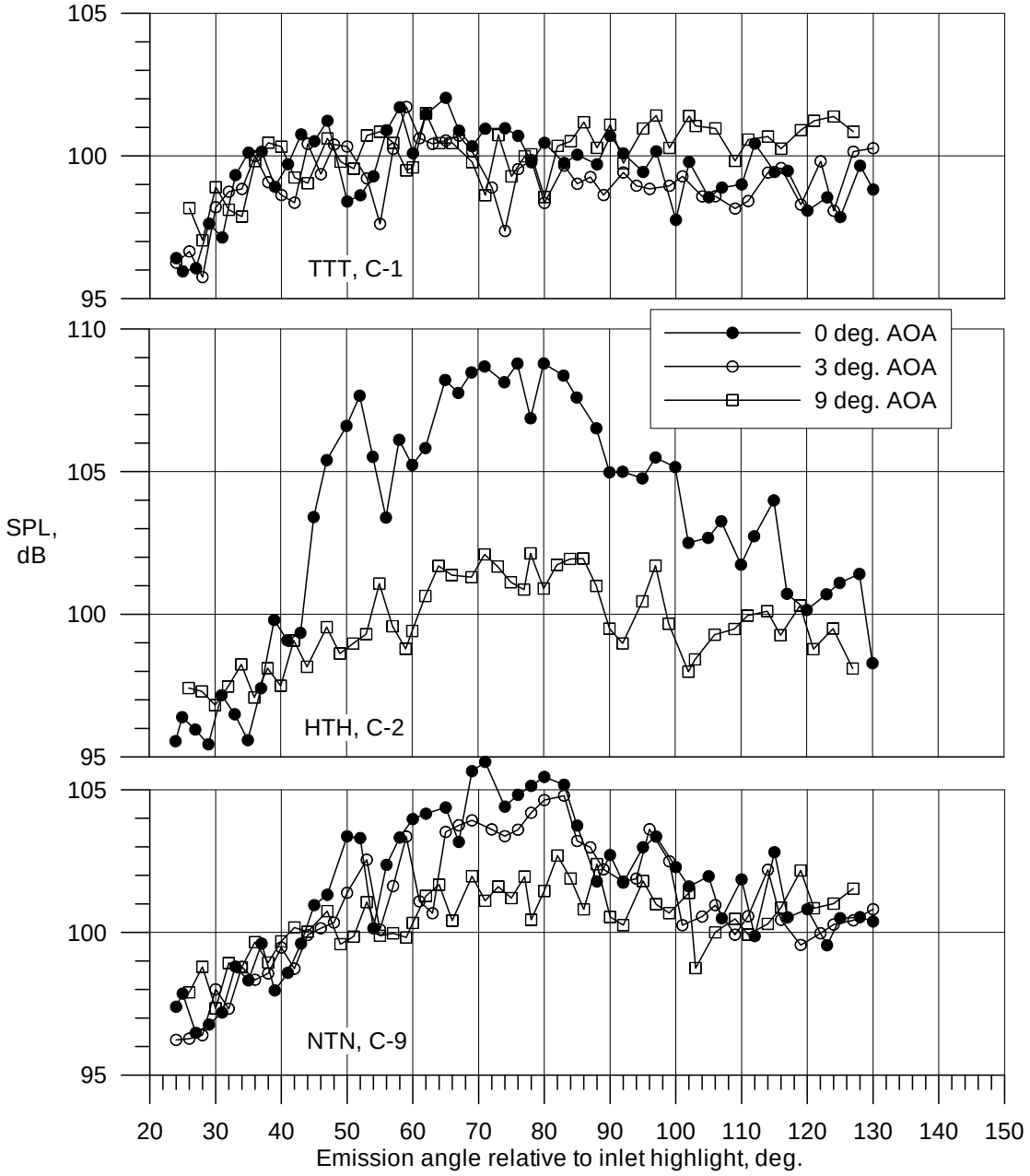

Figure 75.—1/3rd octave directivities at 12000 rpmc showing fan axis angle-of-attack effects (Baseline M4 metal rotor, 2 kHz (1/3rd octave band contains multiple pure tones and broadband)).

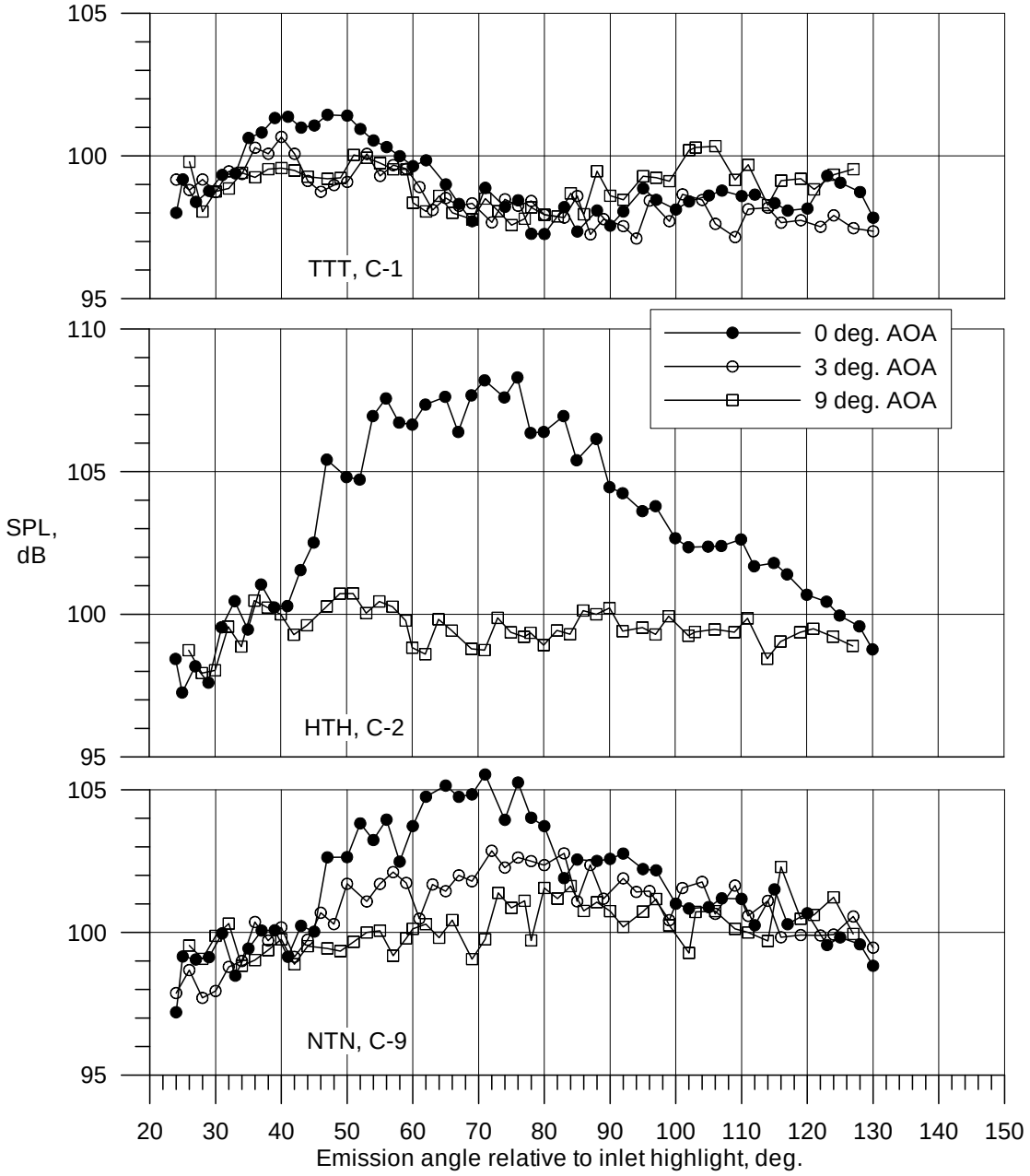

Figure 76.—1/3rd octave directivities at 12000 rpm_c showing fan axis angle-of-attack effects (Baseline M4 metal rotor, 4 kHz (1/3rd octave band contains bypass BPF and multiple pure tones)).

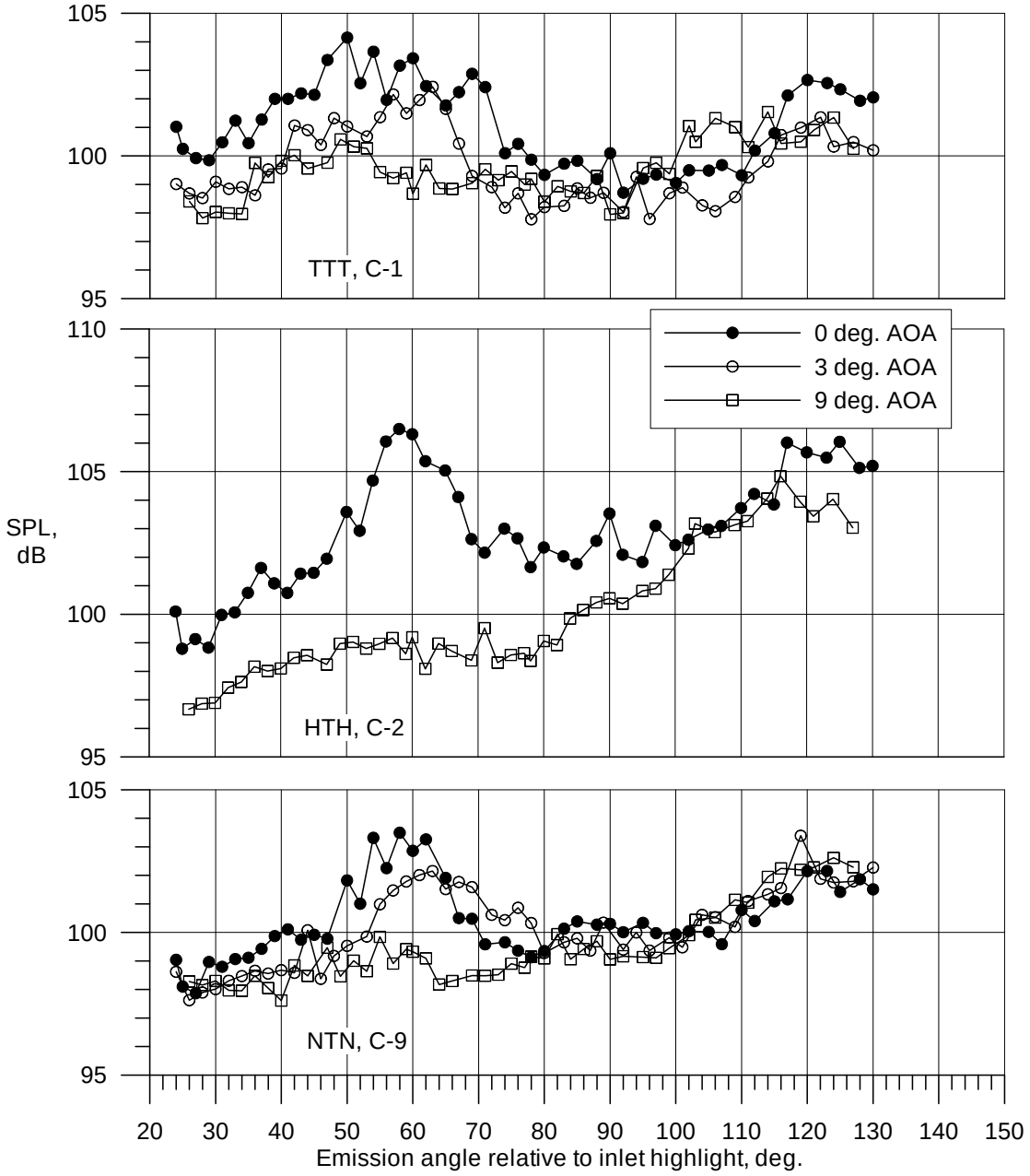

Figure 77.—1/3rd octave directivities at 12000 rpm_c showing fan axis angle-of-attack effects (Baseline M4 metal rotor, 8 kHz (1/3rd octave band contains bypass 2BPF and multiple pure tones)).

REPORT DOCUMENTATION PAGE	Form Approved OMB No. 0704-0188

1. REPORT DATE *(DD-MM-YYYY)*	2. REPORT TYPE	3. DATES COVERED *(From - To)*
01-05-2012	Technical Memorandum	

4. TITLE AND SUBTITLE
Acoustic Performance of the GEAE UPS Research Fan in the NASA Glenn 9- by 15-Foot Low-Speed Wind Tunnel

5a. CONTRACT NUMBER

5b. GRANT NUMBER

5c. PROGRAM ELEMENT NUMBER

6. AUTHOR(S)
Woodward, Richard, P.; Hughes, Christopher, E.

5d. PROJECT NUMBER

5e. TASK NUMBER

5f. WORK UNIT NUMBER
WBS 561581.02.08.03.45.02.04

7. PERFORMING ORGANIZATION NAME(S) AND ADDRESS(ES)
National Aeronautics and Space Administration
John H. Glenn Research Center at Lewis Field
Cleveland, Ohio 44135-3191

8. PERFORMING ORGANIZATION REPORT NUMBER
E-18180

9. SPONSORING/MONITORING AGENCY NAME(S) AND ADDRESS(ES)
National Aeronautics and Space Administration
Washington, DC 20546-0001

10. SPONSORING/MONITOR'S ACRONYM(S)
NASA

11. SPONSORING/MONITORING REPORT NUMBER
NASA/TM-2012-217450

12. DISTRIBUTION/AVAILABILITY STATEMENT
Unclassified-Unlimited
Subject Category: 01
Available electronically at http://www.sti.nasa.gov
This publication is available from the NASA Center for AeroSpace Information, 443-757-5802

13. SUPPLEMENTARY NOTES

14. ABSTRACT
A model advanced turbofan was acoustically tested in the NASA Glenn 9- by 15-Foot Low-Speed Wind Tunnel in 1994. The Universal Propulsion Simulator fan was designed and manufactured by General Electric Aircraft Engines, and included an active core, as well as bypass, flow paths. The fan was tested with several rotors featuring unswept, forward-swept and aft-swept designs of both metal and composite construction. Sideline acoustic data were taken with both hard and acoustically treated walls in the flow passages. The fan was tested within an airflow at a Mach number of 0.20, which is representative of aircraft takeoff/approach conditions. All rotors showed similar aerodynamic performance. However, the composite rotors typically showed higher noise levels than did corresponding metal rotors. Aft and forward rotor sweep showed at most modest reductions of transonic multiple pure tone levels. However, rotor sweep often introduced increased rotor-stator interaction tone levels. Broadband noise was typically higher for the composite rotors and also for the aft-swept metal rotor. Transonic MPT generation was reduced with increasing fan axis angle of attack (AOA); however, higher downstream noise levels did increase with AOA resulting in higher overall Effective Perceived Noise Level.

15. SUBJECT TERMS
Acoustic emission; Jet aircraft noise; Engine noise; Noise reduction

16. SECURITY CLASSIFICATION OF:			17. LIMITATION OF ABSTRACT	18. NUMBER OF PAGES	19a. NAME OF RESPONSIBLE PERSON
a. REPORT	b. ABSTRACT	c. THIS PAGE			STI Help Desk (email:help@sti.nasa.gov)
U	U	U	UU	82	19b. TELEPHONE NUMBER *(include area code)* 443-757-5802